MULTI-REGION LOCAL FIELD POTENTIAL SIGNATURES

AND BRAIN COHERENCE ALTERNATIONS

IN RESPONSE TO MIGRAINE ATTACKS

by

ZHEN WANG

DISSERTATION

Submitted in partial fulfillment of the requirements

for the degree of Doctor of Philosophy at

The University of Texas at Arlington

May, 2022

Arlington, Texas

Supervising Committee:

Dr. Yuan Bo Peng, Supervising Professor (chair)
Dr. Qing Lin, co-chair
Dr. Perry Fuchs
Dr. Pedro Maia
Dr. Phillip Kramer
Dr. J.-C. Chiao

Acknowledgements

I would like to express my sincere gratitude to my mentor, Dr. Yuan Bo Peng, who provides me the opportunity to conduct the graduate study, supports me to carry out the research, advances my understanding of science, guides me to achieve excellence in neuroscience, etc. I am fortunate enough to have the opportunity to work with Dr. Peng, and my graduate life is gorgeous with him. All I gained will prepare me as an independent researcher.

I would also like to thank my dissertation committee members, Dr. Qing Lin (co-chair, Department of Psychology, UTA), Dr. Perry Fuchs (Department of Psychology, UTA), Dr. Pedro Maia (Department of Mathematics, UTA), Dr. Phillip Kramer (Department of Biomedical Sciences, Texas A&M University College of Dentistry), and Dr. J.-C. Chiao (Department of Electrical and Computer Engineering, Southern Methodist University). They have offered profound and insightful inputs into my dissertation, especially in the field of data processing.

Additionally, I want to acknowledge collaborators with Dr. Peng lab, Dr. Hanli Liu and Dr. Sen Xu. We have worked together to examine the feasibility of light stimulation to pain alleviation and related transcriptome analysis. I also want to thank my colleague, Tao Zhang, we hold lots of discussions associated with the ultrasound project, where I have acquired growing interdisciplinary inputs. I would like to thank Christine Safieddine, UTA's Animal Care Facility Manager, for helping us take care of animals and prepare laboratory supplies. I would also like to thank rats and I can not accomplish the dissertation without them.

Last but not least, I would like to thank my caring family and friends who always support me.

May, 2022

Abstract

Multi-region Local Field Potential Signatures and Brain Coherence Alternations in Response to Migraine Attacks

Zhen Wang, Ph.D.

The University of Texas at Arlington, 2022

Supervising Professor: Yuan Bo Peng

Migraine is a recurrent primary headache disorder with moderate to severe disability. It has been ranked as the second leading cause of disability and the sixth most prevalent disease. However, the pathophysiology of migraine headaches remains not fully understood. Consequently, safe and effective therapies to alleviate migraine headaches are limited. Local field potential (LFP) recording, as a neurophysiological tool, has been widely utilized to investigate the combined neuronal activity. The ***purpose*** of this proposed study was to determine differential LFP signatures and brain coherence alternations from multiple brain regions associated with migraine-relevant pain networks, which enabled to remove barriers to understanding the migraine pathophysiology and facilitated the treatment study clinically. We conducted the migraine animal model which was induced by intraperitoneal (i.p.) injection of nitroglycerin (NTG), a well-established migraine model. As an initial part of this study, LFP signals were firstly recorded from anesthetized animals, followed by freely moving animals. Additionally, behavior measurements were implemented in freely moving animals. The ***hypothesis*** was that various brain areas, which are involved in

different orders of neurons in the trigeminovascular system and pain processing, could show different response patterns/signatures with brain coherence changes to migraine attacks. In this study, LFPs from the anterior cingulate cortex (ACC), the posterior nucleus of the thalamus (Po), the trigeminal ganglion (TG), and the primary visual cortex (V1M) were simultaneously recorded. The ***rationale*** was that the trigeminal ganglion, thalamus, and visual cortex are involved in the pathophysiology of migraine attacks, and the ACC as one part of the limbic system is related to emotional processing. There were three specific aims. ***Aim 1***: Determine LFP signatures containing ACC, Po, TG, and V1M when migraine occurs from anesthetized animals; ***Aim 2***: Determine the multi-region LFP signatures in response to migraine attacks from freely moving animals and examine behavioral responses; ***Aim 3***: Examine brain coherence alternations among paired brain sites.

Table of Contents

List of Illustrations

Chapter 1 Introduction

1.1 Overview of migraine

Migraine, as one of the main neurological disorders, has been ranked as the second leading cause of disability and the sixth most prevalent disease with up to 1 billion (1.04 billion in 2016) patients worldwide according to the Global Burden of Disease Study, which brings about enormous socioeconomic burdens (Table 1) (Vos et al., 2017). Affected females (18%) outnumber males (6%) in the ratio of three to one each year in US population studies (Lipton et al., 2007; Burch et al., 2019).

Migraine is a recurrent primary headache disorder with moderate to severe disability, manifesting with attacks of throbbing headache (unilateral usually) lasting 4-72 hours; nausea; vomiting; aggravated by routine physical activity; photophobia, phonophobia, osmophobia, cutaneous allodynia (sensitive to light, sound, odor, and normal touch respectively); etc. Moreover, there are usually four typical linear/chronological ordering phases for migraine: prodrome, aura (recognized as a hallmark of migraine), headache, and postdrome, with overlap mostly as shown in Figure 1 (Burgos-Vega et al., 2015; Dodick, 2018).

Table 1. Leading cause of (**A**) prevalence and (**B**) YLDs. YLD: Years Lived with Disability (Vos et al., 2017)

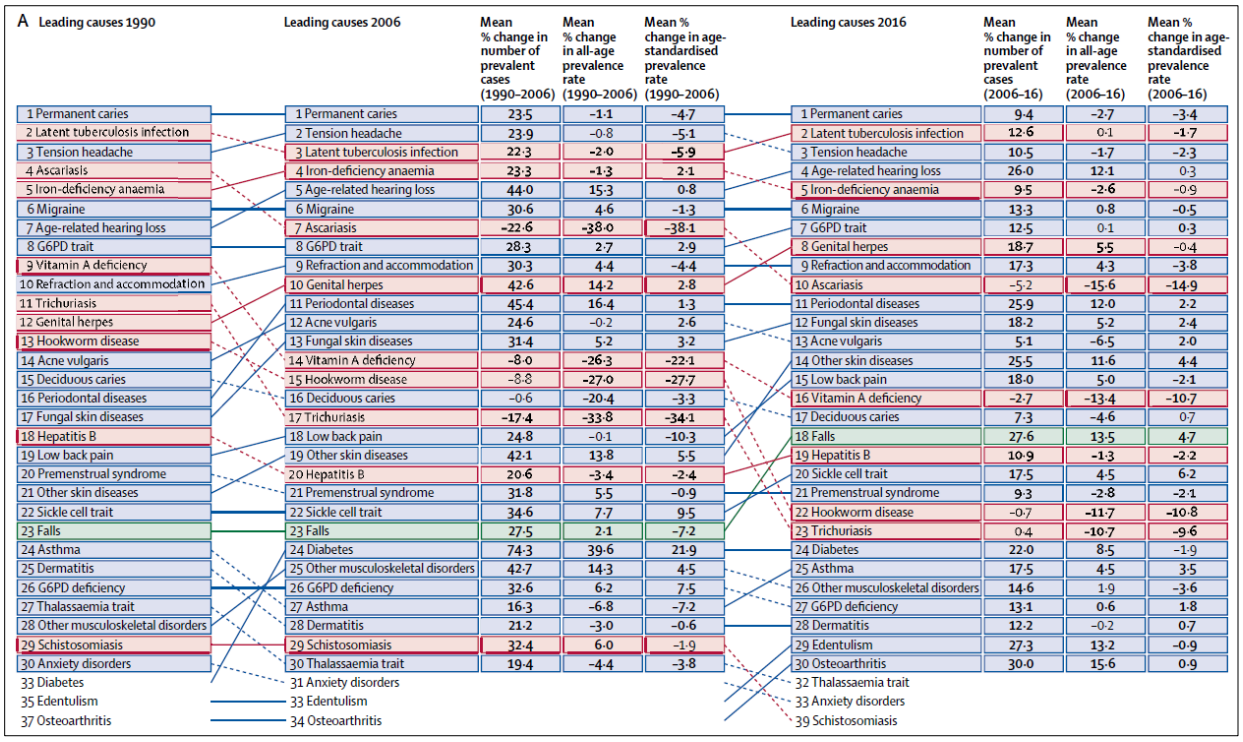

A

Leading causes 1990	Leading causes 2006	Mean % change in number of prevalent cases (1990–2006)	Mean % change in all-age prevalence rate (1990–2006)	Mean % change in age-standardised prevalence rate (1990–2006)	Leading causes 2016	Mean % change in number of prevalent cases (2006–16)	Mean % change in all-age prevalence rate (2006–16)	Mean % change in age-standardised prevalence rate (2006–16)
1 Permanent caries	1 Permanent caries	23·5	−1·1	−4·7	1 Permanent caries	9·4	−2·7	−3·4
2 Latent tuberculosis infection	2 Tension headache	23·9	−0·8	−5·1	2 Latent tuberculosis infection	12·6	0·1	−1·7
3 Tension headache	3 Latent tuberculosis infection	22·3	−2·0	−5·9	3 Tension headache	10·5	−1·7	−2·3
4 Ascariasis	4 Iron-deficiency anaemia	23·3	−1·3	2·1	4 Age-related hearing loss	26·0	12·1	0·3
5 Iron-deficiency anaemia	5 Age-related hearing loss	44·0	15·3	0·8	5 Iron-deficiency anaemia	9·5	−2·6	−0·9
6 Migraine	6 Migraine	30·6	4·6	−1·3	6 Migraine	13·3	0·8	−0·5
7 Age-related hearing loss	7 Ascariasis	−22·6	−38·0	−38·1	7 G6PD trait	12·5	0·1	0·3
8 G6PD trait	8 G6PD trait	28·3	2·7	2·9	8 Genital herpes	18·7	5·5	−0·4
9 Vitamin A deficiency	9 Refraction and accommodation	30·3	4·4	−4·4	9 Refraction and accommodation	17·3	4·3	−3·8
10 Refraction and accommodation	10 Genital herpes	42·6	14·2	2·8	10 Ascariasis	−5·2	−15·6	−14·9
11 Trichuriasis	11 Periodontal diseases	45·4	16·4	1·3	11 Periodontal diseases	25·9	12·0	2·2
12 Genital herpes	12 Acne vulgaris	24·6	−0·2	2·6	12 Fungal skin diseases	18·2	5·2	2·4
13 Hookworm disease	13 Fungal skin diseases	31·4	5·2	3·2	13 Acne vulgaris	5·1	−6·5	2·0
14 Acne vulgaris	14 Vitamin A deficiency	−8·0	−26·3	−22·1	14 Other skin diseases	25·5	11·6	4·4
15 Deciduous caries	15 Hookworm disease	−8·8	−27·0	−27·7	15 Low back pain	18·0	5·0	−2·1
16 Periodontal diseases	16 Deciduous caries	−0·6	−20·4	−3·3	16 Vitamin A deficiency	−2·7	−13·4	−10·7
17 Fungal skin diseases	17 Trichuriasis	−17·4	−33·8	−34·1	17 Deciduous caries	7·3	−4·6	0·7
18 Hepatitis B	18 Low back pain	24·8	−0·1	−10·3	18 Falls	27·6	13·5	4·7
19 Low back pain	19 Other skin diseases	42·1	13·8	5·5	19 Hepatitis B	10·9	−1·3	−2·2
20 Premenstrual syndrome	20 Hepatitis B	20·6	−3·4	−2·4	20 Sickle cell trait	17·5	4·5	6·2
21 Other skin diseases	21 Premenstrual syndrome	31·8	5·5	−0·9	21 Premenstrual syndrome	9·3	−2·8	−2·1
22 Sickle cell trait	22 Sickle cell trait	34·6	7·7	9·5	22 Hookworm disease	−0·7	−11·7	−10·8
23 Falls	23 Falls	27·5	2·1	−7·2	23 Trichuriasis	0·4	−10·7	−9·6
24 Asthma	24 Diabetes	74·3	39·6	21·9	24 Diabetes	22·0	8·5	−1·9
25 Dermatitis	25 Other musculoskeletal disorders	42·7	14·3	4·5	25 Asthma	17·5	4·5	3·5
26 G6PD deficiency	26 G6PD deficiency	32·6	6·2	7·5	26 Other musculoskeletal disorders	14·6	1·9	−3·6
27 Thalassaemia trait	27 Asthma	16·3	−6·8	−7·2	27 G6PD deficiency	13·1	0·6	1·8
28 Other musculoskeletal disorders	28 Dermatitis	21·2	−3·0	−0·6	28 Dermatitis	12·2	−0·2	0·7
29 Schistosomiasis	29 Schistosomiasis	32·4	6·0	−1·9	29 Edentulism	27·3	13·2	−0·9
30 Anxiety disorders	30 Thalassaemia trait	19·4	−4·4	−3·8	30 Osteoarthritis	30·0	15·6	0·9
33 Diabetes	31 Anxiety disorders				32 Thalassaemia trait			
35 Edentulism	33 Edentulism				33 Anxiety disorders			
37 Osteoarthritis	34 Osteoarthritis				39 Schistosomiasis			

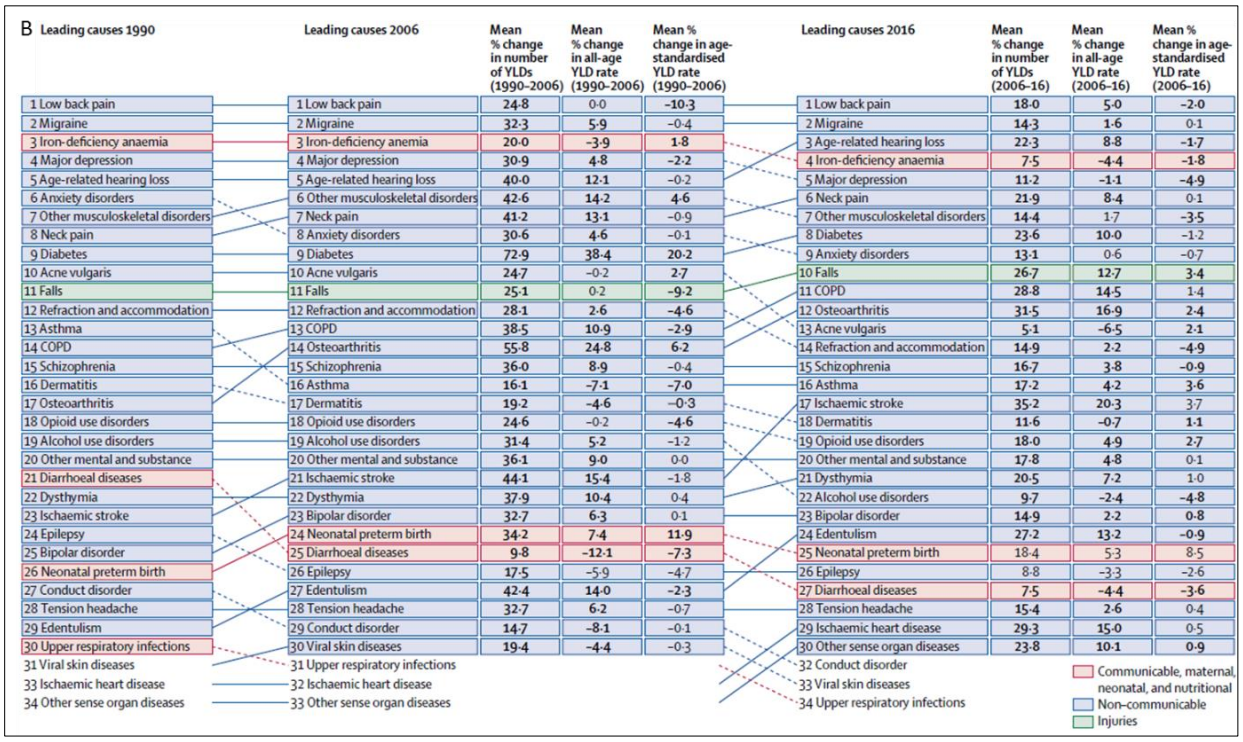

B

Leading causes 1990	Leading causes 2006	Mean % change in number of YLDs (1990–2006)	Mean % change in all-age YLD rate (1990–2006)	Mean % change in age-standardised YLD rate (1990–2006)	Leading causes 2016	Mean % change in number of YLDs (2006–16)	Mean % change in all-age YLD rate (2006–16)	Mean % change in age-standardised YLD rate (2006–16)
1 Low back pain	1 Low back pain	24·8	0·0	−10·3	1 Low back pain	18·0	5·0	−2·0
2 Migraine	2 Migraine	32·3	5·9	−0·4	2 Migraine	14·3	1·6	0·1
3 Iron-deficiency anaemia	3 Iron-deficiency anemia	20·0	−3·9	1·8	3 Age-related hearing loss	22·3	8·8	−1·7
4 Major depression	4 Major depression	30·9	4·8	−2·2	4 Iron-deficiency anaemia	7·5	−4·4	−1·8
5 Age-related hearing loss	5 Age-related hearing loss	40·0	12·1	−0·2	5 Major depression	11·2	−1·1	−4·9
6 Anxiety disorders	6 Other musculoskeletal disorders	42·6	14·2	4·6	6 Neck pain	21·9	8·4	0·1
7 Other musculoskeletal disorders	7 Neck pain	41·2	13·1	−0·9	7 Other musculoskeletal disorders	14·4	1·7	−3·5
8 Neck pain	8 Anxiety disorders	30·6	4·6	−0·1	8 Diabetes	23·6	10·0	−1·2
9 Diabetes	9 Diabetes	72·9	38·4	20·2	9 Anxiety disorders	13·1	0·6	−0·7
10 Acne vulgaris	10 Acne vulgaris	24·7	−0·2	2·7	10 Falls	26·7	12·7	3·4
11 Falls	11 Falls	25·1	0·2	−9·2	11 COPD	28·8	14·5	1·4
12 Refraction and accommodation	12 Refraction and accommodation	28·1	2·6	−4·6	12 Osteoarthritis	31·5	16·9	2·4
13 Asthma	13 COPD	38·5	10·9	−2·9	13 Acne vulgaris	5·1	−6·5	2·1
14 COPD	14 Osteoarthritis	55·8	24·8	6·2	14 Refraction and accommodation	14·9	2·2	−4·9
15 Schizophrenia	15 Schizophrenia	36·0	8·9	−0·4	15 Schizophrenia	16·7	3·8	−0·9
16 Dermatitis	16 Asthma	16·1	−7·1	−7·0	16 Asthma	17·2	4·2	3·6
17 Osteoarthritis	17 Dermatitis	19·2	−4·6	−0·3	17 Ischaemic stroke	35·2	20·3	3·7
18 Opioid use disorders	18 Opioid use disorders	24·6	−0·2	−4·6	18 Dermatitis	11·6	−0·7	1·1
19 Alcohol use disorders	19 Alcohol use disorders	31·4	5·2	−1·2	19 Opioid use disorders	18·0	4·9	2·7
20 Other mental and substance	20 Other mental and substance	36·1	9·0	0·0	20 Other mental and substance	17·8	4·8	0·1
21 Diarrhoeal diseases	21 Ischaemic stroke	44·1	15·4	−1·8	21 Dysthymia	20·5	7·2	1·0
22 Dysthymia	22 Dysthymia	37·9	10·4	0·4	22 Alcohol use disorders	9·7	−2·4	−4·8
23 Ischaemic stroke	23 Bipolar disorder	32·7	6·3	0·1	23 Bipolar disorder	14·9	2·2	0·8
24 Epilepsy	24 Neonatal preterm birth	34·2	7·4	11·9	24 Edentulism	27·2	13·2	−0·9
25 Bipolar disorder	25 Diarrhoeal diseases	9·8	−12·1	−7·3	25 Neonatal preterm birth	18·4	5·3	8·5
26 Neonatal preterm birth	26 Epilepsy	17·5	−5·9	−4·7	26 Epilepsy	8·8	−3·3	−2·6
27 Conduct disorder	27 Edentulism	42·4	14·0	−2·3	27 Diarrhoeal diseases	7·5	−4·4	−3·6
28 Tension headache	28 Tension headache	32·7	6·2	−0·7	28 Tension headache	15·4	2·6	0·4
29 Edentulism	29 Conduct disorder	14·7	−8·1	−0·1	29 Ischaemic heart disease	29·3	15·0	0·5
30 Upper respiratory infections	30 Viral skin diseases	19·4	−4·4	−0·3	30 Other sense organ diseases	23·8	10·1	0·9
31 Viral skin diseases	31 Upper respiratory infections				32 Conduct disorder			
33 Ischaemic heart disease	32 Ischaemic heart disease				33 Viral skin diseases			
34 Other sense organ diseases	33 Other sense organ diseases				34 Upper respiratory infections			

Communicable, maternal, neonatal, and nutritional
Non-communicable
Injuries

According to the 3rd edition of the *International Classification of Headache Disorders* (ICHD-3), migraine can be classified into six subtypes: migraine without aura, migraine with aura, chronic migraine, complications of migraine, probable migraine, episodic syndromes that may be associated with migraine (Table 2). There are two major subtypes which are with or without aura. Migraine without aura (MO) accounting for 70% comprises the symptoms of recurrent headache, lasting 4-72 hours, unilateral location, pulsating quality, nausea, photophobia, phonophobia, etc. Migraine with aura (MA) accounting for 20% is described as recurrent attacks, lasting minutes, fully reversible visual unilaterally, followed by headache usually, etc. According to the frequency of migraine attacks, it is also categorized as episodic or chronic migraine. Chronic migraine is decided if a headache (without medication overuse) occurs on 15 or more days per month for more than 3 months, which at least 8 days per month have the features of migraine headache (Olesen, 2018).

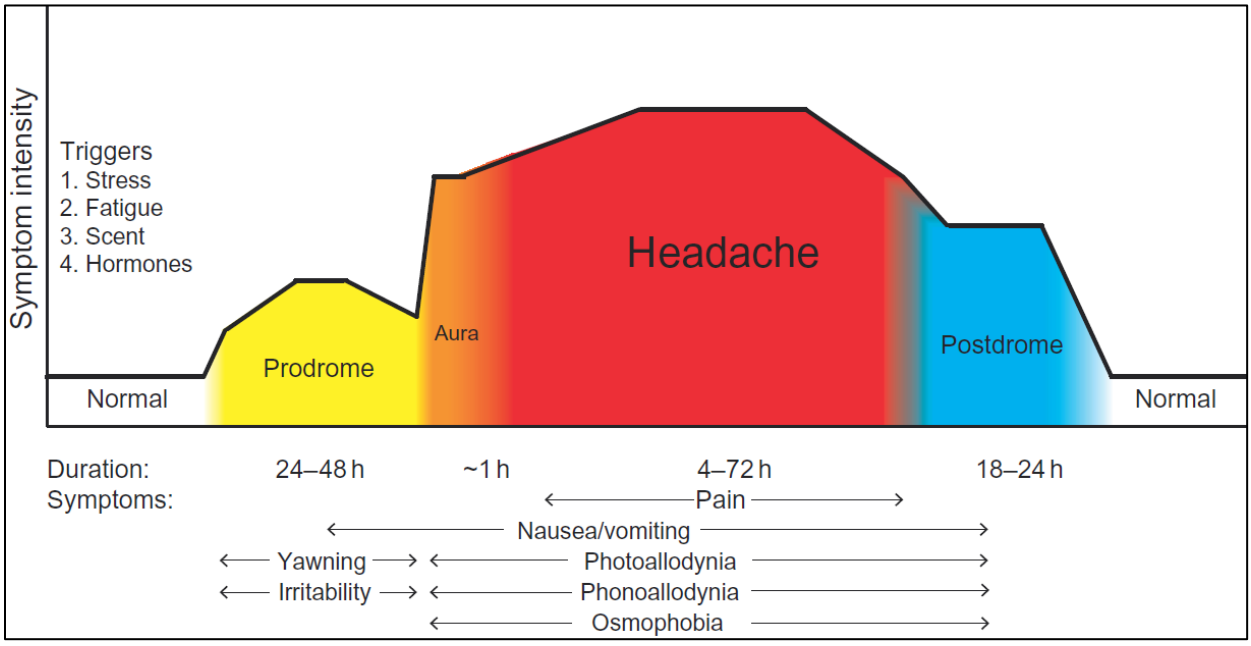

Figure 1. Four typical phases of migraine with various symptoms (Burgos-Vega et al., 2015).

Table 2. Classification of migraine (Olesen, 2018)

Migraine	Migraine without aura			
	Migraine with aura	Migraine with typical aura	Typical aura with headache	
			Typical aura without headache	
		Migraine with brainstem aura		
		Hemiplegic migraine	Familial hemiplegic migraine (FHM)	Familial hemiplegic migraine type 1 (FHM1)
				Familial hemiplegic migraine type 2 (FHM2)
				Familial hemiplegic migraine type 3 (FHM3)
				Familial hemiplegic migraine, other loci
			Sporadic hemiplegic migraine (SHM)	
		Retinal migraine		
	Chronic migraine			
	Complications of migraine	Status migrainosus		
		Persistent aura without infarction		
		Migrainous infarction		
		Migraine aura-triggered seizure		
	Probable migraine	Probable migraine without aura		
		Probable migraine with aura		
	Episodic syndromes that may be associated with migraine	Recurrent gastrointestinal disturbance	Cyclical vomiting syndrome	
			Abdominal migraine	
		Benign paroxysmal vertigo		
		Benign paroxysmal torticollis		

1.2 Pathophysiology of migraine

Migraine is considered a disorder of the sensory network. Although the complete pathophysiology of migraine has not been clear, the trigeminovascular system consisting of neurons in a trigeminal ganglion that innervates the cerebral vasculature (or the network of nerves associated with cerebral blood vessels) currently accounts for the major explanation of migraine pathophysiology supported by growing evidence (Borsook et al., 2015).

1.2.1 General migraine networks

There are three orders of neurons in the trigeminovascular system. The first-order neurons located in the trigeminal ganglion receive input information from dural blood vessels innervated by trigeminal afferents densely. The information is then transmitted to the second-order neurons in the spinal trigeminal nucleus, and the third-order neurons in the thalamic nuclei finally (Fig. 2) (Landy et al., 2004; Bernstein and Burstein, 2012).

In detail, the trigeminal ganglion receives input information from dural blood vessels innervated by trigeminal afferents densely. The input is then transmitted to the spinal trigeminal nucleus (SpV). The neurons in the trigeminal nucleus caudalis (TNC) project to the ventral posteromedial (VPM), posterior (Po), and lateral posterior (LP) nuclei of the thalamus. VPM neurons project primarily to the primary and secondary somatosensory cortices (S1 and S2), and insular, while Po neurons project to the insula, somatosensory, auditory, visual cortices, etc. LP neurons project to the motor, somatosensory, and visual cortices. The neurons in TNC also project to the nucleus tractus solitarius (NTS) and parabrachial nucleus (PB), and then information is transmitted to the hypothalamus, amygdala, prefrontal cortex, anterior cingulate cortex, etc. which are involved in the affective response. The neurons in TNC also project to the periaqueductal gray (PAG) and superior salivatory nucleus (SSN) (Noseda and Burstein, 2013; Pietrobon and Moskowitz, 2013). Single-Unit action potential recording demonstrates increased activities of the trigeminal ganglion, spinal trigeminal nucleus, and thalamic nuclei after different orders of neurons sensitization (A.M. Strassman, S.A. Raymond, 1996; Burstein et al., 2000, 2010).

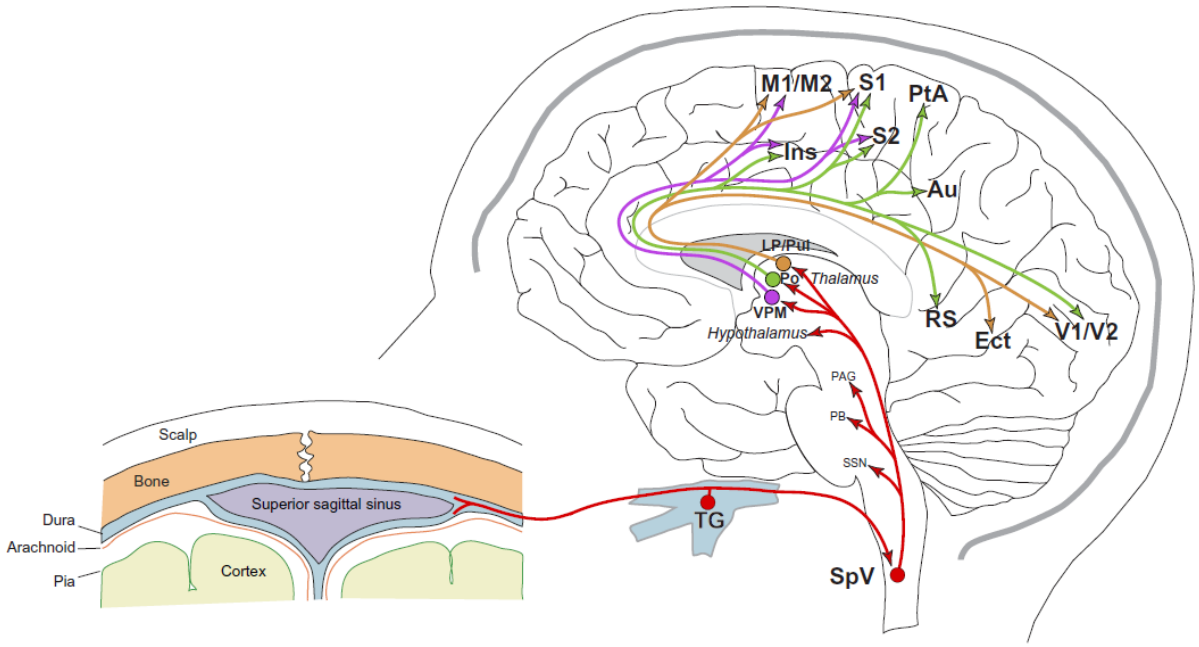

Figure 2. The ascending pathways of the trigeminovascular system (Noseda and Burstein, 2013).

1.2.2 Cortical spreading depression (CSD)

Cortical spreading depression (CSD) is a slowly propagating wave of depolarization of neuronal and glial cells across the cortex with the involvement of the cerebellum, basal ganglia, thalamus, and hippocampus, which is recognized to be associated with migraine aura. The activation of nociceptors in meningeal blood vessels by CSD results in the phase of headache with nausea, throbbing pain, phonophobia, photophobia, etc. H+, K+, and other agents are released to the extracellular space when CSD occurs, which gives rise to the depolarization of trigeminal nerve endings. Then trigeminal nucleus (TGN) and trigeminal ganglion (TGG) is activated. The activation of the axon of neurons in the TGG leads to the release of inflammatory peptides in meninges and innervating blood vessels, which induces meningeal inflammation. After the TGN activation, signals are transmitted from the superior salivatory nucleus (SSN) to the sphenopalatine

ganglion (SPG), which releases vasoactive agents at the terminals causing vasodilation of meningeal blood vessels (Fig. 3) (Leao, 1944; Iadecola, 2002).

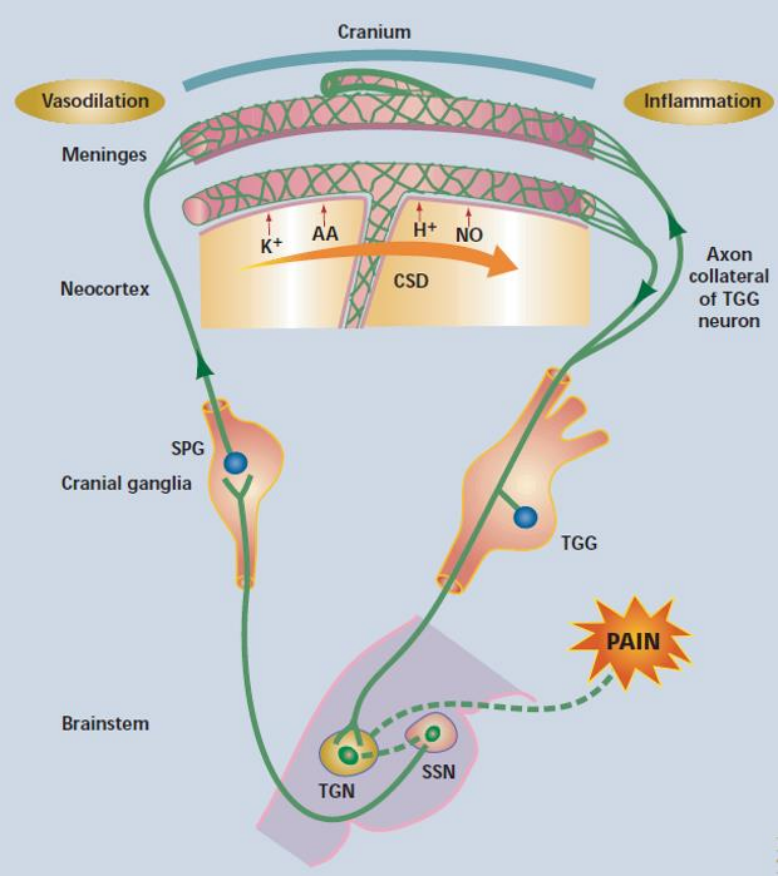

Figure 3. Cortical spreading depression (CSD) and migraine (Iadecola, 2002).

1.2.3 Photophobia and migraine

The underlying mechanism of photophobia (hypersensitivity to visual stimuli) might be that the recurrent activation of the trigeminovascular pathway disturbs the normal function of the visual cortex, as shown in Figure 4. The phenomenon of photophobia is hypothesized to be associated with the findings that light-sensitive neurons in the lateral posterior nucleus (LP) and

pulvinar (Pul) thalamus receive convergent input information from intrinsically photosensitive retinal ganglion cells (ipRGCs), retinal ganglion cells (RGCs), and trigeminal afferents in the dura, and project to primary and secondary visual cortices (V1 and V2) (Noseda et al., 2010, 2011; Noseda and Burstein, 2011).

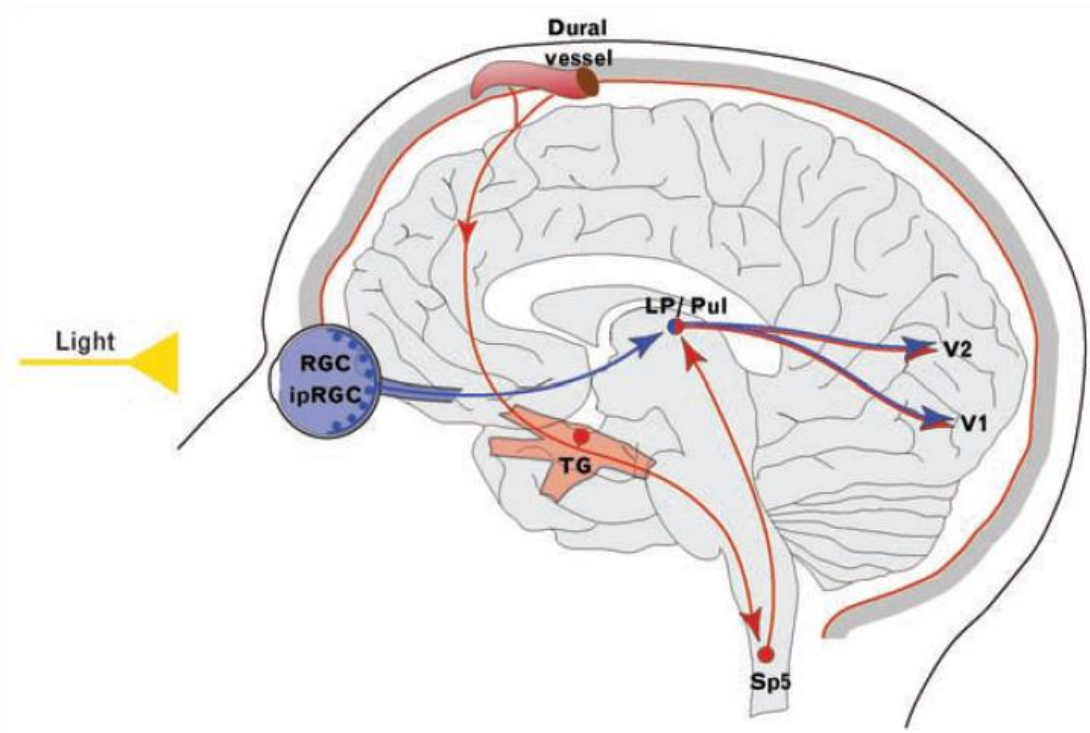

Figure 4. The probable mechanism of photophobia during migraine via the convergence of trigeminovascular pathways and visual pathways (Noseda and Burstein, 2011).

1.3 Local field potential (LFP)

Local field potential (LFP) reflects action potentials and transmembrane currents in a small neuronal volume ranging from several hundred micrometers to a few millimeters (radius) located around the vicinity of the electrode (Buzsáki et al., 2012; Bozer et al., 2017). LFP demonstrates the low-frequency activity of neurons with a frequency of less than 500 Hz (typically <100 Hz)

(Lindén et al., 2011). When analyzing LFP, we separate it into different frequency bands: delta (0.1-3 Hz), theta (3-7 Hz), alpha (7-12 Hz), beta (12-30 Hz), and gamma (30-100 Hz) (H. et al., 2016). In our previous study, we succeeded in recording the different LFP changes under various noxious stimuli: electrical, mechanical (pinch), and chemical (carrageenan) (Harris-Bozer and Peng, 2016; Li et al., 2016). In addition, we deciphered multi-region LFP signatures and brain coherence changes in response to the formalin-induced stimulus (Wang and Peng, 2022). Brain coherence, an emerging approach to measure the similarity (synchronization) between different signals in targeted frequency content, has been commonly harnessed to examine brain functional connectivity (Bowyer, 2016).

1.4 Nitroglycerin induced migraine model

Animal models are recognized to play a crucial role in deciphering the underlying mechanisms of migraine headaches and novel discoveries of treatments. Currently, many manipulations (stimulations) including electrical, chemical, physical, and genetic are conducted to create animal models mimicking the disorders occurring in humans clinically (Chen et al., 2016; Harriott et al., 2019; Tardiolo et al., 2019).

Nitric oxide (NO) has been found to cause vasodilatation and activation of the trigeminovascular system. Nitroglycerin (NTG) as a NO donor is used to develop a migraine animal model commonly through sensitization of trigeminal endings and vasodilation of cranial blood vessels, which can display migraine-like symptoms, such as hyperalgesia, allodynia, and photophobia. NTG-induced migraine is widely applied so far both in animal and human models (Ashina et al., 2000; Lambert et al., 2000; Iversen, 2001; Thomsen and Olesen, 2001; Demartini

et al., 2019). In this study, we recorded LFP changes from the migraine animal model created by injection (i.p.) of NTG with a single dose of 10 mg/kg.

1.5 Specific aims

The ***purpose*** of this proposed study was to determine differential LFP signatures and brain coherence alternations from multiple brain regions associated with migraine-relevant pain networks, which enabled to remove barriers to understanding the migraine pathophysiology and facilitated the treatment study clinically. We conducted the migraine animal model which was induced by intraperitoneal (i.p.) injection of nitroglycerin (NTG), a well-established migraine model. As an initial part of this study, LFP signals were firstly recorded from anesthetized animals, followed by freely moving animals. Additionally, behavior measurements were implemented in freely moving animals. The ***hypothesis*** was that various brain areas, which are involved in different orders of neurons in the trigeminovascular system and pain processing, could show different response patterns/signatures with brain coherence changes to migraine attacks.

In this study, LFPs from the anterior cingulate cortex (ACC), the posterior nucleus of the thalamus (Po), the trigeminal ganglion (TG), and the primary visual cortex (V1M) were simultaneously recorded. The ***rationale*** was that the trigeminal ganglion, thalamus, and visual cortex are involved in the pathophysiology of migraine attacks, and the ACC as one part of the limbic system is related to emotional processing. There were three specific aims:

***Aim 1*:** Determine LFP signatures containing ACC, Po, TG, and V1M when migraine occurs from anesthetized animals.

Methods: Recorded simultaneous multi-region LFPs in response to migraine attacks in anesthetized animals; Compared the response differences among these brain regions [For example, whether the ACC demonstrated a more intense reaction to migraine headache than other regions with the method of mixed analysis of variance (mixed ANOVA)]; Tested the relationship of LFP changes at various bands in different regions using a Pearson's *r* correlation.

The **hypothesis** was that different LFP signatures would be seen among these brain regions in response to the migraine attacks in anesthetized animals.

***Aim 2*:** Determine the multi-region LFP signatures in response to migraine attacks from freely moving animals and examine behavioral responses.

Methods: Recorded simultaneous multi-region LFPs in response to migraine attacks in freely-moving animals; Contrasted the response differences among these brain regions; Tested the relationship of LFP changes at various bands in different regions using a Pearson's *r* correlation; Measured the behavioral responses (light-aversive behavior test).

We **hypothesized** various brain regions would demonstrate different LFP patterns in response to migraine attacks in freely moving animals, which were different from the anesthetized ones.

***Aim 3*:** Examine brain coherence alternations among paired brain sites.

Methods: Tested brain coherence alternations among paired brain regions using Spike2 with the following formula:

$$\mathrm{COH}_{mn}(f) = \frac{|\mathrm{P}_{mn}(f)|^2}{\mathrm{P}_{mm}(f)\,\mathrm{P}_{nn}(f)}$$

which mainly examined the similarity between different signals in targeted frequency content (frequency-domain).

The **hypothesis** was that brain coherence altered (synchronization or desynchronization) with the input of migraine attacks.

Chapter 2 Materials and Methods

2.1 Animals

Forty-four male Sprague Dawley rats weighed 300-400g were used in this study. The rats were housed in Animal Care Facility with a 12 h light/dark cycle. Water and food pellets were available *ad libitum*. All procedures were approved by the Institutional Animal Care and Use Committee (IACUC) of the University of Texas at Arlington. A heating pad was used to keep the rats' temperature during the surgery. Figure 5 demonstrated the experimental design for wireless multi-region LFP recordings.

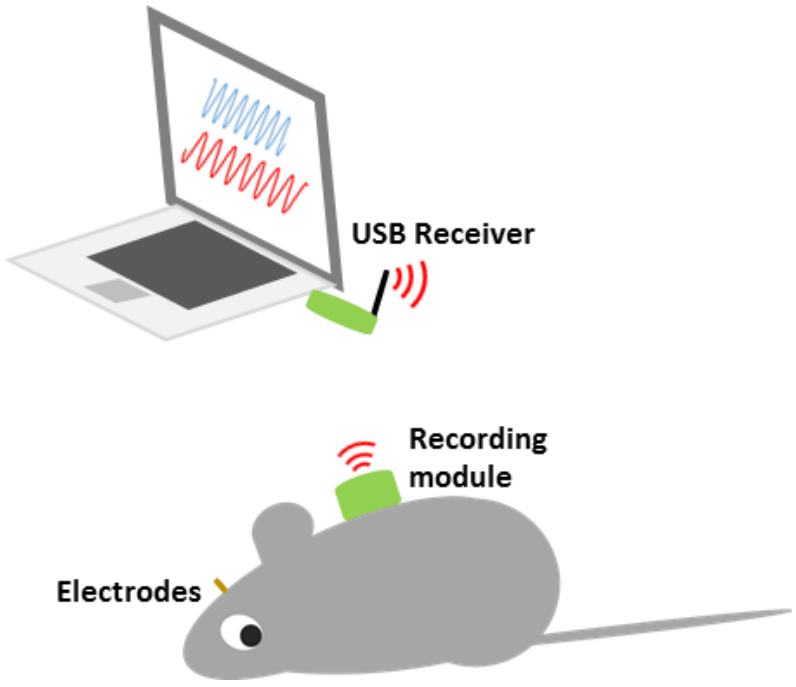

Figure 5. Schematic diagram of multi-region local field potential (LFP) recordings by the wireless closed-loop neural recording control system.

2.2 Drug administration

NTG was in a stock solution of 5 mg/mL in alcohol and propylene glycol (American Regent, Inc.). It was freshly diluted in 0.9% saline to a dose of 10 mg/kg (Tang et al., 2018). The vehicle control solution contained the same volume of alcohol and propylene glycol in 0.9% saline. Intraperitoneal (i.p.) injection of a single dose (10 mg/kg) of NTG was given to rats under brief isoflurane anesthesia (induction: 5%; maintenance: 1.5-3%). For the vehicle control group, rats received the i.p. injection of vehicle solution.

2.3 Electrode implantation

The rat was firstly placed in the induction chamber with 5% isoflurane inhaled anesthesia, and then transferred to a stereotaxic frame under 1.5-3% isoflurane for maintenance. In accordance with the brain atlas (6^{th} edition) by Paxinos and Watson, four bipolar stainless steel electrodes (diameter of 0.01 inch, Plastics One, Inc. 81MS3031SPCE) were separately implanted into four regions (Fig. 6A): the right ACC at 0 mm posterior to bregma, 0.70 mm lateral to the right, 3.20 mm deep; the right Po at 3.72 mm posterior to bregma, 2.20 mm lateral to the right, 5.60 mm deep; the left TG at 4.30 mm posterior to bregma, 3.40 mm lateral to the left, 10.00 mm deep; and the right V1M at 7.44 mm posterior to bregma, 3.40 mm lateral to the right, 1.60 mm deep. One screw was placed under the skull with a wire serving as ground and reference. Dental cement and two anchor screws were finally harnessed to fix electrodes on the skull (Fig. 6B). For the animals in the anesthesia group, the recording was initialized immediately after the electrode fixation. With regard to the animals in the freely moving group, subcutaneous (s.c.) buprenorphine SR (1mg/kg) was injected. After one week of recovering from the surgery, LFP was recorded with NTG/vehicle solution injection.

2.4 LFP recordings

The four electrodes and ground/reference wire were connected to the wireless module (SiChuan NeoSource BioTektronics Limited) to acquire the brain signals from the targeted areas of the brain. A USB dongle (receiver) inserted into a computer transmitted the signal data from the recording module to the software wirelessly (Fig. 5). For the anesthesia group, after connecting the recording module, the LFP recording was carried out immediately. The LFP signals were firstly recorded under 1.5-3% isoflurane anesthesia for 30 minutes as the baseline. NTG was then given (i.p.) to rats after baseline recordings. The recording was continued for up to four hours under isoflurane finally. For the vehicle control group, vehicle solution was injected with the same procedures (see flowchart for the anesthesia group). For the freely moving group, after the module setup under isoflurane anesthesia, rats were returned to the cage and the LFP signals were recorded for 30 minutes as the baseline. After NTG or vehicle solution injection (i.p.), the recording lasted for four hours. In the meanwhile, we measured behavior responses (light aversion) by following procedures (see flowchart for the freely moving group). After finishing the recording and behavior test (only existing in the freely moving group), rats were euthanized with CO_2. In order to verify the electrode placement, a histology analysis was carried out. Specifically, the brain was immediately extracted and stored in 10% formalin for fixation (at least 24 h), and then in 30% sucrose for dehydration (at least 24 h). The sliced sections of the brain by a microtome with 80 μm thickness were stained with thionin and observed using a digital microscope to confirm the placement of the electrode tip finally (Fig. 6C).

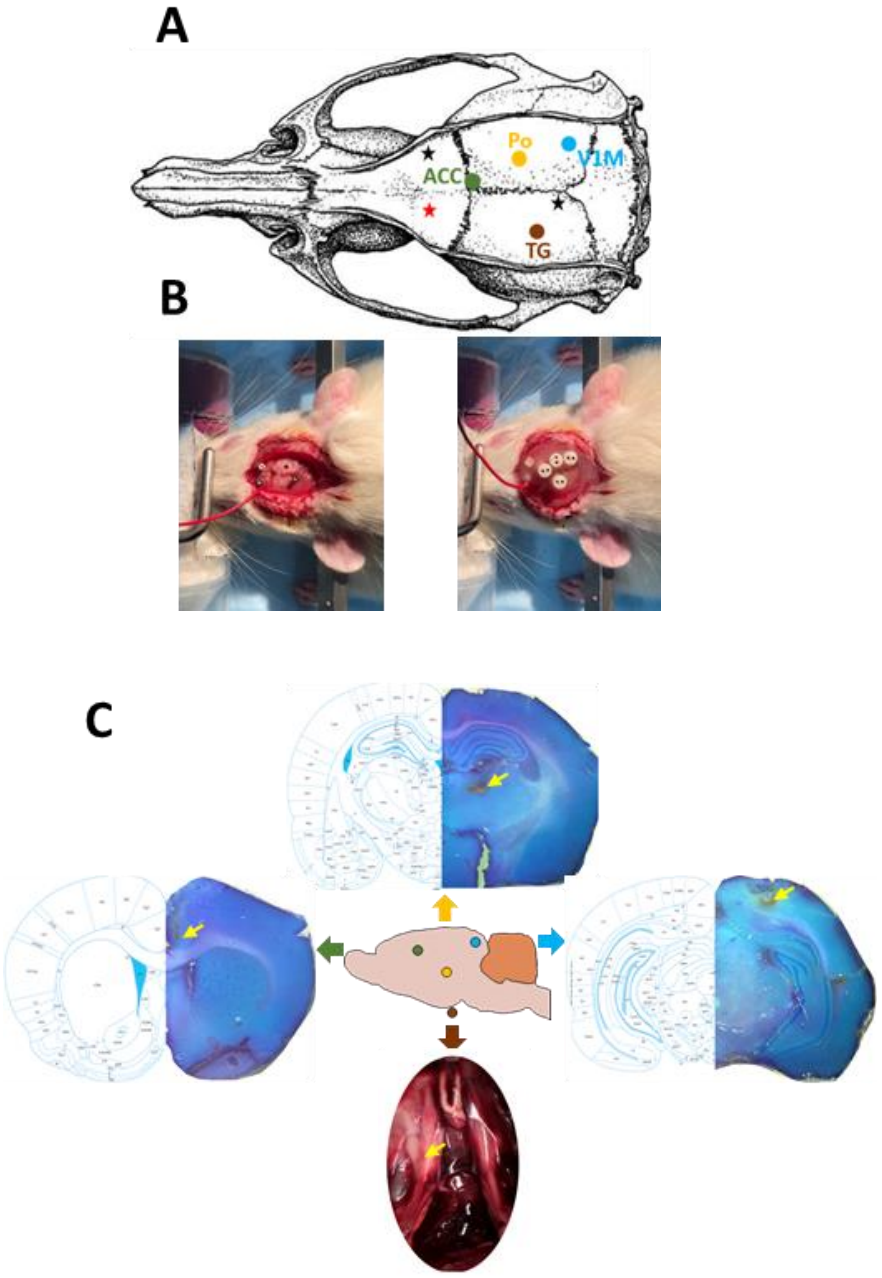

Figure 6. Stereotaxic coordinates.

(**A**) Stereotaxic coordinates of the anterior cingulate cortex (ACC, green), the posterior nucleus of the thalamus (Po, yellow), the trigeminal ganglion (TG, gray), and the primary visual cortex (V1M, blue). (**B**) Surgical craniotomies (four holes for electrodes, two screws for anchors, and one with a red wire for grounding/reference). Electrodes were finally fixed with dental cement. (**C**)

Schematic representation of the placement of electrodes in the ACC, Po, TG, and V1M. The yellow arrows point to the electrode tip location.

The flowchart for the anesthesia group:

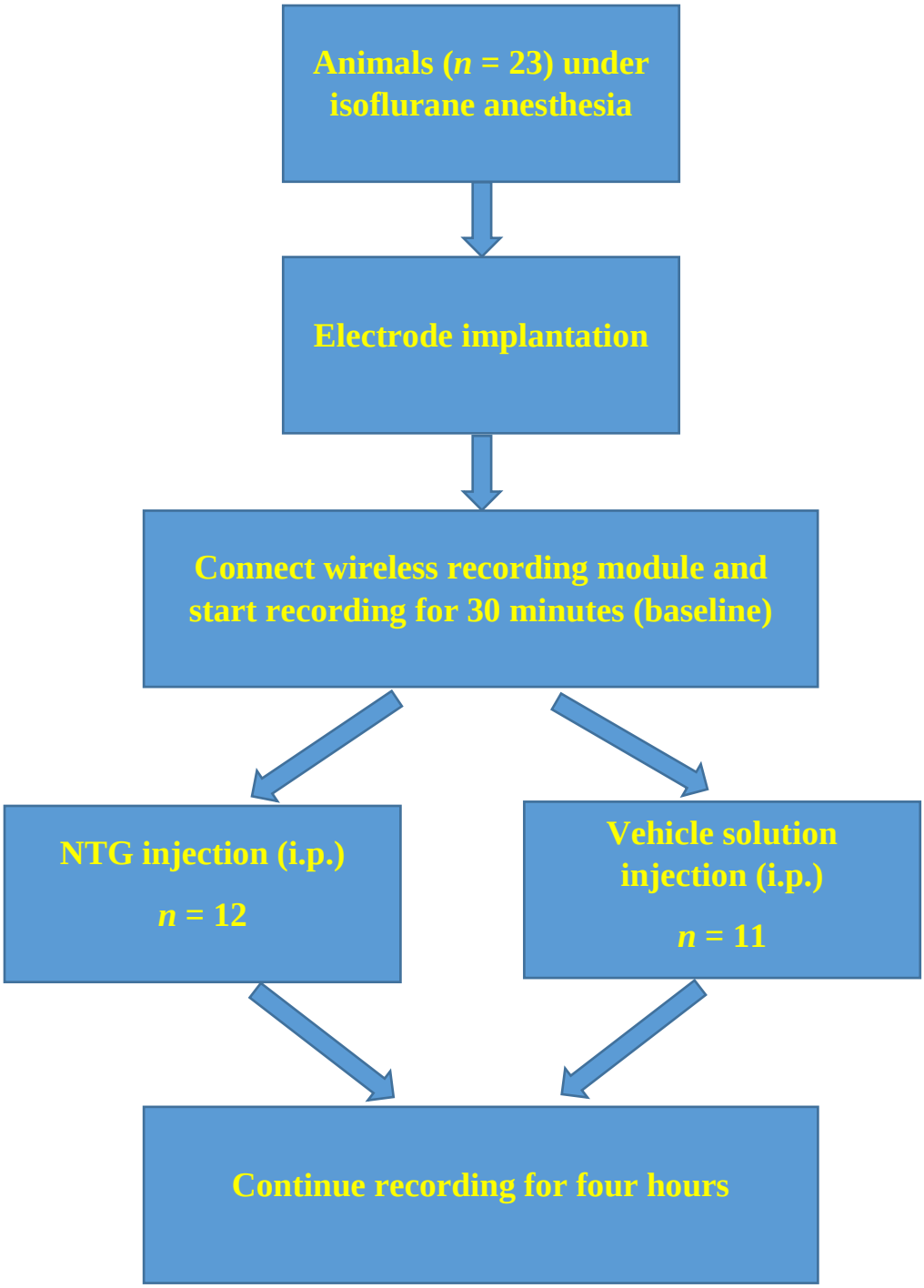

The flowchart for the freely moving group:

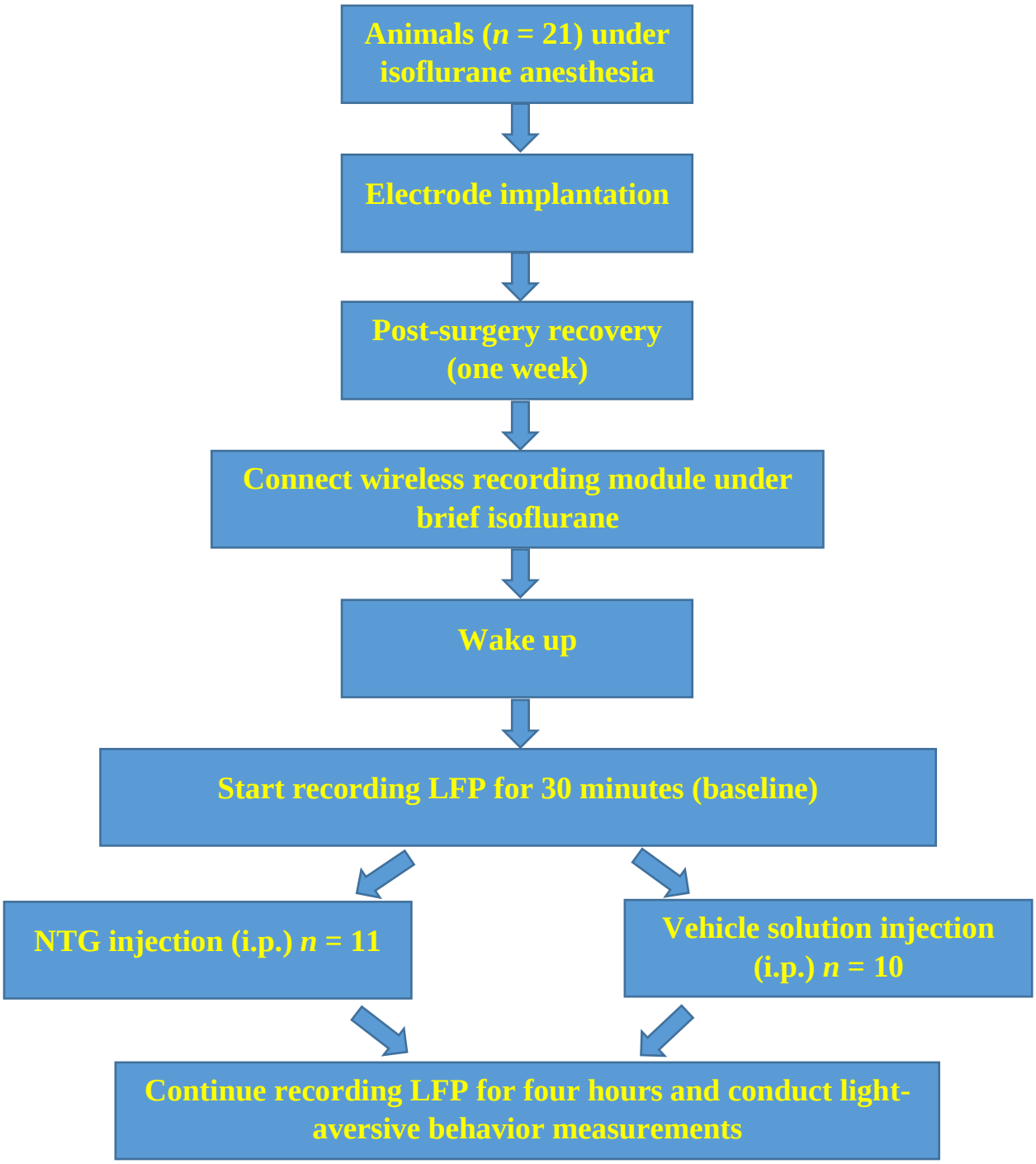

2.5 Light-aversive behavior test

Rats exclusively in the freely moving group underwent a light-aversive behavior test following administration of NTG/vehicle solution, accompanied by LFP recordings. A custom-made light-dark box (60 cm length by 30 cm width by 30 cm height) with two equally-sized compartments was exerted as shown in the following figure. White papers were utilized to cover the side of the light compartment with a LED light (1000 Lux) on the top. Conversely, the dark compartment was shielded with black papers and a dark lid. Rats were allowed to move freely to the light or dark compartment through a gate (10 cm by 10 cm). One test lasted for 30 minutes (time bin = 30 minutes) under the recording of a camera, the percentage of time in the dark compartment was calculated finally. Before injection, the time spent in the dark compartment was counted as the baseline of light-aversive behavior (Farkas et al., 2016; Tang et al., 2018).

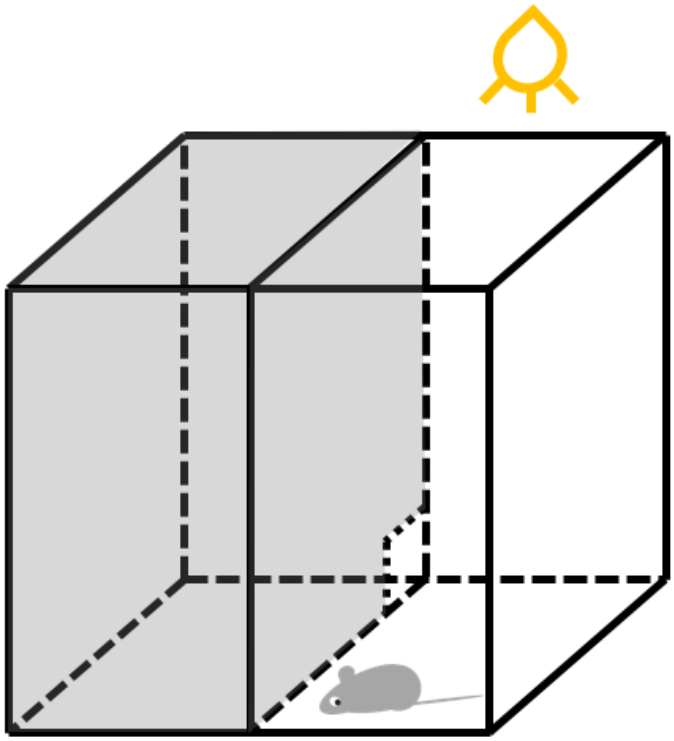

2.6 Data analysis

The software of Spike2 and MATLAB 2017a was applied to process the raw data. The representative raw trace (waveform) and power spectrum of LFP recorded from the module (Figs. 7A-H, 8A-H) at a sampling frequency of 10 kHz were processed by power spectrum analysis in Spike2 (CED, UK). The LFP power or intensity was calculated by fast Fourier transform (FFT) in MATLAB with a time window of 10 seconds and then divided into five frequency bands: delta (0.1-3 Hz), theta (3-7 Hz), alpha (7-12 Hz), beta (12-30 Hz), and gamma (30-100 Hz). In order to compare the changes in LFP between the NTG group and vehicle control group, the data were normalized by the average power of the first 30 minutes. Additionally, the heatmap was generated with the normalized power spectrum in a time window of 5 minutes using customized code in MATLAB.

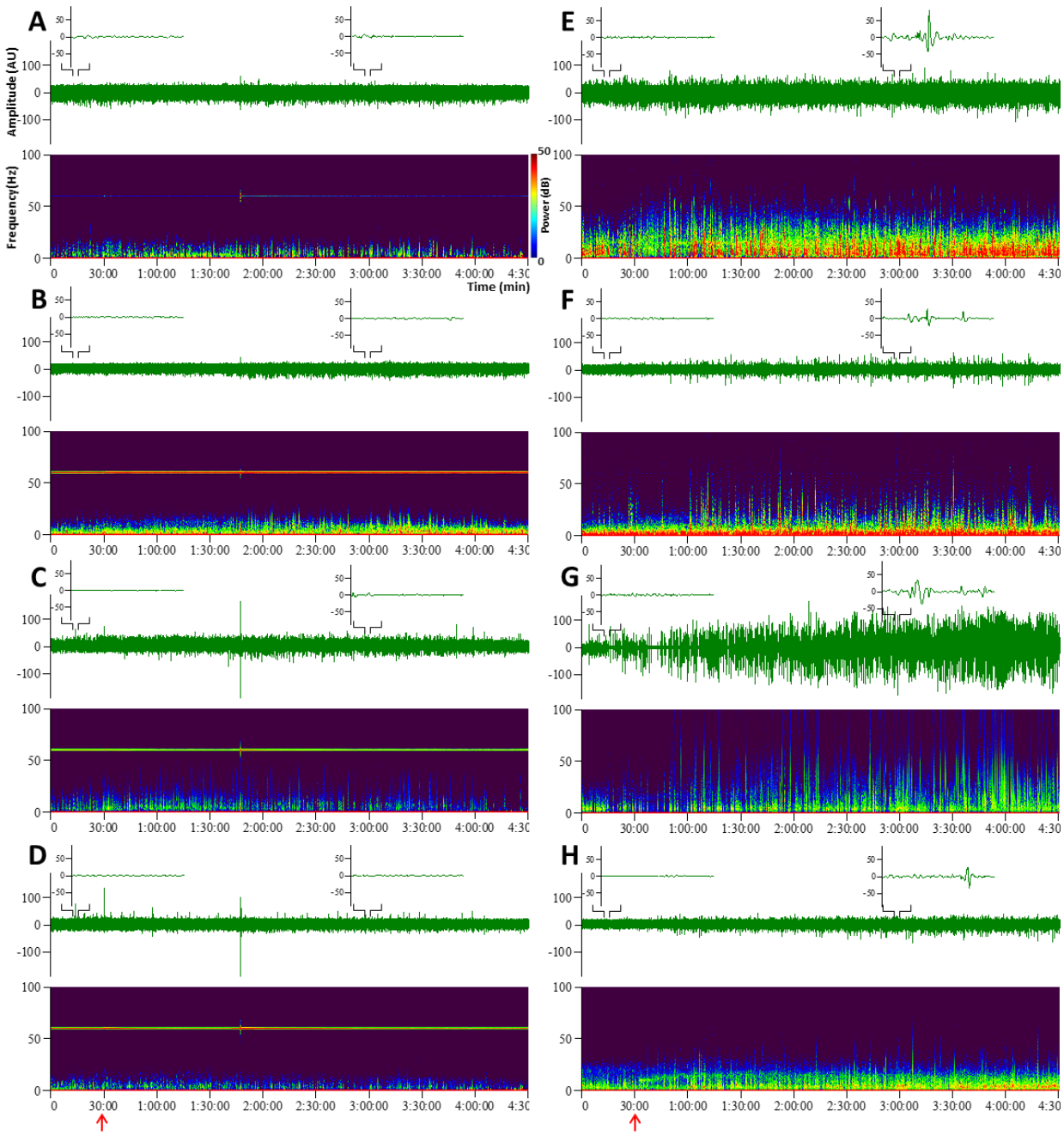

Figure 7. Representative LFP activities from anesthetized animals.

Representative LFP activities after vehicle injection in (**A**) ACC, (**B**) Po, (**C**) TG, and (**D**) V1M were recorded from anesthetized animals. LFP activities after NTG injection in (**E**) ACC, (**F**) Po, (**G**) TG, and (**H**) V1M. In each figure, raw trace (top) and power spectrum (bottom) were plotted by Spike2. For raw trace, the x-axis is the time in minutes, and the y-axis is the LFP amplitude (AU). For the power spectrum, the x-axis is the time in minutes, and the y-axis is the frequency

(Hz). The color bar represents power intensity. The red arrows denote the timepoint of NTG/vehicle solution injection. AU, arbitrary unit.

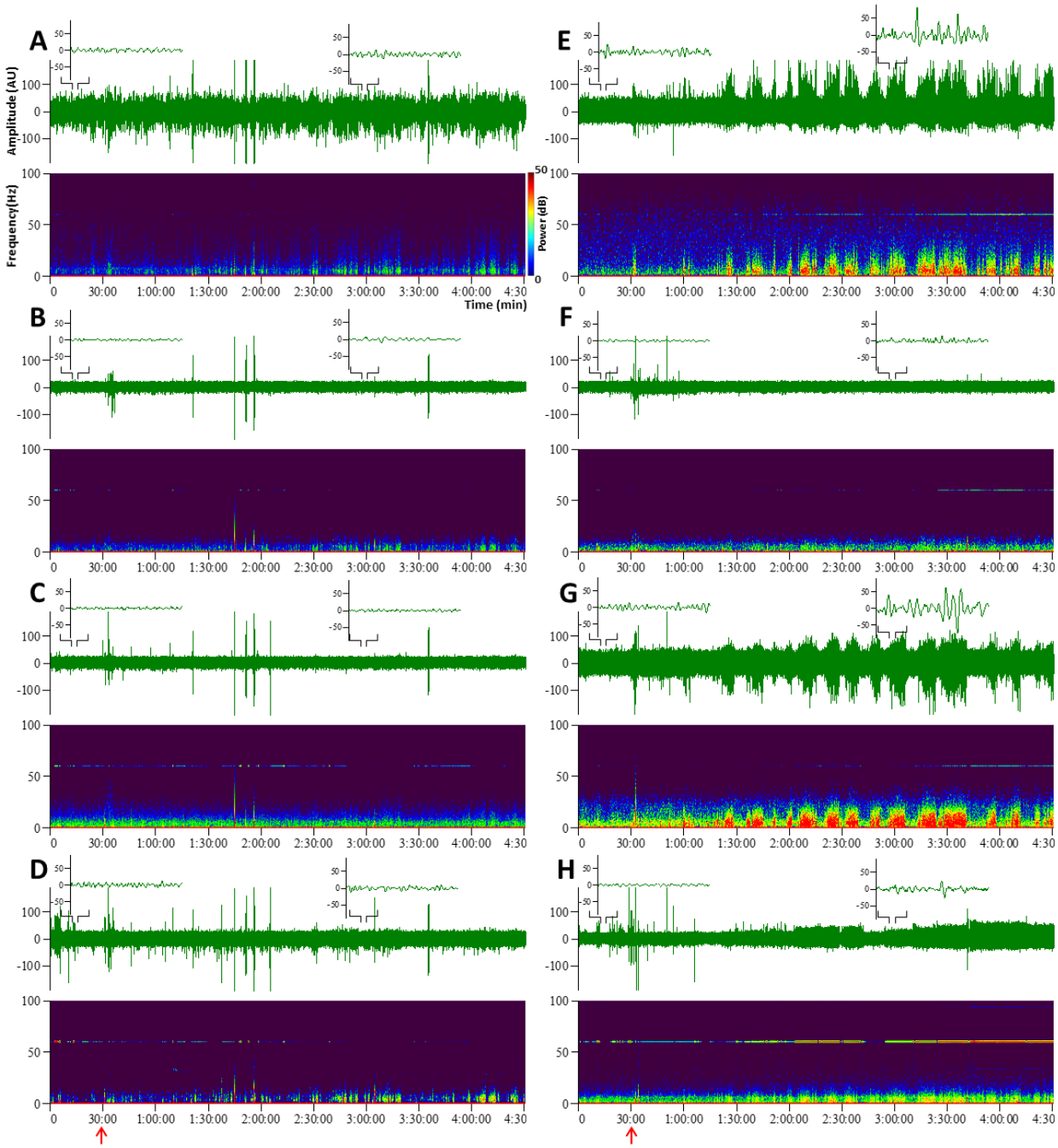

Figure 8. Representative LFP activities from freely moving animals.

Representative LFP activities after vehicle injection in (**A**) ACC, (**B**) Po, (**C**) TG, and (**D**) V1M were recorded from freely moving animals. LFP activities after NTG injection in (**E**) ACC, (**F**) Po, (**G**) TG, and (**H**) V1M. In each figure, raw trace (top) and power spectrum (bottom) were plotted by Spike2. For raw trace, the x-axis is the time in minutes, and the y-axis is the LFP amplitude (AU). For the power spectrum, the x-axis is the time in minutes, and the y-axis is the frequency (Hz). The color bar represents power intensity. The red arrows represent the timepoint of NTG/vehicle solution injection. AU, arbitrary unit.

2.7 Brain coherence

The brain coherence (COH) between any paired brain sites was calculated in Spike2 with the following formula (Sakkalis, 2011):

$$\mathrm{COH}_{mn}(f) = \frac{|\mathrm{P}_{mn}(f)|^2}{\mathrm{P}_{mm}(f)\ \mathrm{P}_{nn}(f)}$$

where the power spectrum densities of the signal (e.g., signal *m* and *n* here) are denoted by the elements $P_{mm}(f)$, $P_{nn}(f)$ in the spectral matrix **P**. The magnitude-squared spectrum coherence, $COH_{mn}(f)$, at frequency *f* is a function of cross-power spectrum densities $P_{mn}(f)$ and power spectrum density of each signal $P_{mm}(f)$, $P_{nn}(f)$. Since the similarity of two signals can be calculated in any frequency content, the coherence from 1 Hz to 100 Hz was firstly calculated with a 0.6 Hz-window. Thereafter, it was combined to the delta, theta, alpha, beta, and gamma bands to compare the difference. In this study, we calculated the changes of coherence (alternations) before and after injection between paired brain sites (ACC and Po, ACC and TG, ACC and V1M, Po and TG, Po and V1M, TG and V1M), and then examined the difference of alternations between the vehicle control group and NTG group.

2.8 Statistical analysis

The SPSS software was adopted to test statistical significance between the NTG and vehicle control groups. A mixed analysis of variance (mixed ANOVA) with LSD posthoc was implemented to test the differences in LFP power, coherence changes, and time spent in the dark box between the NTG group and vehicle control group. A repeated measures factorial ANOVA with LSD posthoc test was carried out to test whether the LFP power responses were different among these four regions. A Pearson's *r* correlation was conducted to test the relationship of LFP changes among paired brain regions. All data were presented as mean ± SEM. A significance was determined at a $p < 0.05$ level.

Chapter 3 Results

3.1 LFP signatures and brain coherence alternations from anesthetized animals

3.1.1 Significant elevations of LFP intensity with various response patterns following NTG injection were observed from anesthetized animals (see summary in Tables 3, 4)

The heatmap of normalized LFP power (ratio) indicated that the LFP activities in the ACC, Po, TG, and V1M at the delta, theta, alpha, beta, and gamma bands were elevated with different patterns after NTG injection from the anesthetized animals (Fig. 9A,B). The following were details:

The observation results from the ACC indicated that LFP powers (intensities) of the delta, theta, alpha, beta, and gamma bands in the NTG group (n = 12) increased significantly compared with the vehicle control group (n = 11) (Fig. 10A). Notably, at the delta band, LFP power increased significantly after NTG injection at 180-210 min (p = 0.044) and 240-270 min (p = 0.027). At the theta band, LFP intensity ascended at 60-90 min (p = 0.036), 210-240 min (p = 0.018), and 240-270 min (p = 0.005). At the alpha band, significant raises were detected at 60-90 min (p = 0.016), 90-120 min (p = 0.028), 180-210 min (p = 0.042), and 210-270 min (p = 0.012). At the beta band, LFP power elevated at 60-90 min (p = 0.006), 90-120 min (p = 0.004), 120-150 min (p = 0.023), 150-180 min (p = 0.025), 180-210 min (p = 0.007), and 210-270 min (p = 0.004). At the gamma band, significant increases were observed at 60-90 min (p = 0.039), 90-120 min (p = 0.014), 120-150 min (p = 0.041), 150-180 min (p = 0.029), 180-210 min (p = 0.004), 210-240 min (p = 0.007), and 240-270 min (p = 0.010).

From the Po, LFP powers (intensities) of the delta, theta, alpha, and beta bands in the NTG group (n = 12) elevated significantly compared with the vehicle control group (n = 11), but not for the gamma band (Fig. 10B). Specifically, at the delta and theta bands, significant increases were only tracked at 30-60 min (p = 0.030, p = 0.016, respectively). At the alpha band, LFP power enhanced at 30-60 min (p = 0.003), 60-90 min (p = 0.004), 90-120 min (p = 0.006), 180-210 min (p = 0.039), 210-240 min (p = 0.023), and 240-270 min (p = 0.012). At the beta band, LFP intensity improved at 180-210 min (p = 0.045), 210-240 min (p = 0.010), and 240-270 min (p = 0.005). However, there were no significant changes in the gamma band.

From the TG, LFP powers (intensities) of the theta, alpha, beta, and gamma bands in the NTG group (n = 12) increased significantly compared with the vehicle control group (n = 11), but not for the delta band (Fig. 10C). In detail, at the theta band, significant changes were found at 180-210 min (p = 0.033), 210-240 min (p = 0.028), and 240-270 min (p = 0.017). Similar results were detected for the alpha band, which increased at 180-210 min (p = 0.023), 210-240 min (p = 0.020), and 240-270 min (p = 0.019). At the beta band, LFP intensity enhanced significantly at 150-180 min (p = 0.030), 180-210 min (p = 0.004), 210-240 min (p = 0.002), and 240-270 min (p = 0.001). At the gamma band, it mounted at 60-90 min (p = 0.043), 90-120 min (p = 0.028), 120-150 min (p = 0.013), 150-180 min (p = 0.011), 180-210 min (p = 0.003), 210-240 min (p = 0.002), and 240-270 min (p = 0.001). However, no significant changes were detected in the delta band.

From the V1M, LFP powers (intensities) of the delta, theta, alpha, beta, and gamma bands in the NTG group (n = 12) increased significantly compared with the vehicle control group (n = 11) (Fig. 10D). At the delta band, LFP power enhanced at 90-120 min (p = 0.043), 120-150 min (p = 0.047), and 240-270 min (p = 0.016). At the theta band, significant increases were observed at 90-120 min (p = 0.041), 150-180 min (p = 0.041), 180-210 min (p = 0.018), 210-240 min (p =

0.010), and 240-270 min (p = 0.005). At the alpha band, LFP intensity kept rising immediately after NTG injection at 30-60 min (p = 0.030), 60-90 min (p = 0.002), 90-120 min (p = 0.001), 120-150 min (p = 0.006), 150-180 min (p = 0.008), 180-210 min (p = 0.003), 210-240 min (p = 0.002), and 240-270 min (p = 0.001). At the beta band, LFP power promoted at 60-90 min (p = 0.006), 90-120 min (p = 0.002), 120-210 min (p = 0.001), 210-240 min (p < 0.001), and 240-270 min (p = 0.001). At the gamma band, the significant increase was detected at 240-270 min (p = 0.021) merely.

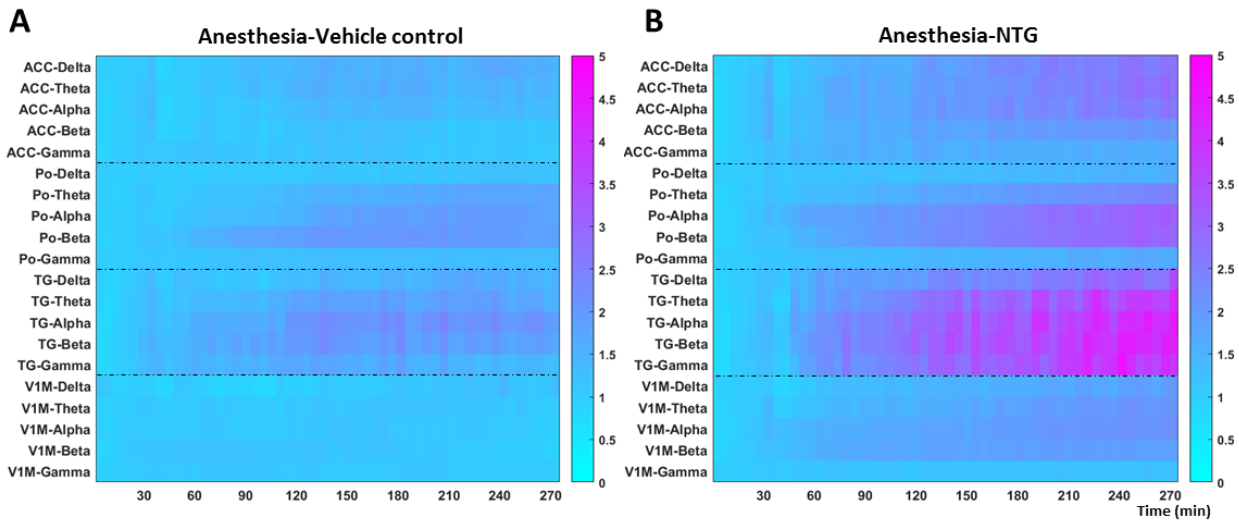

Figure 9. Heatmap of local field potential power at various brain regions in the (**A**) vehicle control group (n = 11) and (**B**) NTG group (n = 12) from anesthetized animals. In each figure, the x-axis is the time in minutes, and the y-axis is the brain region with different frequency bands. The color bar represents the LFP intensity.

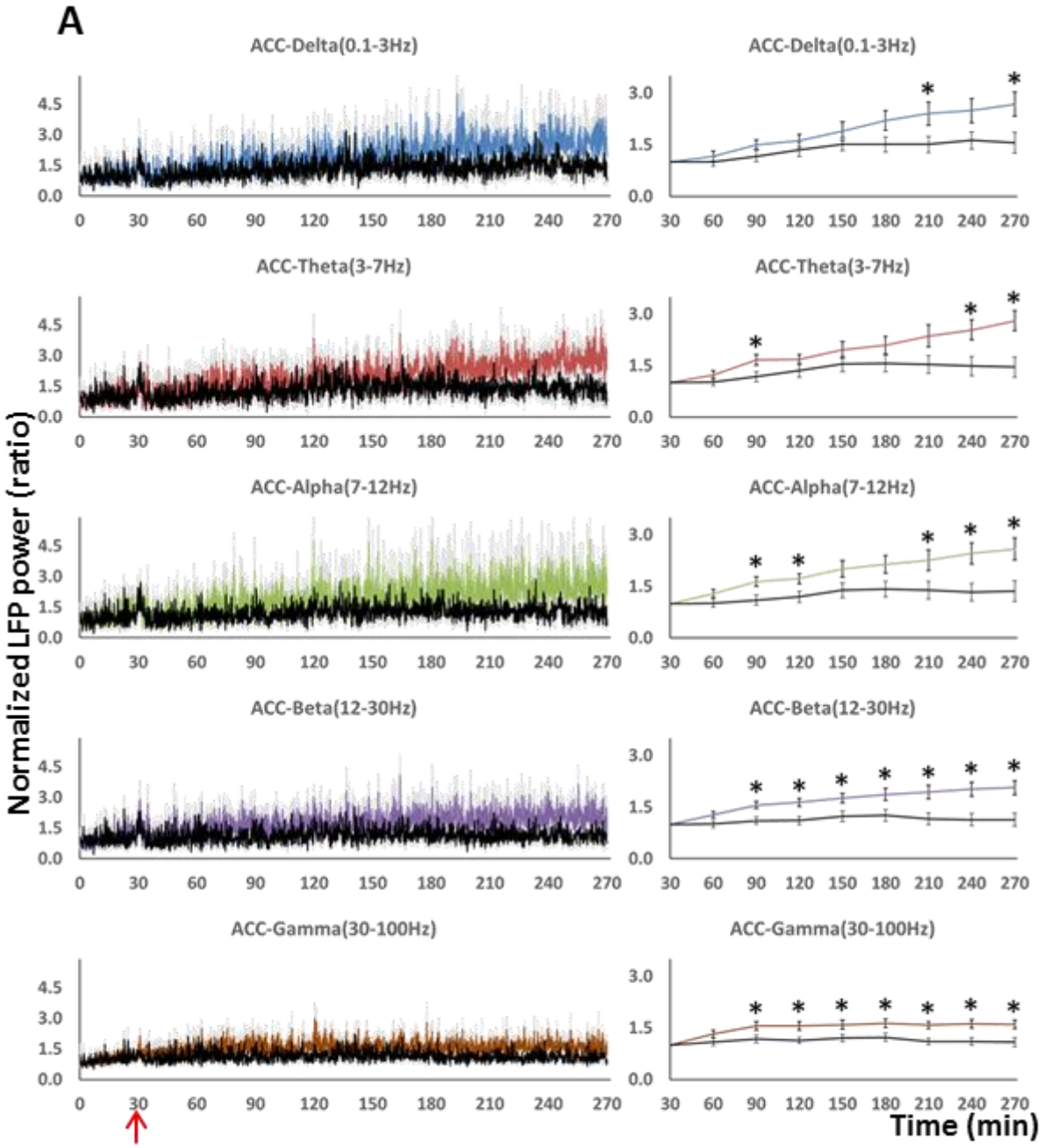
A
ACC-Delta(0.1-3Hz)
ACC-Delta(0.1-3Hz)
ACC-Theta(3-7Hz)
ACC-Theta(3-7Hz)
ACC-Alpha(7-12Hz)
ACC-Alpha(7-12Hz)
ACC-Beta(12-30Hz)
ACC-Beta(12-30Hz)
ACC-Gamma(30-100Hz)
ACC-Gamma(30-100Hz)
Normalized LFP power (ratio)
Time (min)

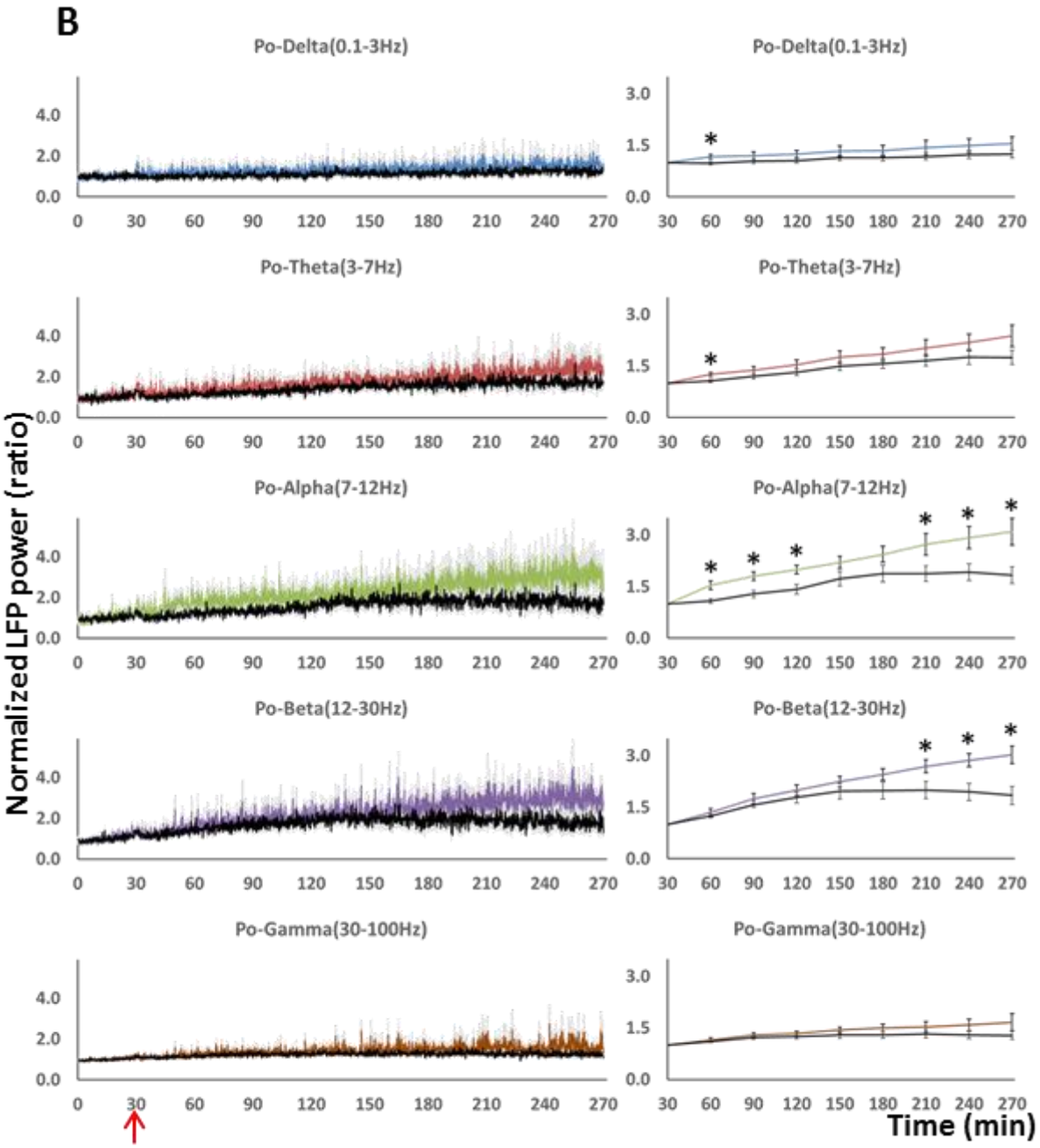
B
Po-Delta(0.1-3Hz)
Po-Delta(0.1-3Hz)
Po-Theta(3-7Hz)
Po-Theta(3-7Hz)
Po-Alpha(7-12Hz)
Po-Alpha(7-12Hz)
Po-Beta(12-30Hz)
Po-Beta(12-30Hz)
Po-Gamma(30-100Hz)
Po-Gamma(30-100Hz)
Normalized LFP power (ratio)
Time (min)

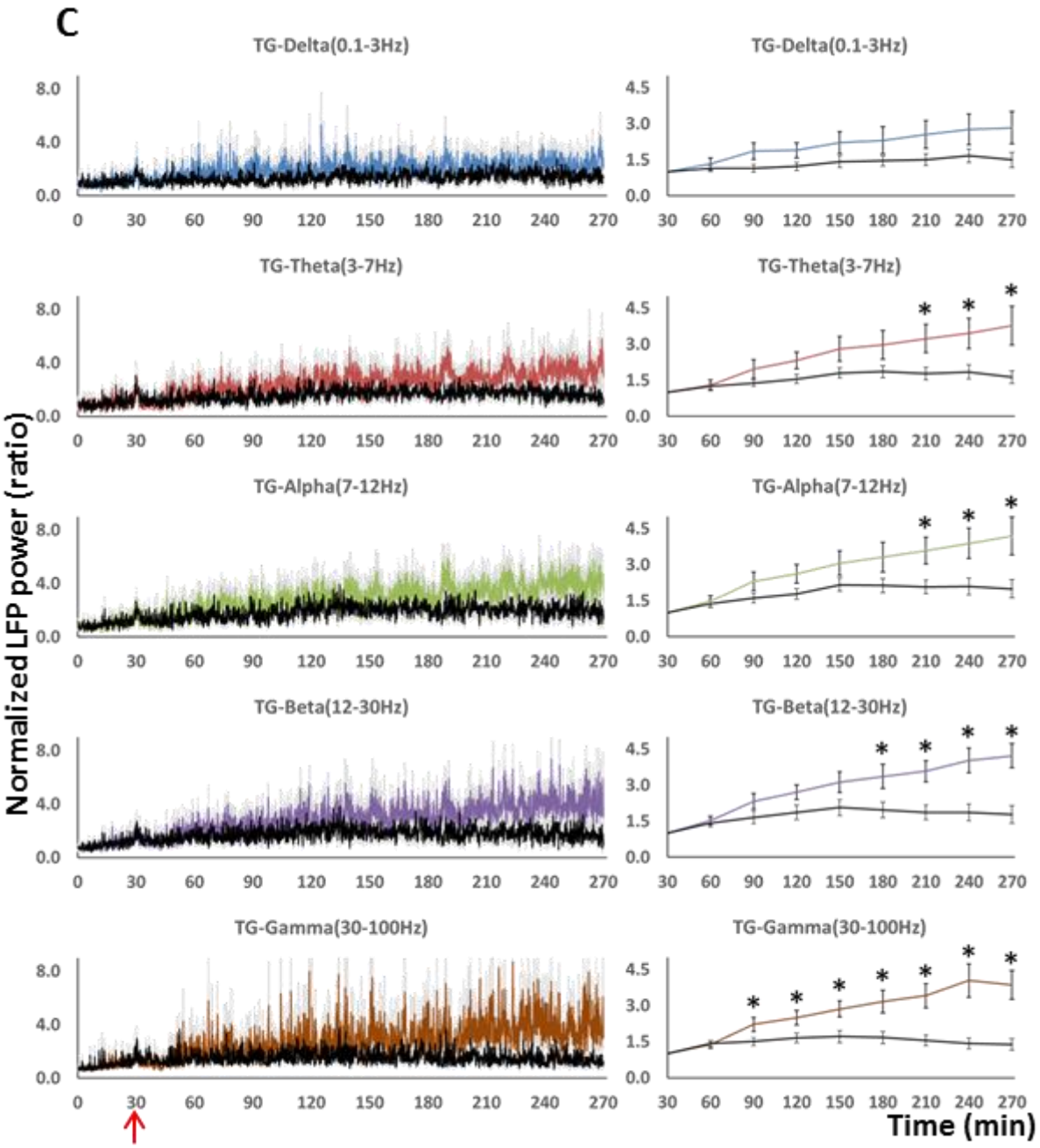
C
TG-Delta(0.1-3Hz)
TG-Delta(0.1-3Hz)
TG-Theta(3-7Hz)
TG-Theta(3-7Hz)
TG-Alpha(7-12Hz)
TG-Alpha(7-12Hz)
TG-Beta(12-30Hz)
TG-Beta(12-30Hz)
TG-Gamma(30-100Hz)
TG-Gamma(30-100Hz)
Normalized LFP power (ratio)
Time (min)

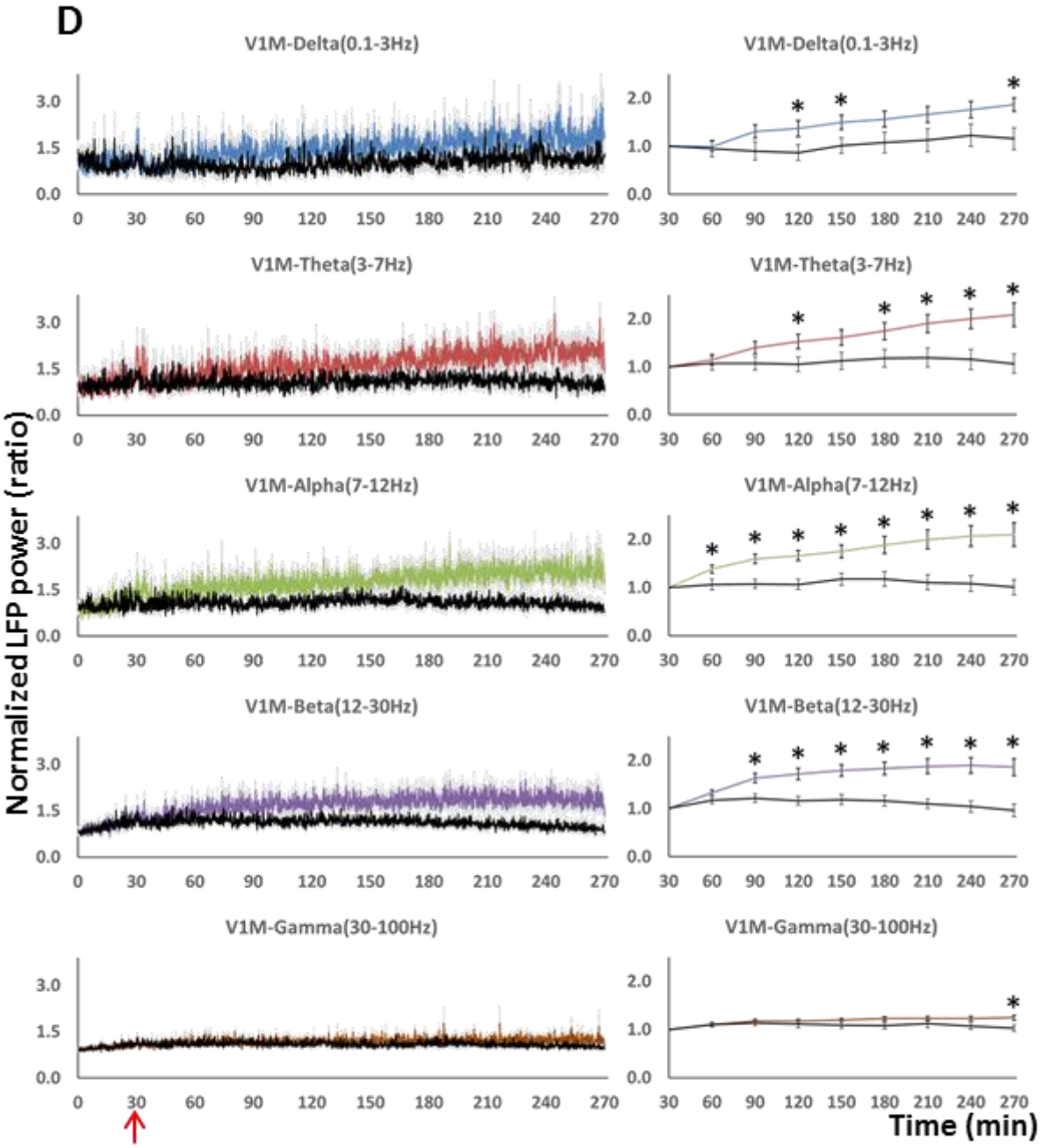

Figure 10. LFP power/intensity changes from anesthetized animals.

LFP power/intensity changes in the delta, theta, alpha, beta, and gamma bands at (**A**) ACC, (**B**) Po, (**C**) TG, and (**D**) V1M between the NTG group (n = 12) and vehicle control group (n = 11) from anesthetized animals. On the left column, the power is represented every 10 seconds, whereas

on the right column, it is averaged every 30 minutes. The x-axis is the time in minutes, and the y-axis is the normalized LFP power (ratio). The color lines are LFP changes in the NTG group, and black lines represent LFP changes in the vehicle control group. All data are shown as mean ± SEM. *$p < 0.05$ versus control group. The red arrows denote the timepoint of NTG/vehicle solution injection.

3.1.2 The LFP power responses were different among these four regions at the alpha, beta, and gamma bands

A repeated measures factorial ANOVA with LSD post-hoc test was also conducted to test whether the LFP power responses were different among these four regions. The results illustrated that significant LFP differences of frequency bands among various brain regions were detected from anesthetized animals. At the delta band, there was no main effect for brain regions, $F(3, 33) = 2.889$, $p = 0.079$, suggesting no significant differences for the LFP power responses among these four regions (ACC, Po, TG, and V1M). The same results were detected at the theta band, $F(3, 33) = 3.645$, $p = 0.051$. At the alpha band, there was a main effect for brain regions, $F(3, 33) = 5.021$, $p = 0.007$. In detail, the TG ($M = 2.827$, $SE = 0.395$) responded more strongly than that of the ACC ($M = 1.898$, $SE = 0.187$), $p = 0.022$, and the V1M ($M = 1.716$, $SE = 0.132$), $p = 0.023$. The Po ($M = 2.194$, $SE = 0.179$) responded more intensely than that of the V1M, $p = 0.049$. There were no significant differences among remaining areas. At the beta band, there was a main effect for brain regions, $F(3, 33) = 11.507$, $p < 0.001$. Notably, the Po ($M = 2.151$, $SE = 0.133$) responded more strongly than that of the ACC ($M = 1.679$, $SE = 0.124$), $p = 0.022$, and the V1M ($M = 1.658$, $SE = 0.101$), $p = 0.026$. The TG ($M = 2.874$, $SE = 0.296$) responded more strongly than that of the ACC ($p = 0.001$) and the V1M ($p = 0.002$). There were no differences among remaining sites. At the gamma band, there was a main effect for brain regions, $F(3, 33) = 17.238$, $p = 0.001$. The TG (M

= 2.715, *SE* = 0.316) responded more strongly than that of the ACC (*M* = 1.494, *SE* = 0.099), *p* = 0.003, the Po (*M* = 1.388, *SE* = 0.088), *p* = 0.004, and the V1M (*M* = 1.174, *SE* = 0.032), *p* = 0.001. The ACC responded more strongly than that of the V1M (*p* = 0.015). There were no differences among left regions.

3.1.3 Significant relationships were detected after NTG injection among these four regions at different bands (see summary in Table 5)

In order to test the correlations of LFP changes among these four brain regions, a Pearson's *r* correlation was conducted. The results demonstrated that significant relationships of LFP changes among different brain sites were observed from anesthetized animals (Fig. 11, Table 5). Specifically, at the delta band, there was a positive correlation of LFP changes between the ACC and the Po, $r(7) = 0.974$, $p < 0.001$, which meant LFP activities in ACC fluctuated along with that in the Po. The similar relationships were seen between the ACC and the TG, $r(7) = 0.983$, $p < 0.001$, the V1M, $r(7) = 0.987$, $p < 0.001$; the Po and the TG, $r(7) = 0.979$, $p < 0.001$, the V1M , $r(7) = 0.959$, $p < 0.001$; the TG and the V1M, $r(7) = 0.988$, $p < 0.001$. The similar results were detected at the theta, alpha, and beta bands ($p < 0.001$). Notably, there were positive correlations between the ACC and the Po ($r = 0.992$, $r = 0.994$, $r = 0.988$, in the theta, alpha, and beta bands, respectively), the TG ($r = 0.988$, $r = 0.998$, $r = 0.992$, respectively), and the V1M ($r = 0.993$, $r = 0.983$, $r = 0.971$, respectively); the Po and the TG ($r = 0.985$, $r = 0.989$, $r = 0.997$, respectively), the V1M ($r = 0.989$, $r = 0.986$, $r = 0.925$, respectively); the TG and the V1M ($r = 0.994$, $r = 0.983$, $r = 0.940$, respectively). Additionally, at the gamma band, there was a positive relationship of LFP changes between the ACC and the Po, $r(7) = 0.873$, $p = 0.002$, the TG, $r(7) = 0.841$, $p = 0.005$, the

V1M, $r(7) = 0.967$, $p < 0.001$; between the Po and the TG, the V1M ($r = 0.985$, $r = 0.961$, respectively), $p < 0.001$; between the TG and the V1M ($r = 0.931$, $p < 0.001$).

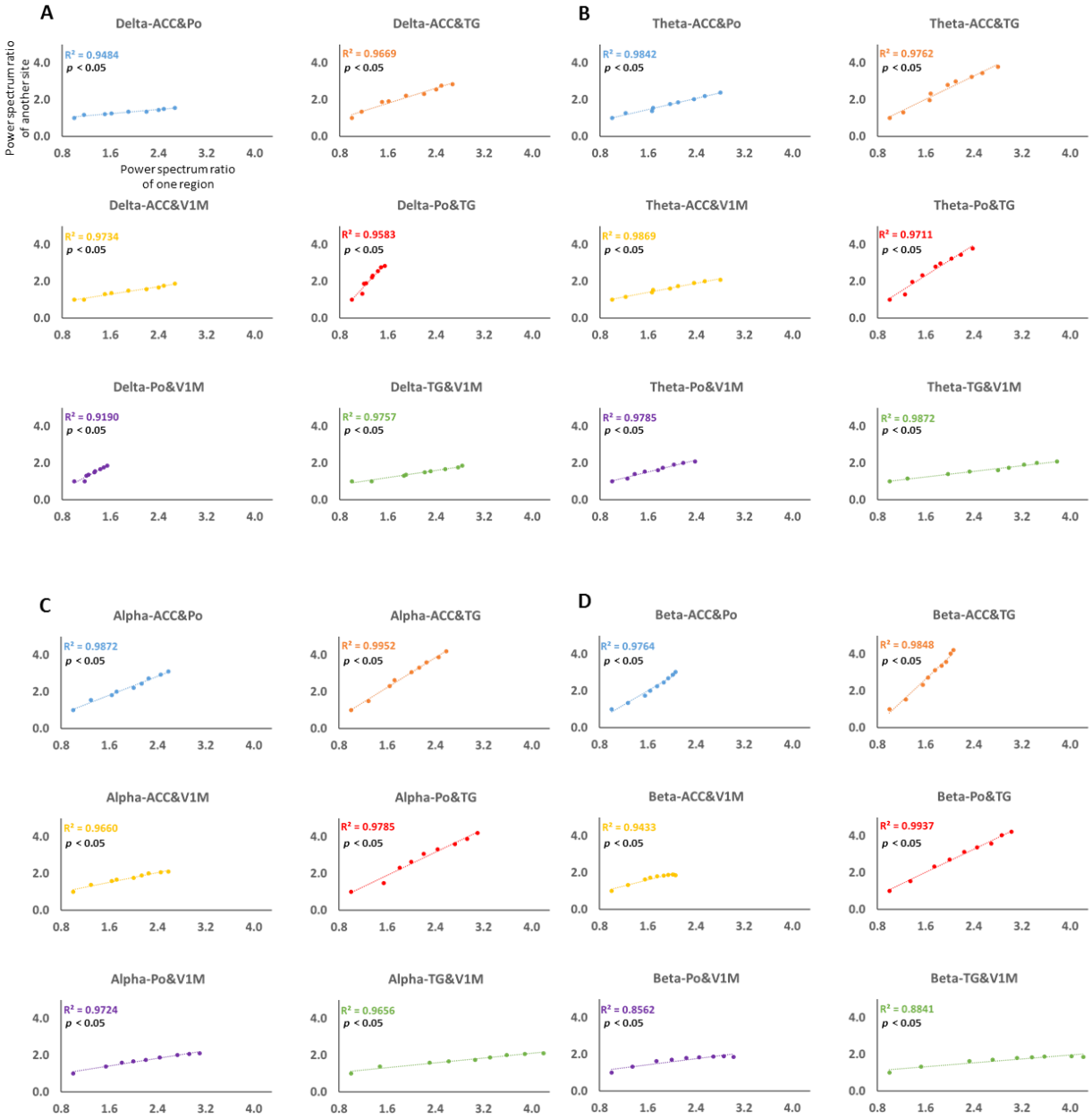

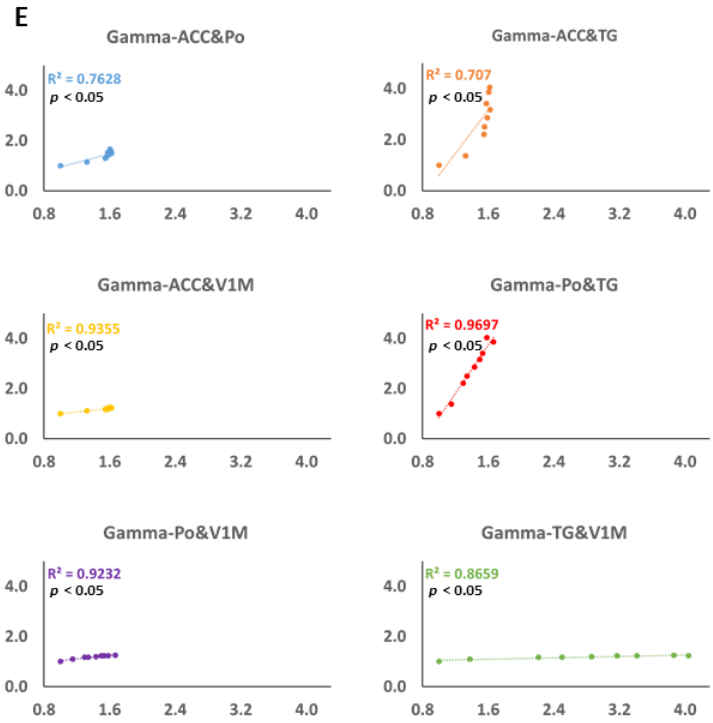

Figure 11. Correlations of LFP intensity changes among paired brain regions at (**A**) delta band, (**B**) theta band, (**C**) alpha band, (**D**) beta band, and (**E**) gamma band from anesthetized animals. The x and y axes were the normalized LFP power (ratio). The results indicated all correlations in this figure were significant ($p < 0.05$, see Table 5).

3.1.4 No obvious brain coherence changes after NTG injection detected from anesthetized animals (see summary in Tables 6, 7)

The coherence changes under 100 Hz were acquired by using Spike2, and then merged into the delta, theta, alpha, beta, and gamma bands. The topographical brain coherence in six pairings (ACC & Po, ACC & TG, ACC & V1M, Po & TG, Po & V1M, TG & V1M) showed there were no obvious brain coherence changes between the vehicle control group (n = 11) and NTG group

(n = 12) detected from anesthetized animals (Fig. 12A,B). The mean coherence change matrices also depicted no alternations between these two groups (Fig. 13A,B). Furthermore, a mixed ANOVA with LSD posthoc test was employed to test the difference in coherence changes between the NTG group (n = 12) and the vehicle control group (n = 11). All data were presented as mean + SEM. A significance was determined at a $p < 0.05$ level. The results showed that there were no significant brain coherence changes between these two groups at the delta, theta, alpha, beta, and gamma bands among any paired brain regions, overall (Fig. 14). However, the changes of coherence in the NTG group between the ACC and the Po at the delta and theta bands increased significantly in contrast to the vehicle control group. A similar result was observed between the Po and the V1M at the alpha band merely.

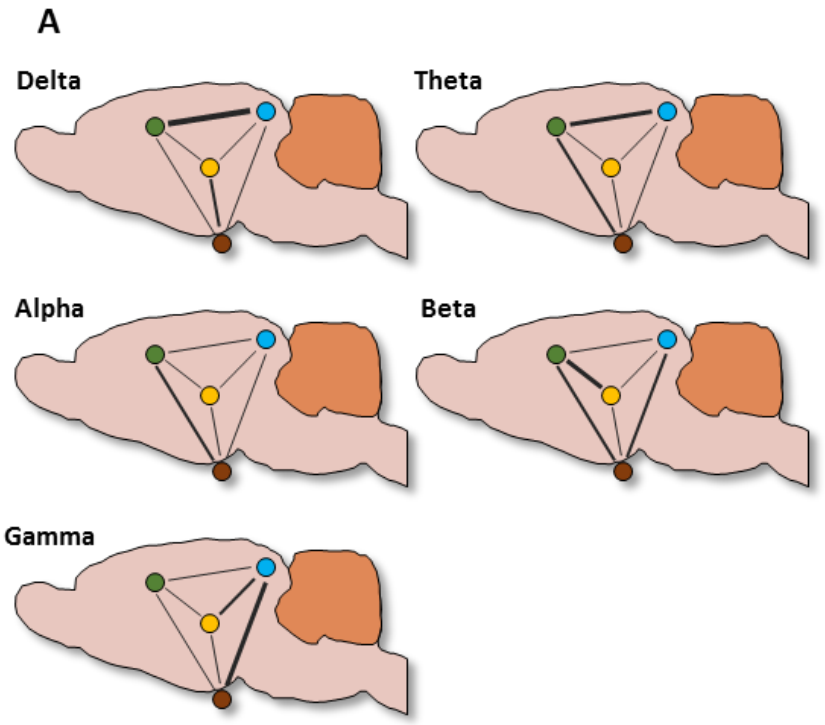

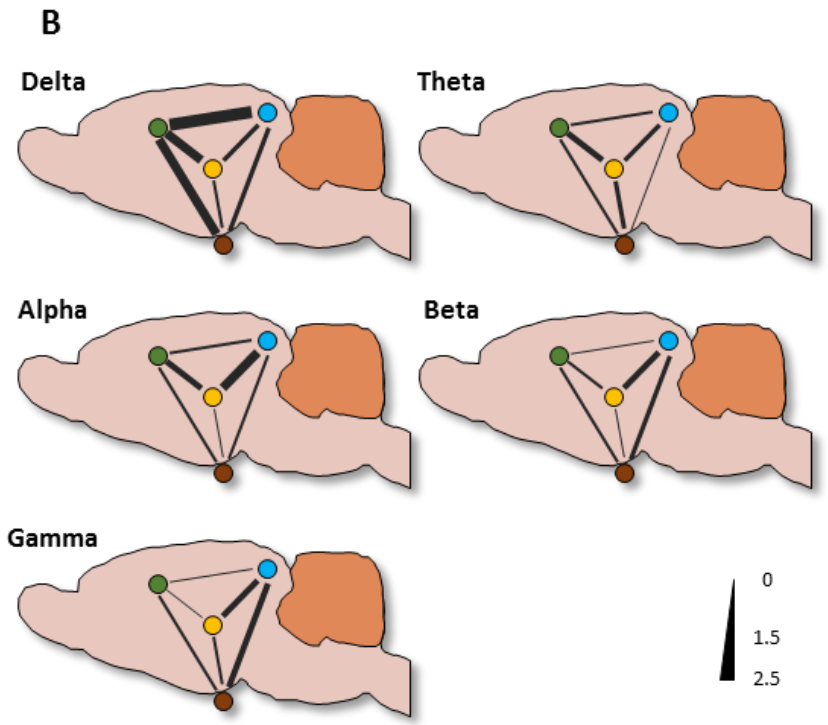

Figure 12. Topographical brain coherence at the delta, theta, alpha, beta, and gamma bands between any paired brain regions (ACC-green, Po-yellow, TG-gray, V1M-blue) in the (**A**) vehicle control (n = 11) and (**B**) NTG group (n = 12) from anesthetized animals. The solid line represents the coherence between paired regions, and the line thickness reflects the magnitude of the coherence.

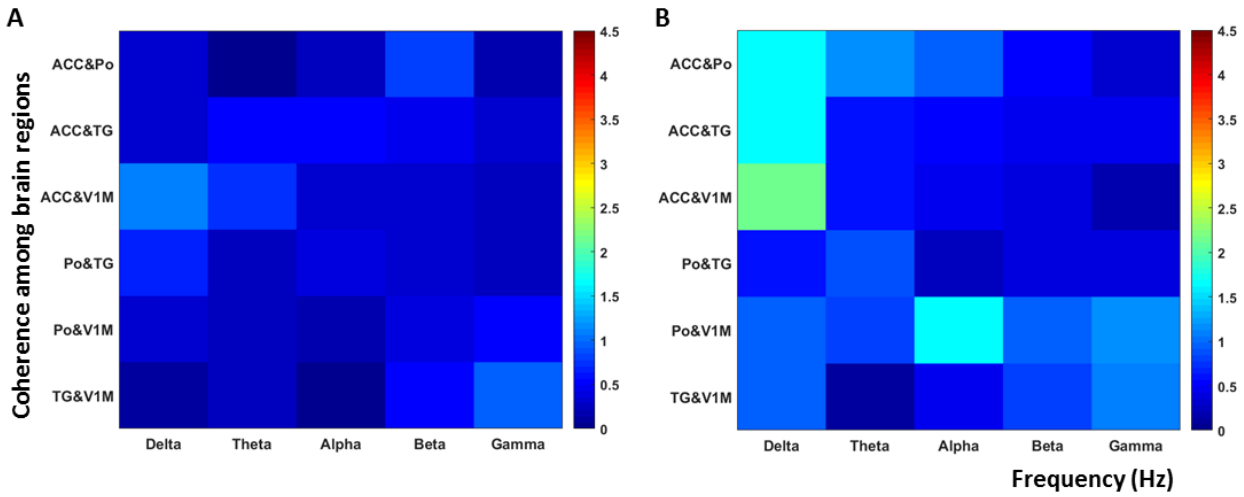

Figure 13. Mean coherence change matrices of the (**A**) vehicle control (n = 11) and (**B**) NTG group (n = 12) from anesthetized animals. The color bar denotes coherence change values.

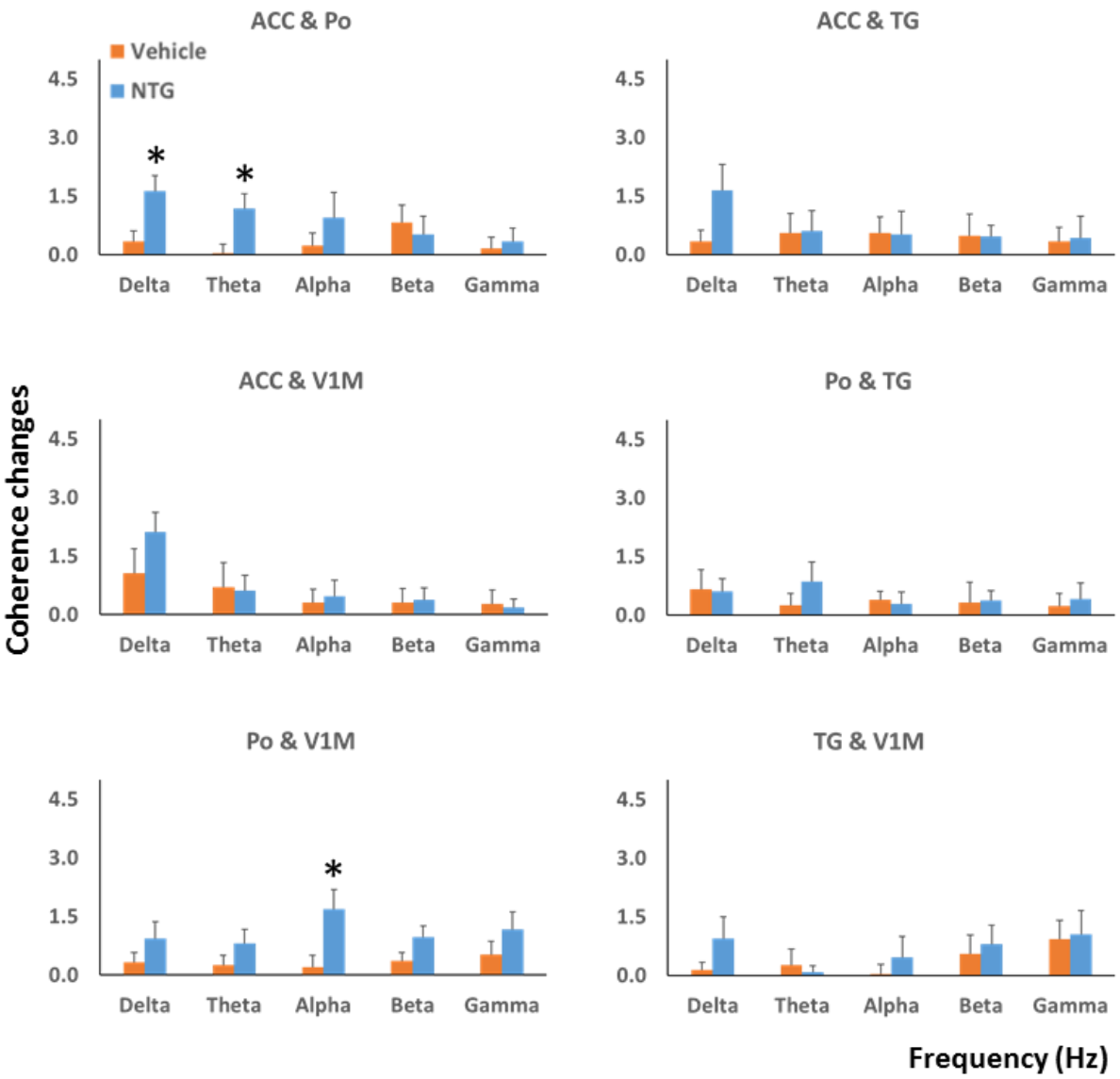

Figure 14. Coherence changes in each paring at different bands between the vehicle control (n = 11) and NTG group (n = 12) from anesthetized animals. All data are shown as mean + SEM. *p < 0.05 versus control group. The x-axis is frequency bands (delta, theta, alpha, beta, and gamma), and the y-axis is the coherence change.

3.2 Light-aversive behavior test, LFP signatures, and brain coherence alternations from freely moving animals

3.2.1 Light-aversive behavior measurement

The animals in the freely moving group were placed in the light-dark box immediately following NTG/vehicle injection (Fig. 15A). During the light-aversive behavior test, rats moved freely through the gate connecting the two compartments. The measurement lasted 30 minutes under a camera, and the time spent on the dark side was counted. In the end, a mixed ANOVA with LSD posthoc test was applied to test the difference in time in the dark compartment. The results indicated that there was a significant increase in time spent in the dark box between the NTG group (M = 94.89%, SE = 0.015) and the vehicle control group (M = 75.55%, SE = 0.034), $p < 0.05$, as shown in Figure 15B, suggesting NTG induced the phenomenon of photophobia.

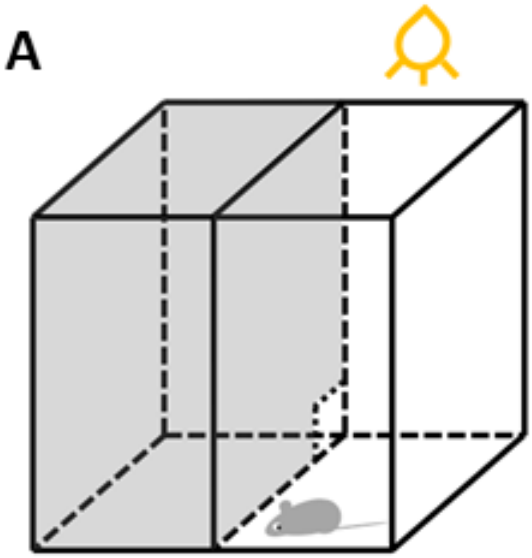

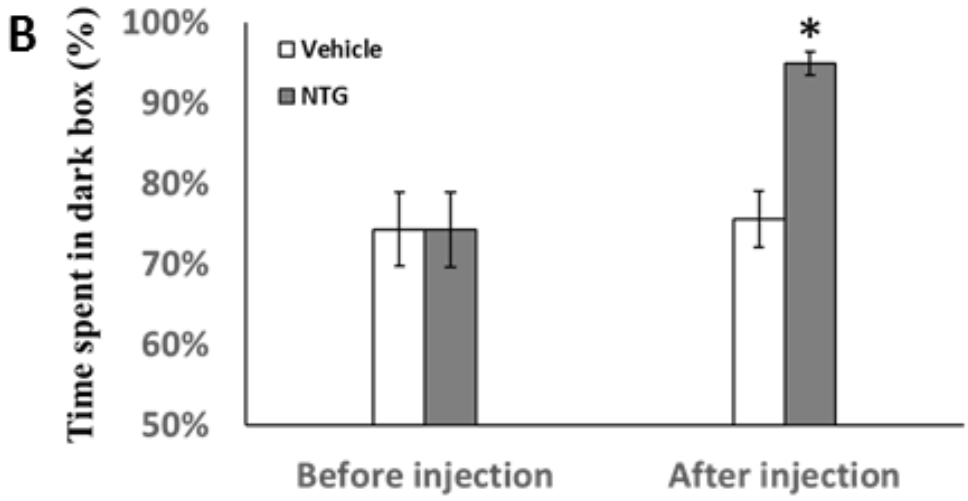

Figure 15. Light-aversive behavior test. (**A**) Test apparatus. (**B**) Time spent in the dark box between the NTG group (n = 11) and vehicle control group (n = 10). The y-axis is the time spent in the dark box (%). *$p < 0.05$ versus control group.

3.2.2 Different brain sites showed various increases in power at various frequency bands after NTG injection observed from freely moving animals (see summary in Tables 8, 9)

A mixed ANOVA with LSD posthoc test was used to test the difference in LFP intensity between the vehicle control group (n = 10) and NTG group (n = 11). All data were presented as mean ± SEM. A significance was determined at a $p < 0.05$ level.

The heatmap of normalized LFP power (ratio) demonstrated that the LFP power in the ACC, Po, TG, and V1M at the delta, theta, alpha, beta, and gamma bands were increased after NTG injection from freely moving animals (Fig. 16A,B). Thereafter, the results of a mixed ANOVA with LSD posthoc test indicated that, from the ACC, LFP powers (intensities) of the delta, theta, alpha, beta, and gamma bands in the NTG group (n = 11) increased significantly

compared with the vehicle control group (n = 10) (Fig. 17A). In detail, at the delta band, LFP power increased immediately after NTG injection at 30-60 min (p = 0.020), 60-90 min (p = 0.017), 90-120 min (p = 0.035), 120-150 min (p = 0.013), 150-180 min (p = 0.002), 180-210 min (p = 0.024), 210-240 min (p = 0.007), and 240-270 min (p = 0.015). At the theta band, significant increases of LFP intensity were observed at 30-60 min (p = 0.003), 60-90 min (p = 0.016), 90-120 min (p = 0.022), 150-180 min (p = 0.039), 210-240 min (p = 0.042), and 240-270 min (p = 0.049). At the alpha band, it improved at 30-60 min (p = 0.005), 60-90 min (p = 0.018), 150-180 min (p = 0.044), and 210-240 min (p = 0.047). At the beta band, LFP intensity ascended at 30-60 min (p = 0.001), 60-90 min (p = 0.004), 150-180 min (p = 0.016), 180-210 min (p = 0.028), and 210-240 min (p = 0.013). At the gamma band, LFP power increased at 30-60 min (p = 0.001), 60-90 min (p = 0.012), 150-180 min (p = 0.041), and 210-240 min (p = 0.023).

With regard to the Po, LFP powers (intensities) of the delta, theta, alpha, and gamma bands in the NTG group (n = 11) increased significantly compared with the vehicle control group (n = 10) (Fig. 17B). Notably, at the delta band, LFP intensity enhanced at 30-60 min (p = 0.004), 120-150 min (p = 0.049), 150-180 min (p = 0.016), 210-240 min (p = 0.028), and 240-270 min (p = 0.018). At the theta band, LFP intensity increased at 30-60 min (p = 0.001), 60-90 min (p = 0.043), 120-150 min (p = 0.011), 210-240 min (p = 0.001), and 240-270 min (p = 0.043). At the alpha band, LFP intensity increased at 30-60 min (p = 0.009), 90-120 min (p = 0.008), 120-150 min (p = 0.035), and 210-240 min (p = 0.003). At the gamma band, LFP intensity improved at 30-60 min (p = 0.006), 90-120 min (p = 0.010), 120-150 min (p = 0.012), and 180-210 min (p = 0.047). At the beta band, however, the significant increase was exclusively seen at 30-60 min (p = 0.014).

From the TG, LFP powers (intensities) of the delta, theta, alpha, beta, and gamma bands in the NTG group (n = 11) increased significantly compared with the vehicle control group (n = 10)

(Fig. 17C). At the delta band, LFP intensity increased at 60-90 min ($p = 0.008$), 90-120 min ($p = 0.049$), 120-150 min ($p = 0.017$), 150-180 min ($p = 0.012$), 180-210 min ($p = 0.015$), 210-240 min ($p = 0.008$), and 240-270 min ($p < 0.001$). At the theta band, LFP intensity mounted at 30-60 min ($p = 0.014$), 60-90 min ($p = 0.005$), 90-120 min ($p = 0.003$), 120-150 min ($p = 0.004$), 150-180 min ($p = 0.007$), 180-210 min ($p = 0.019$), 210-240 min ($p = 0.003$), and 240-270 min ($p = 0.001$). Similar results were observed for the beta band, which elevated at 30-60 min ($p = 0.017$), 60-90 min ($p = 0.006$), 90-120 min ($p = 0.013$), 120-150 min ($p = 0.003$), 150-180 min ($p = 0.012$), 180-210 min ($p = 0.025$), 210-240 min ($p = 0.002$), and 240-270 min ($p = 0.004$). At the alpha band, significant increases were detected at 30-60 min ($p = 0.024$), 60-90 min ($p = 0.014$), 90-120 min ($p = 0.006$), 120-150 min ($p = 0.019$), 150-180 min ($p = 0.031$), 210-240 min ($p = 0.009$), and 240-270 min ($p = 0.001$). At the gamma band, it ascended at 120-150 min ($p = 0.014$), 150-180 min ($p = 0.024$), 180-210 min ($p = 0.047$), 210-240 min ($p = 0.011$), and 240-270 min ($p = 0.002$).

From the V1M, LFP powers (intensities) of the delta, theta, alpha, and beta bands in the NTG group ($n = 11$) enhanced significantly compared with the vehicle control group ($n = 10$) from the V1M (Fig. 17D). Specifically, at the delta band, LFP power surged at 60-90 min ($p = 0.049$), 90-120 min ($p = 0.049$), 120-150 min ($p = 0.016$), 150-180 min ($p = 0.002$), 180-210 min ($p = 0.025$), 210-240 min ($p = 0.028$), and 240-270 min ($p = 0.012$). At the theta band, LFP power promoted at 150-180 min ($p = 0.039$), 210-240 min ($p = 0.021$), and 240-270 min ($p = 0.007$). At the alpha band, significant changes were tracked at 210-240 min ($p = 0.027$) and 240-270 min ($p = 0.005$). At the beta band, LFP power kept increasing at 150-180 min ($p = 0.012$), 180-210 min ($p = 0.031$), 210-240 min ($p = 0.016$), and 240-270 min ($p = 0.009$). However, at the gamma band, the significant increase was only observed at 90-120 min ($p = 0.038$).

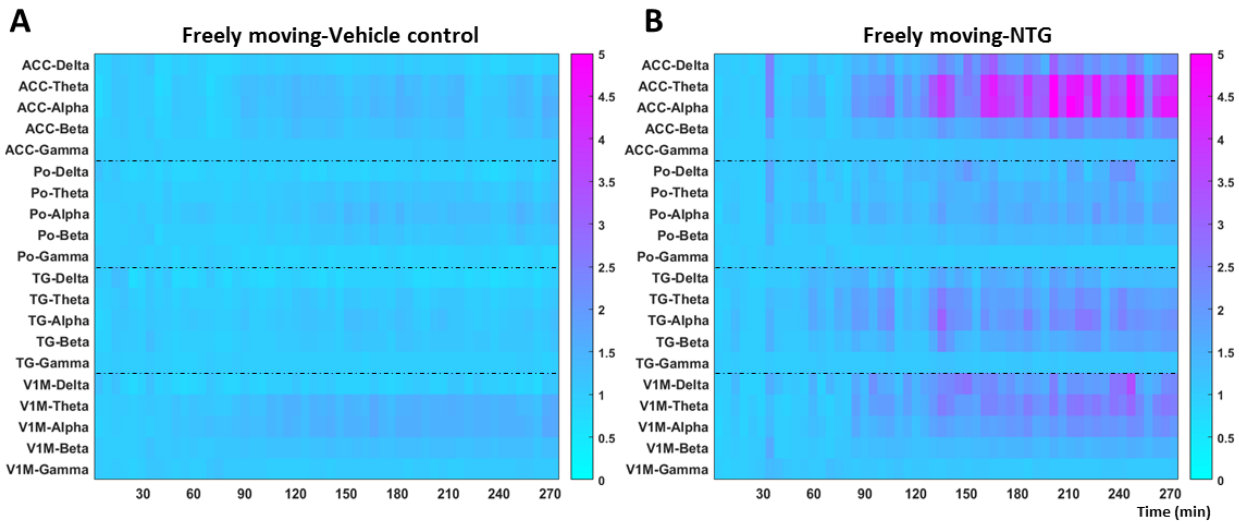

Figure 16. Heatmap of local field potential power at various brain regions in the (**A**) vehicle control group (n = 10) and (**B**) NTG group (n = 11) from freely moving animals. In each figure, the x-axis is the time in minutes, and the y-axis is the brain region with different frequency bands. The color bar represents the LFP intensity.

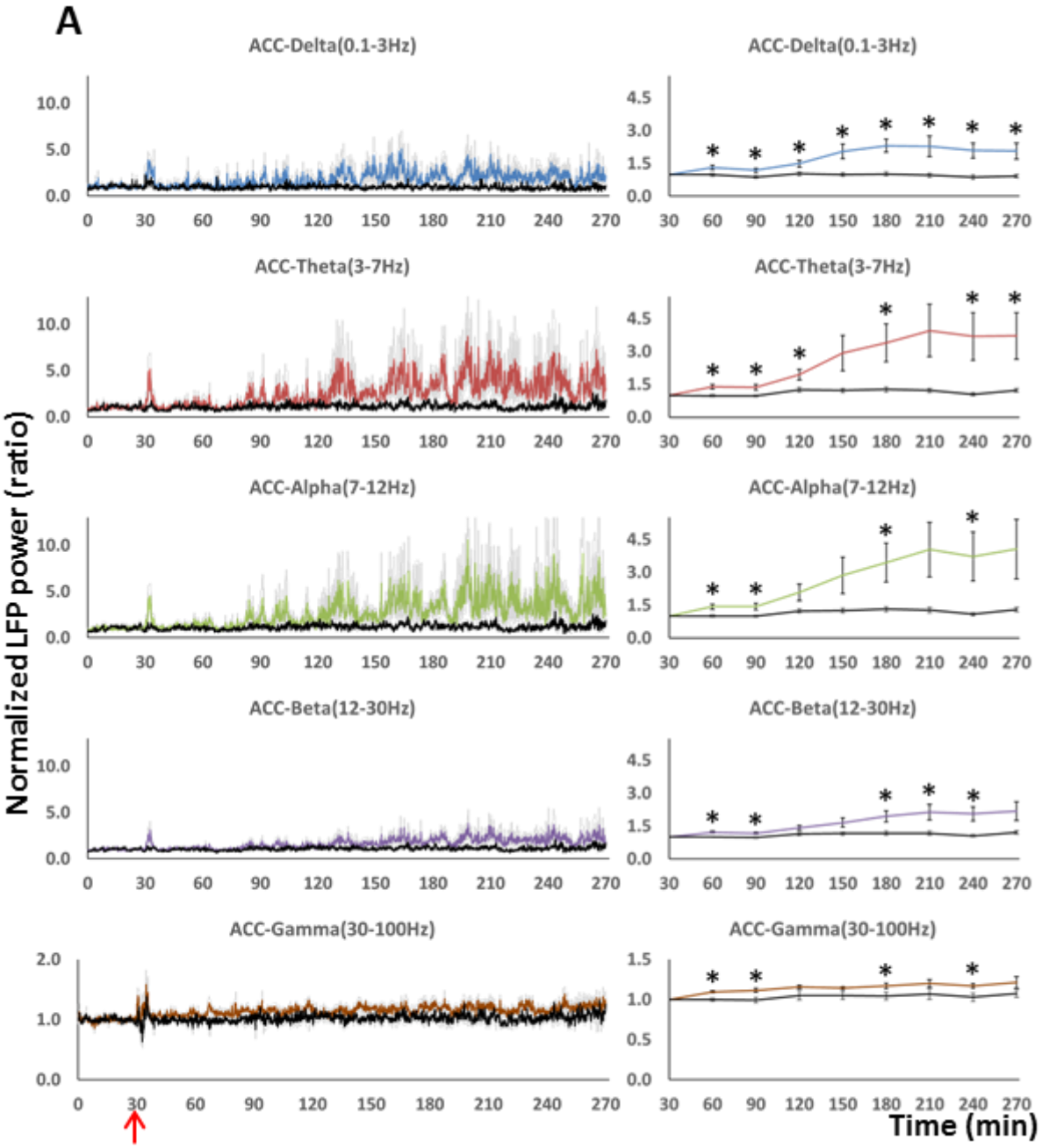
A
ACC-Delta(0.1-3Hz)
ACC-Delta(0.1-3Hz)
ACC-Theta(3-7Hz)
ACC-Theta(3-7Hz)
ACC-Alpha(7-12Hz)
ACC-Alpha(7-12Hz)
ACC-Beta(12-30Hz)
ACC-Beta(12-30Hz)
ACC-Gamma(30-100Hz)
ACC-Gamma(30-100Hz)
Normalized LFP power (ratio)
Time (min)

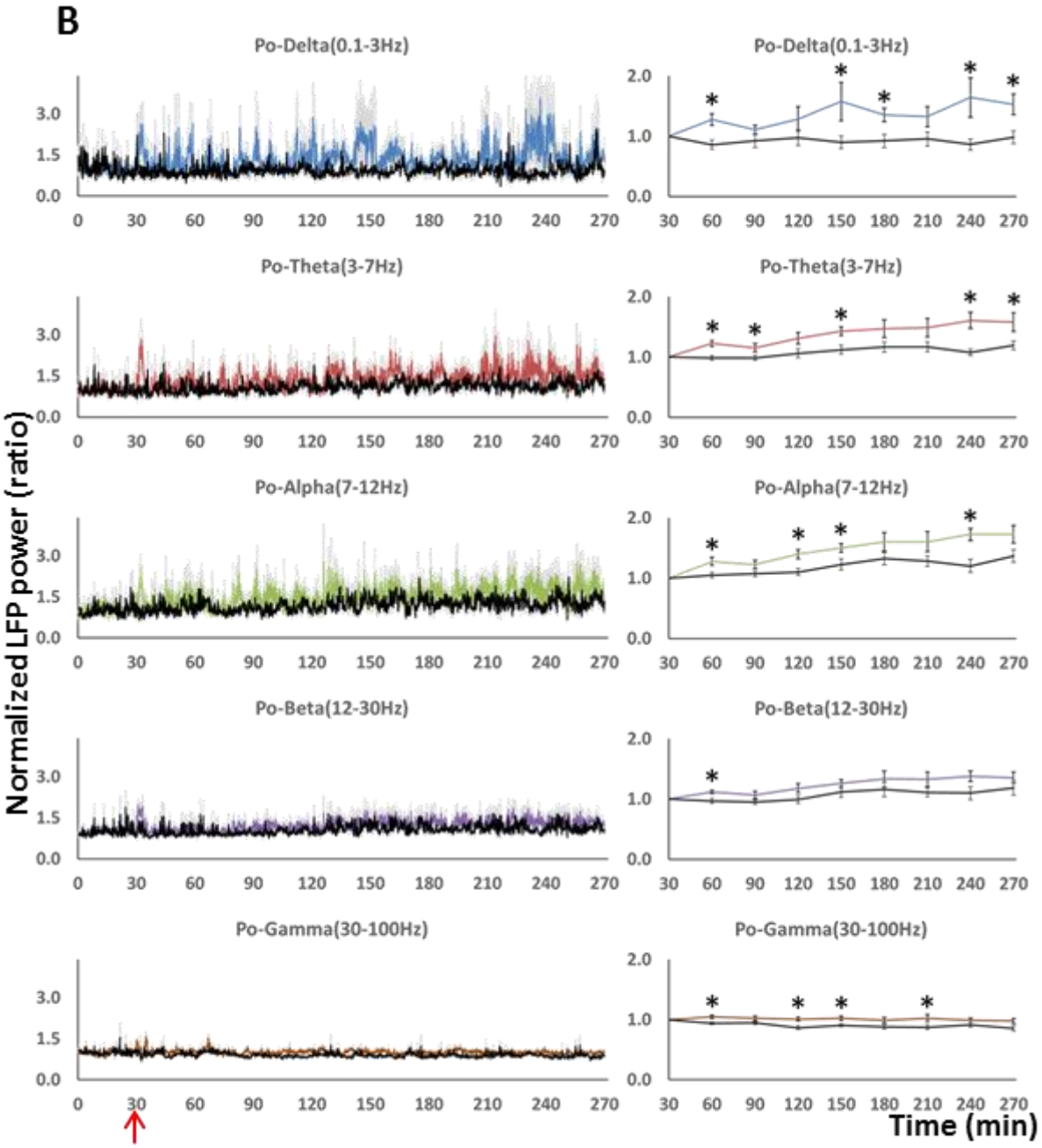
B
Po-Delta(0.1-3Hz)
Po-Delta(0.1-3Hz)
Po-Theta(3-7Hz)
Po-Theta(3-7Hz)
Po-Alpha(7-12Hz)
Po-Alpha(7-12Hz)
Po-Beta(12-30Hz)
Po-Beta(12-30Hz)
Po-Gamma(30-100Hz)
Po-Gamma(30-100Hz)
Normalized LFP power (ratio)
Time (min)

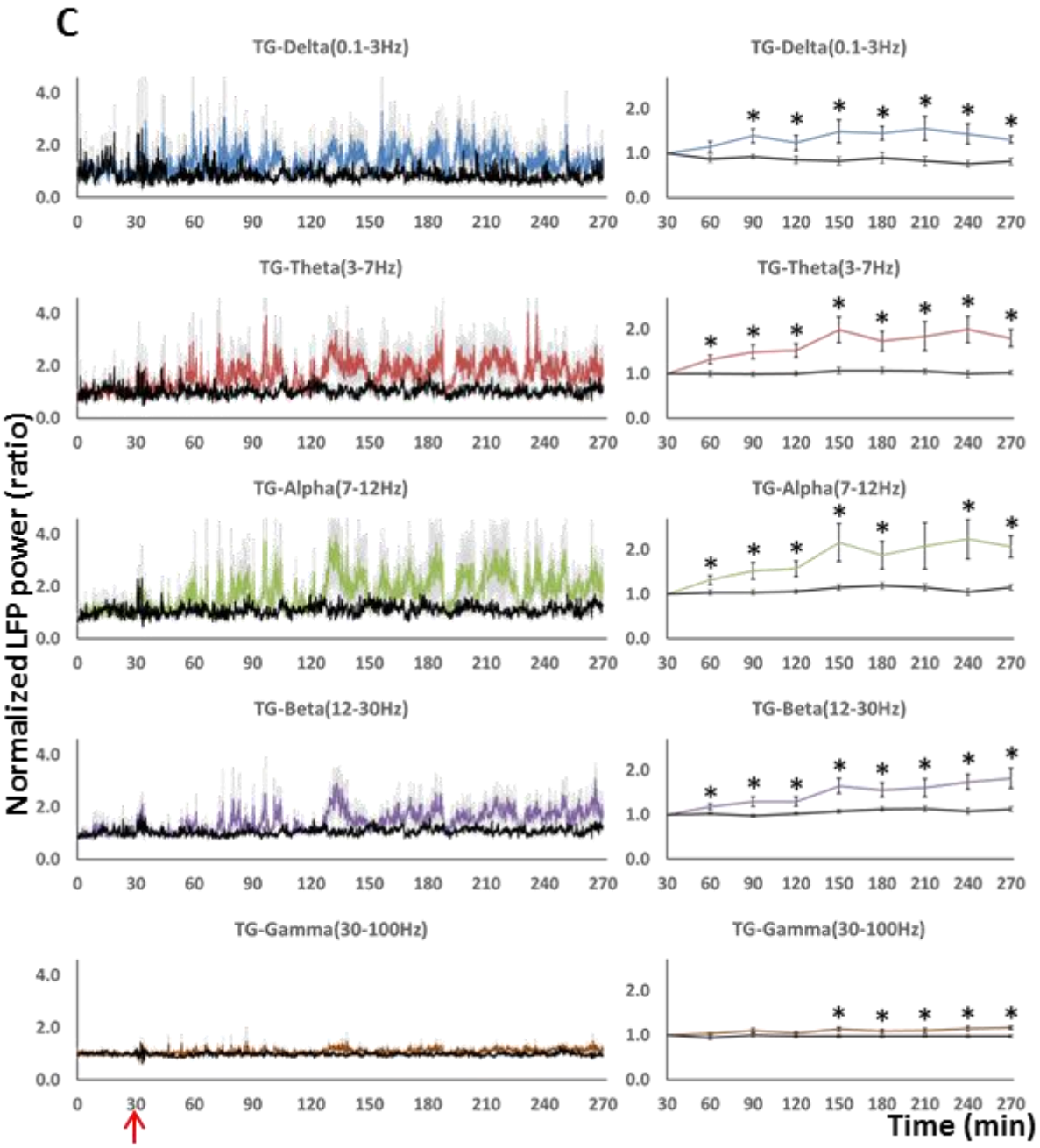
C
TG-Delta(0.1-3Hz)
TG-Delta(0.1-3Hz)
TG-Theta(3-7Hz)
TG-Theta(3-7Hz)
TG-Alpha(7-12Hz)
TG-Alpha(7-12Hz)
TG-Beta(12-30Hz)
TG-Beta(12-30Hz)
TG-Gamma(30-100Hz)
TG-Gamma(30-100Hz)
Normalized LFP power (ratio)
Time (min)

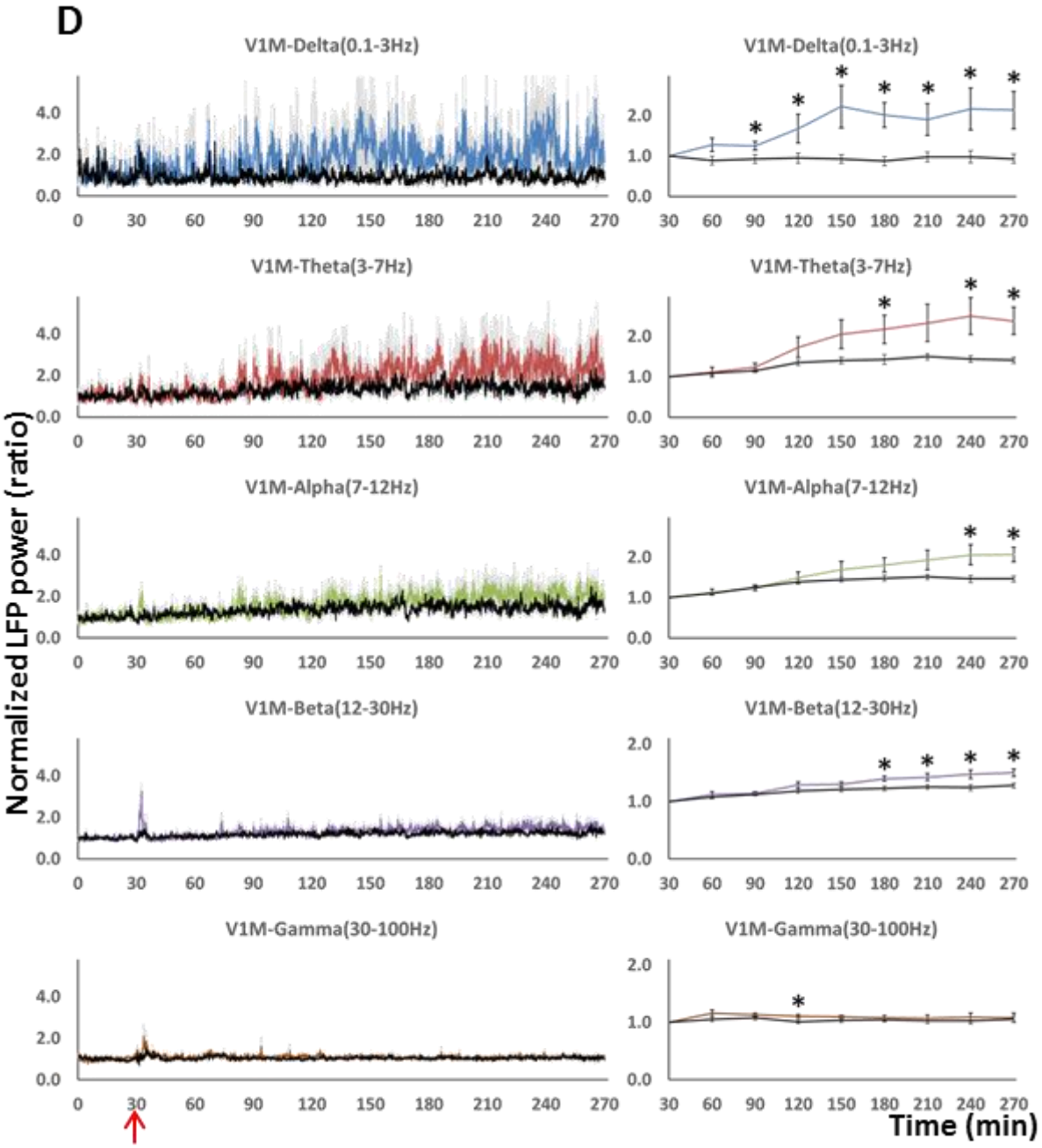

Figure 17. LFP power/intensity changes from freely moving animals.

LFP power/intensity changes in the delta, theta, alpha, beta, and gamma bands at (**A**) ACC, (**B**) Po, (**C**) TG, and (**D**) V1M between the NTG group (*n* = 11) and vehicle control group (*n* = 10) from freely moving animals. On the left column, the power is represented every 10 seconds,

whereas on the right column, it is averaged every 30 minutes. The x-axis is the time in minutes, and the y-axis is the normalized LFP power (ratio). The color lines are LFP changes in the NTG group, and black lines represent LFP changes in the vehicle control group. All data are shown as mean ± SEM. *$p < 0.05$ versus control group. The red arrows denote the timepoint of NTG/vehicle solution injection.

3.2.3 No significant differences of the LFP power response (except the gamma band) were observed among these four regions

A repeated measures factorial ANOVA with LSD posthoc test was implemented to examine whether the LFP power responses were different among the ACC, Po, TG, and V1M. The results indicated no significant differences in frequency bands (except gamma band) among various brain areas from freely moving animals. Notably, at the delta band, there was no main effect for brain regions, $F(3, 30) = 1.457$, $p = 0.255$, suggesting no significant differences in the LFP power responses among these four regions. The same results were observed at the theta band, $F(3, 30) = 2.587$, $p = 0.125$; at the alpha band, $F(3, 30) = 2.372$, $p = 0.151$; and at the beta band, $F(3, 30) = 3.184$, $p = 0.090$. At the gamma band, however, there was a main effect for brain regions, $F(3, 30) = 3.140$, $p = 0.047$. Specifically, the ACC ($M = 1.140$, $SE = 0.021$) responded more strongly than that of the Po ($M = 1.010$, $SE = 0.028$), $p = 0.024$. There were no significant changes among the remaining regions.

3.2.4 Significant relationships were found after NTG injection among these four regions at the delta, theta, alpha, and beta bands (see summary in Table 10)

The results a Pearson's *r* correlation test indicated that there were Significant relationships of LFP changes among different brain sites from freely moving animals (Fig.18, Table 10). At the

delta band, there was a positive relationship of LFP changes between the ACC and the Po, $r(7) = 0.768$, $p = 0.016$, which indicated LFP activities in ACC fluctuated along with that in the Po. The similar correlations were detected between the ACC and the TG, $r(7) = 0.807$, $p = 0.009$, the V1M, $r(7) = 0.921$, $p < 0.001$; the Po and the V1M, $r(7) = 0.922$, $p < 0.001$; the TG and the V1M, $r(7) = 0.745$, $p = 0.021$. At the theta band, there were positive correlations between the ACC and the Po ($r = 0.950$, $p < 0.001$), the TG ($r = 0.875$, $p = 0.002$), and the V1M ($r = 0.978$, $p < 0.001$); the Po and the TG ($r = 0.916$, $p = 0.001$), the V1M ($r = 0.968$, $p < 0.001$); the TG and the V1M ($r = 0.907$, $p = 0.001$). The similar results were seen at the alpha and beta bands ($p < 0.001$). In detail, there were positive correlations between the ACC and the Po ($r = 0.957$, $r = 0.977$, in the alpha and beta bands, respectively), the TG ($r = 0.907$, $r = 0.930$, respectively), and the V1M ($r = 0.983$, $r = 0.971$, respectively); the Po and the TG ($r = 0.930$, $r = 0.938$, respectively), the V1M ($r = 0.977$, $r = 0.978$, respectively); the TG and the V1M ($r = 0.939$, $r = 0.940$, respectively). At the gamma band, however, the significant correlation of LFP changes were exclusively observed between the ACC and the TG, $r(7) = 0.792$, $p = 0.011$.

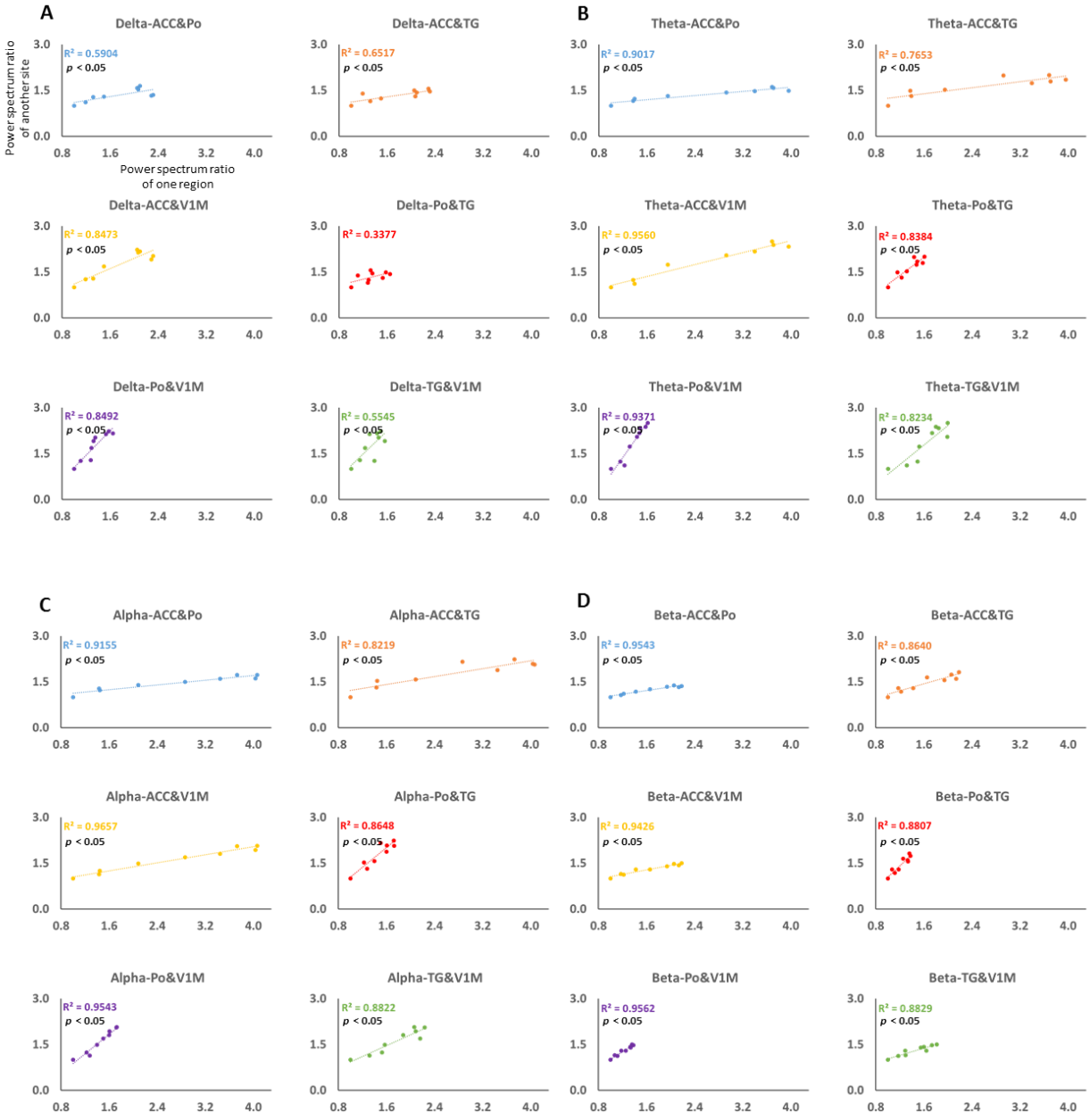
A
Delta-ACC&Po
R² = 0.5904
p < 0.05
Delta-ACC&TG
R² = 0.6517
p < 0.05
Delta-ACC&V1M
R² = 0.8473
p < 0.05
Delta-Po&TG
R² = 0.3377
Delta-Po&V1M
R² = 0.8492
p < 0.05
Delta-TG&V1M
R² = 0.5545
p < 0.05
B
Theta-ACC&Po
R² = 0.9017
p < 0.05
Theta-ACC&TG
R² = 0.7653
p < 0.05
Theta-ACC&V1M
R² = 0.9560
p < 0.05
Theta-Po&TG
R² = 0.8384
p < 0.05
Theta-Po&V1M
R² = 0.9371
p < 0.05
Theta-TG&V1M
R² = 0.8234
p < 0.05
C
Alpha-ACC&Po
R² = 0.9155
p < 0.05
Alpha-ACC&TG
R² = 0.8219
p < 0.05
Alpha-ACC&V1M
R² = 0.9657
p < 0.05
Alpha-Po&TG
R² = 0.8648
p < 0.05
Alpha-Po&V1M
R² = 0.9543
p < 0.05
Alpha-TG&V1M
R² = 0.8822
p < 0.05
D
Beta-ACC&Po
R² = 0.9543
p < 0.05
Beta-ACC&TG
R² = 0.8640
p < 0.05
Beta-ACC&V1M
R² = 0.9426
p < 0.05
Beta-Po&TG
R² = 0.8807
p < 0.05
Beta-Po&V1M
R² = 0.9562
p < 0.05
Beta-TG&V1M
R² = 0.8829
p < 0.05
Power spectrum ratio of another site
Power spectrum ratio of one region
0.0
1.5
3.0
0.8
1.6
2.4
3.2
4.0

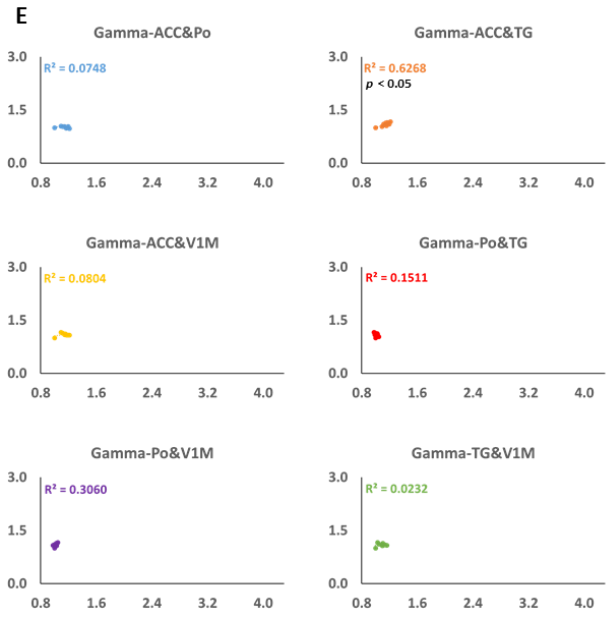

Figure 18. Correlations of LFP intensity changes among paired brain regions at (**A**) delta band, (**B**) theta band, (**C**) alpha band, (**D**) beta band, and (**E**) gamma band from freely moving animals. The x and y axes were the normalized LFP power (ratio). The results demonstrated most correlations in this figure were significant ($p < 0.05$, see Table 10). However, there were no significant correlations between the Po and the TG at the delta band; all pairings except the ACC and the TG at the gamma band.

3.2.5 Surges of coherence induced by NTG injection from freely moving animals (see summary in Tables 11, 12)

The topographical brain coherence showed there were obvious brain coherence changes between the vehicle control group (n = 10) and NTG group (n = 11) in six pairings (ACC & Po, ACC & TG, ACC & V1M, Po & TG, Po & V1M, TG & V1M) from freely moving animals (Fig. 19A,B). The mean coherence change matrices also indicated significant enhancement of brain coherence at the delta, theta, alpha, beta, and gamma bands between these two groups (Fig. 20A,B).

Furthermore, the results of a mixed ANOVA with LSD posthoc test demonstrated that there was significant difference of coherence changes between the vehicle control group (n = 10) and NTG group (n = 11) (Fig. 21). Specifically, the coherence between the ACC and the Po increased significantly in the NTG group compared with the control group at the delta (p = 0.013), alpha (p = 0.021), beta (p = 0.008), and gamma (p = 0.037) bands, but not for theta band. The similar result was detected between the ACC and the TG at the delta (p = 0.037), alpha (p = 0.023), beta (p = 0.002), and gamma (p = 0.004) bands. With respect to the pairings of the ACC and the V1M, the Po and the TG, the Po and the V1M, significant surges of coherence were traced at the delta (p = 0.001, p = 0.017, p < 0.001 , respectively), theta (p = 0.002, p = 0.002, p = 0.009, respectively), alpha (p < 0.001 , p = 0.046, p < 0.001 , respectively), beta (p = 0.020, p = 0.010, p = 0.001, respectively), and gamma (p = 0.034, p = 0.018, p = 0.031, respectively) bands. The significant raise of coherence between the TG and the V1M in the NTG group was exclusively found at the delta (p = 0.008), beta (p = 0.008), and gamma (p = 0.004) bands.

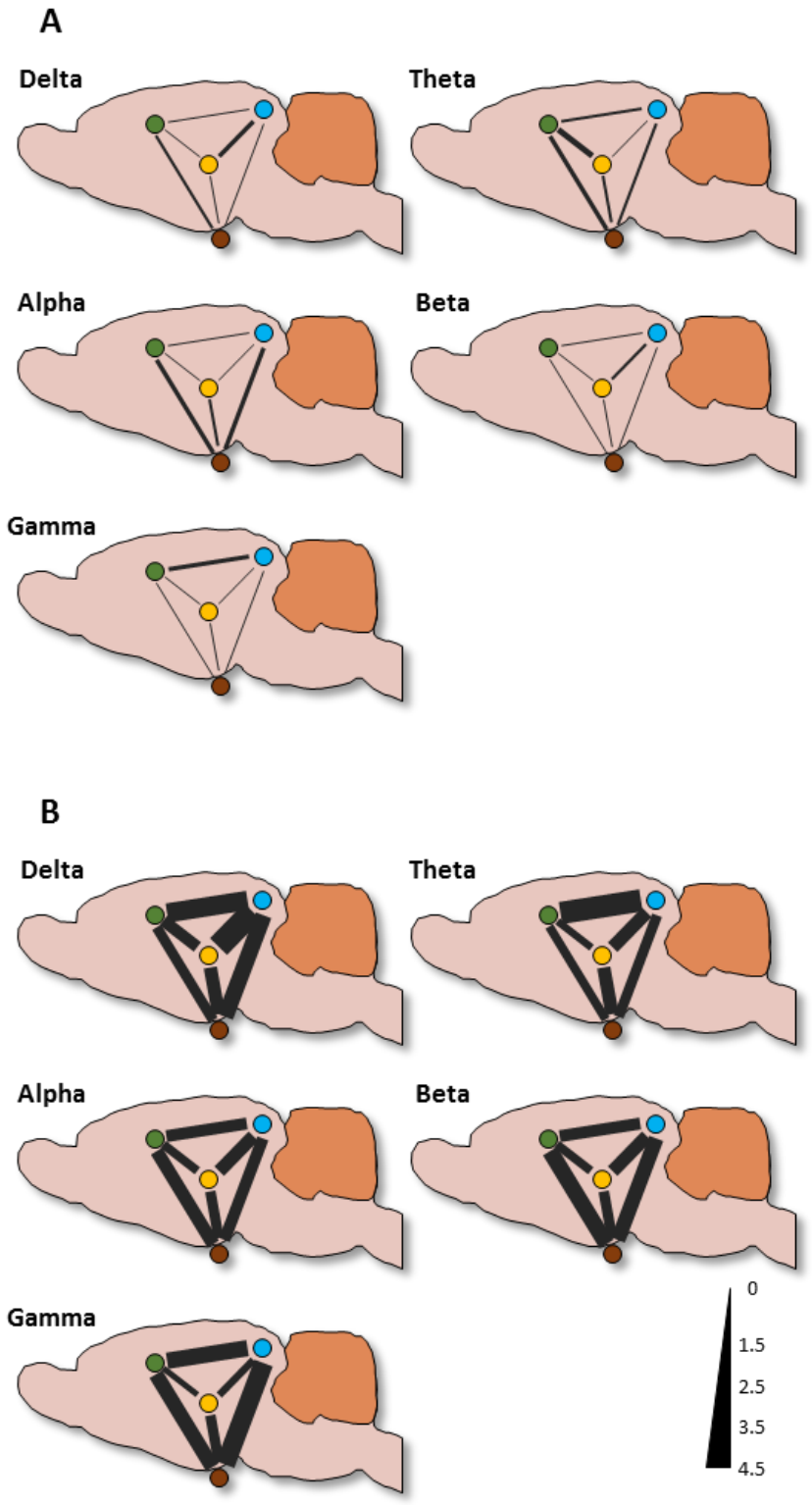

Figure 19. Topographical brain coherence at the delta, theta, alpha, beta, and gamma bands between any paired brain regions (ACC-green, Po-yellow, TG-gray, V1M-blue) in the (**A**) vehicle

control (n = 10) and (**B**) NTG group (n = 11) from freely moving animals. The solid line represents the coherence between paired regions, and the line thickness reflects the magnitude of the coherence.

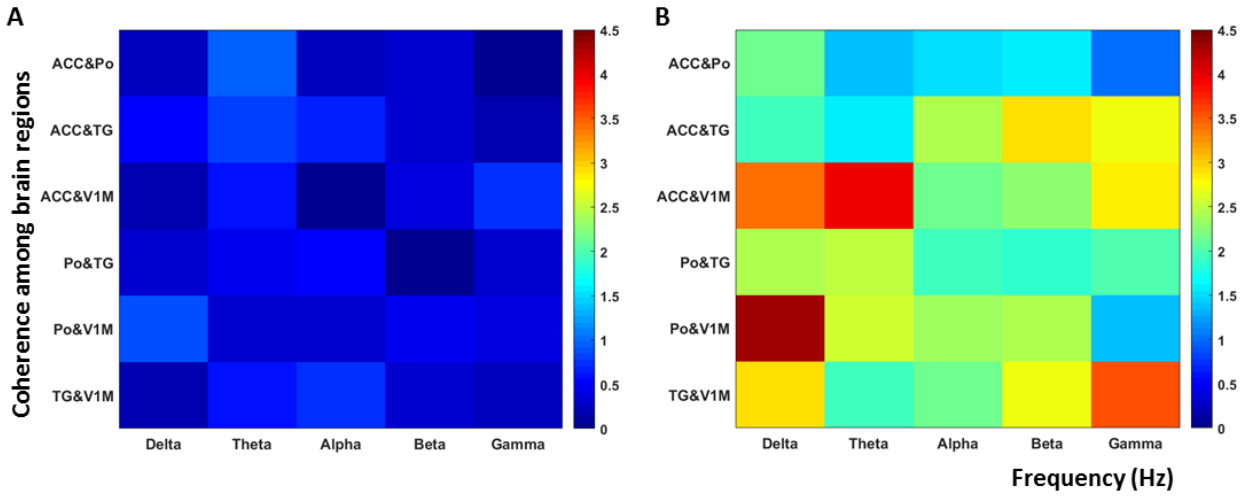

Figure 20. Mean coherence change matrices of the (**A**) vehicle control (n = 10) and (**B**) NTG group (n = 11) from freely moving animals. The color bar denotes coherence change values.

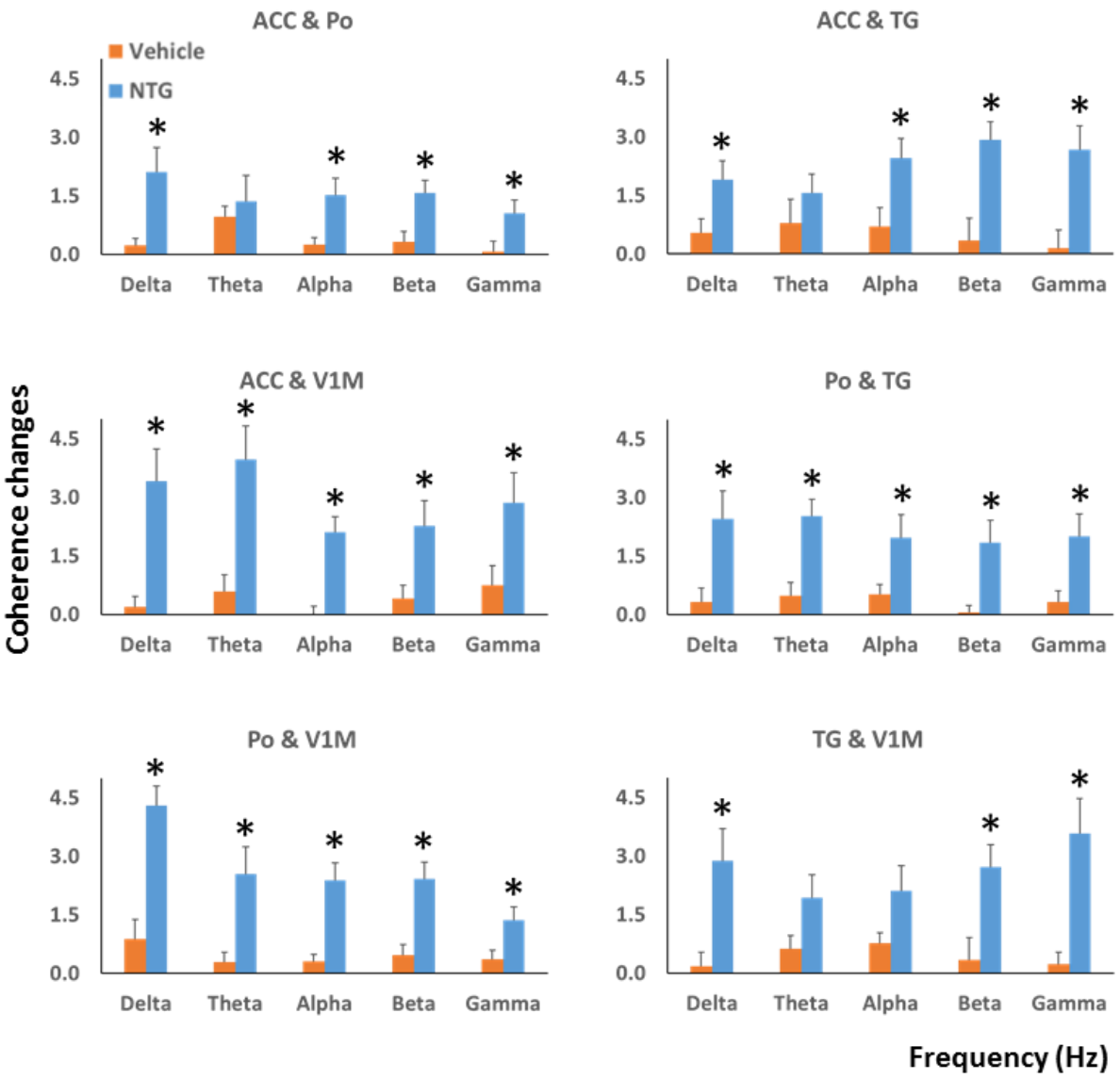

Figure 21. Coherence changes in each paring at different bands between the vehicle control (*n* = 10) and NTG group (*n* = 11) from freely moving animals. All data are shown as mean + SEM. *$p < 0.05$ versus control group. The x-axis is frequency bands (delta, theta, alpha, beta, and gamma), and the y-axis is the coherence change.

Chapter 4 Discussion

In this study, we observed LFP intensity changes after NTG injection from the ACC (Figs. 7E, 9B, 10A), the Po (Figs. 7F, 9B, 10B), the TG (Figs. 7G, 9B, 10C), and the V1M (Figs. 7H, 9B, 10D) with different response patterns simultaneously from anesthetized animals. Additionally, the similar phenomenon was traced in freely moving animals (Figs. 8E-H, 16B, 17). The findings indicate that these regions contribute to the processing of the migraine network, where the trigeminal ganglion, the thalamus, and the visual cortex are involved in the pathway of migraine attacks, and the ACC is related to the emotional reorganization. It is consistence with the probable pathophysiology of migraine. Different orders of neurons are involved, the trigeminal ganglion, the spinal trigeminal nucleus (SpV), the trigeminal nucleus caudalis (TNC), the thalamus, the somatosensory cortices (S1 and S2), the visual cortices, etc. (A.M. Strassman, S.A. Raymond, 1996; Burstein et al., 2000, 2010; Noseda and Burstein, 2013; Pietrobon and Moskowitz, 2013). Differential LFP activities from brain regions in response to NTG injection could be adopted in generating a neural signature for migraine. With future studies involved in more brain areas, these neural signatures may be established and applied to guide the clinical treatment of migraine.

LFP activities in the delta, theta, alpha, beta, and gamma bands among most of the brain regions are enhanced after NTG injection with various patterns (Figs. 10, 17), illustrating different brain sites contribute to migraine pathophysiology in varying degrees. However, significant differences in LFP intensity at the gamma band from the Po (Fig. 10B) and the delta band from the TG (Fig. 10C) were not detected in the anesthetized animals, suggesting possible differential response patterns in these two areas.

Interestingly, in the freely moving animals, NTG created more rhythmic activities than in anesthetized animals (Figs. 8E,G, 17A,C,D). Firstly, the following findings illustrated that the rhythmic activities observed in our study denotes the throbbing of the headache. The single-cell activity indicating throbbing pain was found to fluctuate with the stimulation intensity of meningeal pain fibers (Olesen et al., 2009). Furthermore, growing compelling findings demonstrated that EEG power in various frequencies changes with different subtypes of migraine attacks (episodic migraine, chronic migraine, migraine with or without aura, etc.) (Gastaut et al., 1981; Lev et al., 2010; Porcaro et al., 2017; Gomez-pilar et al., 2020), with ictal or interictal phases (Pisani and Fusco Carlo, 2004; Bjørk and Sand, 2008; Bjørk et al., 2010), etc. However, it was only seen in freely moving animals, which sparks our speculation that the throbbing rhythm is involved in the arterial pulsation change. It is known that inhaled isoflurane interferes with the arterial pulse rate owing to the diminishment in systemic vascular resistances (Torri, 2010; Redfors et al., 2014). Moreover, it has also been investigated that the throbbing rate is related to arterial pulse under temporal patterns (Ahn, 2010; Mirza et al., 2012), but it is different from the pattern we observed (number of oscillations in terms of minutes, see Figures 8E,G, 17A,C,D). To the best of our knowledge, we have not read any detailed clinical descriptions of the similar temporal patterns as we observed in this study. We only detected the rhythm in freely moving animals with the interpretation that the throbbing rhythm was contaminated by the input of isoflurane anesthesia.

Using the repeated measures factorial ANOVA with LSD posthoc test, we deciphered that the brain regions responded differentially when migraine existed. Specifically, the Po and the TG responded more strongly than the V1M, the TG than the ACC in alpha and beta bands; the TG than others, and the ACC than the V1M in the gamma band. With regard to the sequence of information transmitting in the pathway of migraine, the firing inputs initialize from the terminals

(e.g., TG), transmit to third-order neurons (e.g., Po), and final project to different brain cortices (e.g., ACC, V1M). More analysis methods might be suggested to adopt to analyze if there are relationships between these phenomena. Moreover, these four brain regions demonstrated fluctuation simultaneously by Pearson's *r* correlation (Tables 5, 10). With the capability to simultaneously record LFP from multiple regions of the brain, we are able to decipher the relationships of LFP activities involving more brain areas.

In this study, we analyzed correlations of LFP responses among the targeted brain regions, which is time-domain and different from the brain coherence analysis (frequency-domain) (Bastos and Schoffelen, 2016). When it comes to brain coherence, the surge of coherence was exclusively observed among paired brain regions from freely moving rats after NTG injection (Figs. 19-21), and there was no significant difference from anesthetized rats conversely (Figs. 12-14). According to the previous study, anesthesia might partly decrease migraine headache repetitions (suppress severity) (Vosoughian et al., 2021), suggesting the parameter of brain coherence is considered more accurate in this animal study to pinpoint the migraine. The various enhancements of coherence between the ACC and the Po, the ACC and the TG, the ACC and the V1M, the Po and the TG, the Po and the V1M, the TG and the V1M generated in this study might be exploited in the management of migraine and related intervention clinically (Mendonça-de-souza et al., 2012). We calculated brain coherence among the ACC, Po, TG, and V1M. However, brain coherence was also influenced by brain areas (Koeda et al., 1999), and migraine phases (Cao et al., 2016).

The results of the light-aversive behavior test indicated that the time rats spent in the dark compartment increased after NTG injection, suggesting NTG induces the phenomenon of photophobia. The probable mechanism is that the phenomenon results from the interference of the recurrent activation of the trigeminovascular pathway to the visual cortex (Noseda et al., 2010,

2011; Noseda and Burstein, 2011). Our results of LFP activity are consistence with the previous interpretation.

In this study, we recorded LFP by injection (i.p.) of NTG. Similar studies involving different animal models will contribute to the understanding of brain networks. Recently, there are emerging animal models created, for example by the non-invasive stimulation of the dura mater (Burgos-Vega et al., 2019). It is known that aversive environmental stress contributes to the occurrence (Avona et al., 2020) and chronification of migraine with unclear explanations (Liu et al., 2021). Adding such environmental stimulation during the process of chronification will hopefully provide information associated with the cause/origin of migraines. Currently, the explanation of the phenomenon of aura remains not clear. Cortical spreading depression (CSD) is recognized to be associated with migraine aura, which is a slowly propagating wave of depolarization of neuronal and glial cells across the cortex with the involvement of the cerebellum, basal ganglia, thalamus, hippocampus, and brainstem (Leao, 1944; Iadecola, 2002). The involvements of these targeted brain regions need to be explored further.

Several future directions will be conducted. Firstly, it has been reported that migraine affected more females than males each year in US population studies (Lipton et al., 2007; Burch et al., 2019), female rats will be included in the following experiments. With regard to the treatments, multiple kinds of medicines (triptan, sumatriptan, rizatriptan, etc.) have been applied to ameliorate migraine headaches, although the exact mechanisms remain not fully clear. In the near future, we aim to carry out the electrophysiological analysis related to these drugs, then interpret various patterns, and finally offer novel insights into clinical approaches to suppress migraine headaches.

References

A.M. Strassman, S.A. Raymond RB (1996) Sensitization of meningeal sensory neurons and the origin of headaches. Nature 384:356–358.

Ahn AH (2010) On the Temporal Relationship Between Throbbing Migraine Pain and Arterial Pulse. Headache 50:1507–1510.

Ashina M, Bendtsen L, Jensen R, Olesen J (2000) Nitric oxide-induced headache in patients with chronic tension-type headache. Brain 123:1830–1837.

Avona A, Mason BN, Lackovic J, Wajahat N, Motina M, Quigley L, Burgos-vega C, Moldovan C, Garcia-martinez LF, Akopian AN, Price TJ, Dussor G (2020) Repetitive stress in mice causes migraine-like behaviors and calcitonin gene-related peptide-dependent hyperalgesic priming to a migraine trigger. Pain 161:2539–2550.

Bastos AM, Schoffelen JM (2016) A tutorial review of functional connectivity analysis methods and their interpretational pitfalls. Front Syst Neurosci 9:1–23.

Bernstein C, Burstein R (2012) Sensitization of the trigeminovascular pathway: Perspective and implications to migraine pathophysiology. J Clin Neurol 8:89–99.

Bjørk M, Hagen K, Stovner LJ, Sand T (2010) Photic EEG-driving responses related to ictal phases and trigger sensitivity in migraine: A longitudinal, controlled study. Cephalagia 31:444–455.

Bjørk MH, Sand T (2008) Quantitative EEG power and asymmetry increase 36 h before a migraine attack. Cephalagia:960–968.

Borsook D, Maleki N, Burstein R (2015) Migraine. Neurobiol Brain Disord Biol Basis Neurol Psychiatr Disord:693–708.

Bowyer SM (2016) Coherence a measure of the brain networks: past and present. Neuropsychiatr

Electrophysiol:1–12 Available at: http://dx.doi.org/10.1186/s40810-015-0015-7.

Bozer ALH, Uhelski ML, Li AL (2017) Extrapolating meaning from local field potential recordings. J Integr Neurosci 16:107–126.

Burch RC, Buse DC, Lipton RB (2019) Migraine: Epidemiology, Burden, and Comorbidity. Neurol Clin 37:631–649.

Burgos-Vega CC, Moy J, Dussor G (2015) Meningeal Afferent Signaling and the Pathophysiology of Migraine. Elsevier. Available at: http://www.sciencedirect.com/science/article/pii/S1877117315000022 [Accessed April 19, 2016].

Burgos-Vega CC, Quigley LD, Trevisan G, Yan F, Asiedu M, Jacobs B, Motina M, Safdar N, Yousuf H, Avona A, Price TJ, Dussor G (2019) Non-invasive dural stimulation in mice: A novel preclinical model of migraine. Cephalagia 39:123–134.

Burstein R, Cutrer MF, Yarnitsky D (2000) The development of cutaneous allodynia during a migraine attack. Clinical evidence for the sequential recruitment of spinal and supraspinal nociceptive neurons in migraine. Brain 123:1703–1709.

Burstein R, Jakubowski M, Garcia-Nicas E, Kainz V, Bajwa Z, Hargreaves R, Becerra L, Borsook D (2010) Thalamic sensitization transforms localized pain into widespread allodynia. Ann Neurol 68:81–91.

Buzsáki G, Anastassiou CA, Koch C (2012) The origin of extracellular fields and currents-EEG, ECoG, LFP and spikes. Nat Rev Neurosci 13:407–420 Available at: http://dx.doi.org/10.1038/nrn3241.

Cao Z, Lin C, Chuang C, Lai K, Yang AC, Fuh J, Wang S (2016) Resting-state EEG power and coherence vary between migraine phases. J Headache Pain 17:1–9 Available at:

https://thejournalofheadacheandpain.biomedcentral.com/articles/10.1186/s10194-016-0697-7.

Chen SP, Tolner EA, Eikermann-Haerter K (2016) Animal models of monogenic migraine. Cephalalgia 36:704–721 Available at: https://doi.org/10.1177/0333102416645933.

Demartini C, Greco R, Zanaboni AM, Sances G, De Icco R, Borsook D, Tassorelli C (2019) Nitroglycerin as a comparative experimental model of migraine pain: From animal to human and back. Prog Neurobiol 177:15–32 Available at: https://doi.org/10.1016/j.pneurobio.2019.02.002.

Dodick DW (2018) Migraine. Lancet 391:1315–1330.

Farkas S, Bölcskei K, Markovics A, Varga A, Kis-Varga Á, Kormos V, Gaszner B, Horváth C, Tuka B, Tajti J, Helyes Z (2016) Utility of different outcome measures for the nitroglycerin model of migraine in mice. J Pharmacol Toxicol Methods 77:33–44 Available at: http://dx.doi.org/10.1016/j.vascn.2015.09.006.

Gastaut JL, Yermenos E, Bonnefoy M, Cros D (1981) Familial Hemiplegic Migraine: EEG and CT Scan Study of Two Cases. Ann Neurol 10:392–395.

Gomez-pilar J, Garc D, Gomez-lopez-de-san-roman C, Guerrero L, Hornero R (2020) Exploring EEG Spectral Patterns in Episodic and Chronic Migraine During the Interictal State: Determining Frequencies of Interest in the Resting State. Pain Med 21:3530–3538.

H. M, H.R. M, M. M (2016) Methodological note: Neurofeedback: A comprehensive review on system design, methodology and clinical applications. Basic Clin Neurosci 7:143–158 Available at: http://www.embase.com/search/results?subaction=viewrecord&from=export&id=L610031835%0Ahttp://sfx.library.uu.nl/utrecht?sid=EMBASE&issn=2008126X&id=doi:&atitle=Met

hodological+note%3A+Neurofeedback%3A+A+comprehensive+review+on+system+desig n%2C+methodology+a.

Harriott AM, Strother LC, Vila-Pueyo M, Holland PR (2019) Animal models of migraine and experimental techniques used to examine trigeminal sensory processing. J Headache Pain 20.

Harris-Bozer AL, Peng YB (2016) Inflammatory pain by carrageenan recruits low-frequency local field potential changes in the anterior cingulate cortex. Neurosci Lett 632:8–14 Available at: http://dx.doi.org/10.1016/j.neulet.2016.08.016.

Iadecola C (2002) From CSD to headache: A long and winding road. Nat Med 8:110–112.

Iversen HK (2001) Human migraine models. Cephalalgia 21:781–785.

Koeda T, Takeshima T, Matsumoto M, Nakashima K, Takeshita K (1999) Low interhemispheric and high intrahemispheric EEG coherence in migraine. Headache 39:22–23.

Lambert GA, Donaldson C, Boers PM, Zagami AS (2000) Activation of trigeminovascular neurons by glyceryl trinitrate. Brain Res 887:203–210.

Landy S, Rice K, Lobo B (2004) Central sensitisation and cutaneous allodynia in migraine: Implications for treatment. CNS Drugs 18:337–342.

Leao AAP (1944) Spreading Depression of Activity in the Cerebral Cortex. J Neurophysiol 7:359–390.

Lev R, Granovsky Y, Yarnitsky D (2010) Orbitofrontal disinhibition of pain in migraine with aura: An interictal EEG-mapping study. Cephalagia 30:910–918.

Li AL, Yang X, Chiao JC, Peng YB (2016) Reduced local field potential power in the medial prefrontal cortex by noxious stimuli. Brain Res Bull 127:92–99 Available at: http://dx.doi.org/10.1016/j.brainresbull.2016.09.001.

Lindén H, Tetzlaff T, Potjans TC, Pettersen KH, Grün S, Diesmann M, Einevoll GT (2011) Modeling the spatial reach of the LFP. Neuron 72:859–872.

Lipton RB, Bigal ME, Diamond M, Freitag F, Reed ML, Stewart WF (2007) Migraine prevalence, disease burden, and the need for preventive therapy. Neurology 68:343–349.

Liu TH, Wang Z, Xie F, Liu YQ, Lin Q (2021) Contributions of aversive environmental stress to migraine chronification: Research update of migraine pathophysiology. World J Clin Cases 9:2136–2145.

Mendonça-de-souza M, Monteiro UM, Bezerra AS, Ana P, Costa BLSA, Rodrigues MCA (2012) Resilience in migraine brains: decrease of coherence after photic stimulation. Front Hum Neurosci 6:1–6.

Mirza AF, Mo J, Holt JL, Kairalla JA, Heft MW, Ding M, Ahn AH (2012) Is There a Relationship between Throbbing Pain and Arterial Pulsations? J Neurosci 32:7572–7576.

Noseda R, Burstein R (2011) Advances in understanding the mechanisms of migraine-type photophobia. Curr Opin Neurol 24:197–202.

Noseda R, Burstein R (2013) Migraine pathophysiology: Anatomy of the trigeminovascular pathway and associated neurological symptoms, cortical spreading depression, sensitization, and modulation of pain. Pain 154:44–53.

Noseda R, Jakubowski M, Kainz V, Borsook D, Burstein R (2011) Cortical projections of functionally identified thalamic trigeminovascular neurons: Implications for migraine headache and its associated symptoms. J Neurosci 31:14204–14217.

Noseda R, Kainz V, Jakubowski M, Gooley JJ, Saper CB, Digre K, Burstein R (2010) A neural mechanism for exacerbation of headache by light. Nat Neurosci 13:239–245.

Olesen J (2018) Headache Classification Committee of the International Headache Society (IHS)

The International Classification of Headache Disorders, 3rd edition. Cephalalgia 38:1–211.

Olesen J, Burstein R, Ashina M, Tfelt-hansen P, Care C, Israel B (2009) Origin of pain in migraine: evidence for peripheral. Lancet Neurol 8:679–690 Available at: http://dx.doi.org/10.1016/S1474-4422(09)70090-0.

Pietrobon D, Moskowitz MA (2013) Pathophysiology of migraine. Annu Rev Physiol 75:365–391.

Pisani F, Fusco Carlo (2004) Ictal and interictal EEG findings in children with migraine. J Headache Pain 5:23–29.

Porcaro C, Lorenzo G Di, Seri S, Pierelli F, Tecchio F, Coppola G (2017) Impaired brainstem and thalamic high-frequency oscillatory EEG activity in migraine between attacks. Cephalagia 37:915–926.

Redfors B, Shao Y, Omerovic E (2014) Influence of anesthetic agent, depth of anesthesia and body temperature on cardiovascular functional parameters in the rat. Lab Anim 48:6–14.

Sakkalis V (2011) Review of advanced techniques for the estimation of brain connectivity measured with EEG / MEG. Comput Biol Med 41:1110–1117 Available at: http://dx.doi.org/10.1016/j.compbiomed.2011.06.020.

Tang Y, Liu S, Shu H, Xing Y, Tao F (2018) AMPA receptor GluA1 Ser831 phosphorylation is critical for nitroglycerin-induced migraine-like pain. Neuropharmacology 133:462–469 Available at: https://doi.org/10.1016/j.neuropharm.2018.02.026.

Tardiolo G, Bramanti P, Mazzon E (2019) Migraine: Experimental models and novel therapeutic approaches. Int J Mol Sci 20.

Thomsen LL, Olesen J (2001) Nitric oxide in primary headaches. Curr Opin Neurol 14:315–321.

Torri G (2010) Inhalation anesthetics: a review. Minerva Anestesiol 76:215–228.

Vos T et al. (2017) Global, regional, and national incidence, prevalence, and years lived with disability for 328 diseases and injuries for 195 countries, 1990-2016: A systematic analysis for the Global Burden of Disease Study 2016. Lancet 390:1211–1259.

Vosoughian M, Saeedi N, Dabir S (2021) The Effect of Propofol Anesthesia on the Pain Severity and Frequency of Migraine Attacks in Patients with Chronic Migraine Headache over a Six Month Follow Up: An Observational Study. Iran J Pharm Res 20:415–421.

Wang Z, Peng YB (2022) Multi-region local field potential signatures in response to the formalin-induced inflammatory stimulus in male rats. Brain Res 1778:147779 Available at: https://doi.org/10.1016/j.brainres.2022.147779.

Appendix

Table 3. Normalized LFP power at various frequency bands in different brain regions following vehicle solution injection from anesthetized animals

Brain Region	Frequency Band	30 min	60 min	90 min	120 min	150 min	180 min	210 min	240 min	270 min
ACC	Delta	1.000	1.004 ± 0.132	1.167 ± 0.157	1.359 ± 0.205	1.519 ± 0.194	1.509 ± 0.220	1.508 ± 0.237	1.627 ± 0.250	1.561 ± 0.300
	Theta	1.000	1.021 ± 0.118	1.176 ± 0.146	1.364 ± 0.211	1.543 ± 0.223	1.566 ± 0.237	1.531 ± 0.260	1.484 ± 0.280	1.455 ± 0.296
	Alpha	1.000	1.011 ± 0.118	1.102 ± 0.141	1.194 ± 0.164	1.385 ± 0.217	1.424 ± 0.225	1.394 ± 0.255	1.336 ± 0.259	1.357 ± 0.297
	Beta	1.000	1.006 ± 0.100	1.100 ± 0.103	1.106 ± 0.111	1.237 ± 0.154	1.259 ± 0.175	1.157 ± 0.165	1.133 ± 0.171	1.135 ± 0.189
	Gamma	1.000	1.087 ± 0.111	1.177 ± 0.113	1.138 ± 0.095	1.207 ± 0.109	1.222 ± 0.115	1.102 ± 0.102	1.103 ± 0.113	1.080 ± 0.132
Po	Delta	1.000	0.986 ± 0.049	1.033 ± 0.064	1.060 ± 0.072	1.140 ± 0.076	1.135 ± 0.088	1.179 ± 0.103	1.237 ± 0.116	1.250 ± 0.108
	Theta	1.000	1.065 ± 0.049	1.195 ± 0.070	1.316 ± 0.097	1.496 ± 0.120	1.572 ± 0.139	1.662 ± 0.159	1.756 ± 0.216	1.752 ± 0.208
	Alpha	1.000	1.087 ± 0.064	1.284 ± 0.105	1.420 ± 0.137	1.728 ± 0.210	1.877 ± 0.243	1.880 ± 0.226	1.923 ± 0.245	1.833 ± 0.248
	Beta	1.000	1.244 ± 0.043	1.578 ± 0.087	1.784 ± 0.158	1.969 ± 0.226	1.985 ± 0.248	2.001 ± 0.252	1.946 ± 0.251	1.847 ± 0.265
	Gamma	1.000	1.108 ± 0.031	1.214 ± 0.044	1.254 ± 0.072	1.287 ± 0.095	1.292 ± 0.101	1.317 ± 0.112	1.298 ± 0.116	1.279 ± 0.117
TG	Delta	1.000	1.148 ± 0.126	1.145 ± 0.154	1.224 ± 0.177	1.426 ± 0.249	1.461 ± 0.210	1.511 ± 0.246	1.673 ± 0.283	1.498 ± 0.310
	Theta	1.000	1.258 ± 0.113	1.377 ± 0.133	1.552 ± 0.187	1.807 ± 0.212	1.853 ± 0.246	1.785 ± 0.265	1.850 ± 0.292	1.627 ± 0.266

	Alpha	1.000	1.384 ± 0.161	1.609 ± 0.195	1.791 ± 0.221	2.168 ± 0.276	2.133 ± 0.292	2.073 ± 0.279	2.092 ± 0.341	1.998 ± 0.383
	Beta	1.000	1.434 ± 0.171	1.655 ± 0.255	1.866 ± 0.306	2.067 ± 0.342	1.971 ± 0.334	1.875 ± 0.305	1.865 ± 0.348	1.785 ± 0.368
	Gamma	1.000	1.419 ± 0.128	1.503 ± 0.172	1.649 ± 0.200	1.716 ± 0.247	1.671 ± 0.247	1.558 ± 0.225	1.427 ± 0.220	1.387 ± 0.247
V1M	Delta	1.000	0.953 ± 0.169	0.902 ± 0.191	0.867 ± 0.159	1.013 ± 0.165	1.078 ± 0.219	1.128 ± 0.241	1.228 ± 0.229	1.157 ± 0.227
	Theta	1.000	1.076 ± 0.142	1.078 ± 0.144	1.056 ± 0.151	1.122 ± 0.177	1.179 ± 0.188	1.195 ± 0.197	1.155 ± 0.208	1.067 ± 0.199
	Alpha	1.000	1.060 ± 0.108	1.078 ± 0.098	1.064 ± 0.104	1.176 ± 0.124	1.179 ± 0.153	1.109 ± 0.157	1.087 ± 0.162	1.005 ± 0.156
	Beta	1.000	1.169 ± 0.065	1.213 ± 0.089	1.158 ± 0.092	1.186 ± 0.103	1.163 ± 0.109	1.103 ± 0.100	1.041 ± 0.117	0.963 ± 0.132
	Gamma	1.000	1.098 ± 0.040	1.132 ± 0.054	1.108 ± 0.073	1.093 ± 0.072	1.081 ± 0.067	1.118 ± 0.087	1.067 ± 0.066	1.027 ± 0.067

Table 4. Normalized LFP power at various frequency bands in different brain regions following NTG injection from anesthetized animals

Brain Region	Frequency Band	30 min	60 min	90 min	120 min	150 min	180 min	210 min	240 min	270 min
ACC	Delta	1.000	1.162 ± 0.147	1.505 ± 0.133	1.615 ± 0.189	1.898 ± 0.270	2.200 ± 0.288	2.403 ± 0.338*	2.488 ± 0.349	2.673 ± 0.353*
	Theta	1.000	1.223 ± 0.120	1.662 ± 0.158*	1.679 ± 0.148	1.963 ± 0.246	2.095 ± 0.256	2.363 ± 0.319	2.538 ± 0.290*	2.801 ± 0.298*
	Alpha	1.000	1.291 ± 0.120	1.640 ± 0.144*	1.720 ± 0.146*	2.002 ± 0.244	2.133 ± 0.259	2.254 ± 0.300*	2.454 ± 0.304*	2.583 ± 0.326*
	Beta	1.000	1.272 ± 0.098	1.556 ± 0.104*	1.638 ± 0.120*	1.758 ± 0.142*	1.864 ± 0.176*	1.942 ± 0.198*	2.016 ± 0.200*	2.060 ± 0.207*
	Gamma	1.000	1.322 ± 0.107	1.551 ± 0.125*	1.557 ± 0.121*	1.589 ± 0.135*	1.624 ± 0.125*	1.579 ± 0.101*	1.619 ± 0.126*	1.603 ± 0.125*
Po	Delta	1.000	1.173 ± 0.064*	1.200 ± 0.105	1.238 ± 0.112	1.334 ± 0.155	1.344 ± 0.162	1.435 ± 0.210	1.488 ± 0.198	1.550 ± 0.197
	Theta	1.000	1.256 ± 0.061*	1.373 ± 0.109	1.541 ± 0.133	1.761 ± 0.184	1.843 ± 0.193	2.029 ± 0.238	2.183 ± 0.246	2.379 ± 0.317
	Alpha	1.000	1.544 ± 0.124*	1.806 ± 0.122*	1.997 ± 0.128*	2.206 ± 0.176	2.436 ± 0.235	2.728 ± 0.316*	2.927 ± 0.329*	3.098 ± 0.392*
	Beta	1.000	1.344 ± 0.122	1.745 ± 0.154	1.996 ± 0.153	2.241 ± 0.160	2.454 ± 0.172	2.691 ± 0.192*	2.865 ± 0.192*	3.023 ± 0.253*
	Gamma	1.000	1.152 ± 0.058	1.293 ± 0.062	1.340 ± 0.069	1.435 ± 0.090	1.495 ± 0.106	1.531 ± 0.153	1.582 ± 0.174	1.667 ± 0.243
TG	Delta	1.000	1.332 ± 0.257	1.868 ± 0.342	1.899 ± 0.311	2.213 ± 0.447	2.310 ± 0.564	2.552 ± 0.575	2.767 ± 0.641	2.834 ± 0.673
	Theta	1.000	1.292 ± 0.224	1.969 ± 0.378	2.329 ± 0.350	2.803 ± 0.510	2.980 ± 0.596	3.233 ± 0.588*	3.448 ± 0.625*	3.778 ± 0.805*
	Alpha	1.000	1.481 ± 0.228	2.305 ± 0.386	2.622 ± 0.384	3.060 ± 0.518	3.311 ± 0.615	3.587 ± 0.562*	3.884 ± 0.634*	4.196 ± 0.789*

	Beta	1.000	1.523 ± 0.178	2.327 ± 0.319	2.713 ± 0.303	3.120 ± 0.430	3.363 ± 0.497*	3.576 ± 0.431*	4.023 ± 0.510*	4.218 ± 0.502*
	Gamma	1.000	1.375 ± 0.141	2.213 ± 0.284*	2.502 ± 0.301*	2.860 ± 0.338*	3.167 ± 0.480*	3.412 ± 0.501*	4.038 ± 0.701*	3.863 ± 0.596*
V1M	Delta	1.000	0.996 ± 0.105	1.309 ± 0.140	1.370 ± 0.167*	1.497 ± 0.157*	1.562 ± 0.166	1.662 ± 0.167	1.758 ± 0.170	1.865 ± 0.140*
	Theta	1.000	1.152 ± 0.111	1.402 ± 0.131	1.525 ± 0.151*	1.613 ± 0.163	1.745 ± 0.175*	1.904 ± 0.187*	2.004 ± 0.206*	2.085 ± 0.245*
	Alpha	1.000	1.385 ± 0.085*	1.592 ± 0.100*	1.665 ± 0.107*	1.751 ± 0.137*	1.883 ± 0.179*	2.000 ± 0.201*	2.067 ± 0.213*	2.103 ± 0.246*
	Beta	1.000	1.329 ± 0.062	1.630 ± 0.101*	1.712 ± 0.119*	1.790 ± 0.118*	1.831 ± 0.135*	1.878 ± 0.154*	1.894 ± 0.159*	1.861 ± 0.178*
	Gamma	1.000	1.105 ± 0.041	1.170 ± 0.045	1.170 ± 0.041	1.194 ± 0.039	1.225 ± 0.040	1.227 ± 0.045	1.229 ± 0.048	1.244 ± 0.054*

LFP power/intensity changes in the delta, theta, alpha, beta, and gamma bands at the ACC, Po, TG, and V1M from anesthetized animals. All data are shown as mean ± SEM. *$p < 0.05$ versus control group.

Table 5. Correlations of LFP changes among various paired brain regions from anesthetized animals

Delta	ACC	Po	TG	V1M
ACC		$r(7) = .974$ $p < .001$	$r(7) = .983$ $p < .001$	$r(7) = .987$ $p < .001$
Po			$r(7) = .979$ $p < .001$	$r(7) = .959$ $p < .001$
TG				$r(7) = .988$ $p < .001$
V1M				

Theta	ACC	Po	TG	V1M
ACC		$r(7) = .992$ $p < .001$	$r(7) = .988$ $p < .001$	$r(7) = .993$ $p < .001$
Po			$r(7) = .985$ $p < .001$	$r(7) = .989$ $p < .001$
TG				$r(7) = .994$ $p < .001$
V1M				

Alpha	ACC	Po	TG	V1M
ACC		$r(7) = .994$ $p < .001$	$r(7) = .998$ $p < .001$	$r(7) = .983$ $p < .001$
Po			$r(7) = .989$	$r(7) = .986$

			$p < .001$	$p < .001$
TG				$r(7) = .983$ $p < .001$
V1M				

Beta	ACC	Po	TG	V1M
ACC		$r(7) = .988$ $p < .001$	$r(7) = .992$ $p < .001$	$r(7) = .971$ $p < .001$
Po			$r(7) = .997$ $p < .001$	$r(7) = .925$ $p < .001$
TG				$r(7) = .940$ $p < .001$
V1M				

Gamma	ACC	Po	TG	V1M
ACC		$r(7) = .873$ $p = .002$	$r(7) = .841$ $p = .005$	$r(7) = .967$ $p < .001$
Po			$r(7) = .985$ $p < .001$	$r(7) = .961$ $p < .001$
TG				$r(7) = .931$ $p < .001$
V1M				

Table 6. Coherence alternations in each paring following vehicle injection from anesthetized animals

Pairings	Delta	Theta	Alpha	Beta	Gamma
ACC and Po	0.338 ± 0.275	0.040 ± 0.221	0.226 ± 0.324	0.828 ± 0.449	0.155 ± 0.288
ACC and TG	0.334 ± 0.295	0.552 ± 0.507	0.552 ± 0.409	0.489 ± 0.534	0.332 ± 0.359
ACC and V1M	1.067 ± 0.618	0.707 ± 0.618	0.304 ± 0.351	0.310 ± 0.365	0.273 ± 0.351
Po and TG	0.667 ± 0.499	0.259 ± 0.301	0.400 ± 0.207	0.316 ± 0.522	0.234 ± 0.326
Po and V1M	0.323 ± 0.255	0.246 ± 0.262	0.202 ± 0.300	0.362 ± 0.220	0.524 ± 0.340
TG and V1M	0.137 ± 0.201	0.268 ± 0.412	0.037 ± 0.244	0.542 ± 0.498	0.925 ± 0.484

Table 7. Coherence alternations in each paring following NTG injection from anesthetized animals

Pairings	Delta	Theta	Alpha	Beta	Gamma
ACC and Po	1.632 ± 0.396*	1.175 ± 0.377*	0.943 ± 0.646	0.522 ± 0.456	0.333 ± 0.350
ACC and TG	1.648 ± 0.656	0.598 ± 0.522	0.509 ± 0.603	0.462 ± 0.282	0.435 ± 0.543
ACC and V1M	2.115 ± 0.509	0.620 ± 0.383	0.477 ± 0.403	0.385 ± 0.292	0.182 ± 0.220
Po and TG	0.616 ± 0.316	0.860 ± 0.493	0.278 ± 0.313	0.380 ± 0.241	0.407 ± 0.409
Po and V1M	0.941 ± 0.424	0.808 ± 0.363	1.682 ± 0.504*	0.969 ± 0.279	1.162 ± 0.452
TG and V1M	0.941 ± 0.551	0.083 ± 0.170	0.460 ± 0.534	0.802 ± 0.489	1.058 ± 0.595

*$p < 0.05$ versus control group

Table 8. Normalized LFP power at various frequency bands in different brain regions following vehicle solution injection from freely moving animals

Brain Region	Frequency Band	30 min	60 min	90 min	120 min	150 min	180 min	210 min	240 min	270 min
ACC	Delta	1.000	0.981 ± 0.060	0.884 ± 0.060	1.032 ± 0.094	0.986 ± 0.079	1.015 ± 0.092	0.958 ± 0.089	0.873 ± 0.103	0.927 ± 0.079
	Theta	1.000	0.982 ± 0.047	0.975 ± 0.041	1.241 ± 0.100	1.216 ± 0.092	1.262 ± 0.109	1.216 ± 0.098	1.045 ± 0.071	1.233 ± 0.077
	Alpha	1.000	1.004 ± 0.043	0.995 ± 0.035	1.237 ± 0.094	1.252 ± 0.096	1.314 ± 0.123	1.277 ± 0.117	1.080 ± 0.059	1.300 ± 0.095
	Beta	1.000	1.011 ± 0.013	0.976 ± 0.025	1.148 ± 0.076	1.157 ± 0.077	1.176 ± 0.092	1.175 ± 0.096	1.055 ± 0.050	1.210 ± 0.079
	Gamma	1.000	0.997 ± 0.020	0.991 ± 0.033	1.050 ± 0.055	1.048 ± 0.046	1.042 ± 0.047	1.069 ± 0.067	1.027 ± 0.048	1.073 ± 0.048
Po	Delta	1.000	0.861 ± 0.074	0.925 ± 0.112	0.978 ± 0.131	0.897 ± 0.103	0.921 ± 0.111	0.956 ± 0.116	0.863 ± 0.091	0.985 ± 0.105
	Theta	1.000	0.985 ± 0.035	0.988 ± 0.042	1.063 ± 0.077	1.121 ± 0.077	1.166 ± 0.084	1.169 ± 0.082	1.077 ± 0.054	1.197 ± 0.073
	Alpha	1.000	1.046 ± 0.044	1.071 ± 0.044	1.100 ± 0.060	1.227 ± 0.093	1.323 ± 0.106	1.283 ± 0.084	1.201 ± 0.107	1.367 ± 0.103
	Beta	1.000	0.967 ± 0.042	0.949 ± 0.038	0.992 ± 0.064	1.115 ± 0.085	1.161 ± 0.123	1.110 ± 0.076	1.097 ± 0.107	1.185 ± 0.124
	Gamma	1.000	0.936 ± 0.021	0.945 ± 0.024	0.866 ± 0.032	0.904 ± 0.020	0.880 ± 0.039	0.873 ± 0.043	0.914 ± 0.038	0.859 ± 0.047
TG	Delta	1.000	0.879 ± 0.073	0.922 ± 0.045	0.854 ± 0.086	0.830 ± 0.082	0.898 ± 0.122	0.824 ± 0.100	0.762 ± 0.074	0.818 ± 0.069
	Theta	1.000	1.002 ± 0.064	0.989 ± 0.050	1.005 ± 0.043	1.069 ± 0.069	1.072 ± 0.067	1.054 ± 0.058	0.997 ± 0.078	1.026 ± 0.046
	Alpha	1.000	1.043 ± 0.054	1.043 ± 0.052	1.065 ± 0.039	1.154 ± 0.064	1.193 ± 0.071	1.152 ± 0.068	1.045 ± 0.075	1.150 ± 0.062

	Beta	1.000	1.021 ± 0.021	0.976 ± 0.027	1.022 ± 0.025	1.075 ± 0.037	1.124 ± 0.044	1.131 ± 0.059	1.079 ± 0.066	1.115 ± 0.051
	Gamma	1.000	0.945 ± 0.039	1.000 ± 0.040	0.979 ± 0.033	0.981 ± 0.032	0.976 ± 0.027	0.980 ± 0.026	0.974 ± 0.027	0.976 ± 0.031
V1M	Delta	1.000	0.887 ± 0.103	0.930 ± 0.106	0.949 ± 0.126	0.928 ± 0.104	0.872 ± 0.113	0.975 ± 0.120	0.982 ± 0.148	0.932 ± 0.108
	Theta	1.000	1.085 ± 0.040	1.155 ± 0.043	1.354 ± 0.069	1.404 ± 0.080	1.425 ± 0.115	1.500 ± 0.077	1.438 ± 0.082	1.411 ± 0.075
	Alpha	1.000	1.109 ± 0.030	1.252 ± 0.030	1.399 ± 0.060	1.444 ± 0.059	1.482 ± 0.073	1.513 ± 0.060	1.465 ± 0.086	1.465 ± 0.074
	Beta	1.000	1.083 ± 0.030	1.126 ± 0.027	1.187 ± 0.042	1.213 ± 0.041	1.228 ± 0.041	1.258 ± 0.040	1.243 ± 0.049	1.281 ± 0.044
	Gamma	1.000	1.050 ± 0.040	1.080 ± 0.037	1.011 ± 0.029	1.035 ± 0.036	1.041 ± 0.035	1.025 ± 0.050	1.028 ± 0.055	1.057 ± 0.058

Table 9. Normalized LFP power at various frequency bands in different brain regions following NTG injection from freely moving animals

Brain Region	Frequency Band	30 min	60 min	90 min	120 min	150 min	180 min	210 min	240 min	270 min
ACC	Delta	1.000	1.315 ± 0.106*	1.191 ± 0.090*	1.494 ± 0.164*	2.049 ± 0.338*	2.312 ± 0.303*	2.287 ± 0.479*	2.093 ± 0.346*	2.066 ± 0.371*
	Theta	1.000	1.389 ± 0.098*	1.368 ± 0.127*	1.949 ± 0.239*	2.921 ± 0.811	3.395 ± 0.858*	3.958 ± 1.202	3.685 ± 1.088*	3.706 ± 1.065*
	Alpha	1.000	1.433 ± 0.113*	1.443 ± 0.151*	2.085 ± 0.374	2.863 ± 0.826	3.446 ± 0.883*	4.034 ± 1.239	3.727 ± 1.119*	4.064 ± 1.364
	Beta	1.000	1.221 ± 0.043*	1.172 ± 0.048*	1.419 ± 0.098	1.655 ± 0.206	1.940 ± 0.244*	2.139 ± 0.354*	2.058 ± 0.323*	2.182 ± 0.419
	Gamma	1.000	1.094 ± 0.011*	1.115 ± 0.027*	1.156 ± 0.020	1.143 ± 0.019	1.171 ± 0.034*	1.199 ± 0.046	1.168 ± 0.029*	1.214 ± 0.073
Po	Delta	1.000	1.276 ± 0.097*	1.109 ± 0.076	1.288 ± 0.201	1.576 ± 0.318*	1.353 ± 0.114*	1.324 ± 0.168	1.644 ± 0.326*	1.528 ± 0.174*
	Theta	1.000	1.224 ± 0.049*	1.156 ± 0.065*	1.311 ± 0.098	1.431 ± 0.072*	1.473 ± 0.146	1.486 ± 0.152	1.608 ± 0.132*	1.577 ± 0.154*
	Alpha	1.000	1.277 ± 0.065*	1.223 ± 0.070	1.397 ± 0.077*	1.501 ± 0.068*	1.600 ± 0.155	1.605 ± 0.167	1.723 ± 0.099*	1.727 ± 0.143
	Beta	1.000	1.115 ± 0.031*	1.068 ± 0.061	1.178 ± 0.075	1.256 ± 0.067	1.333 ± 0.136	1.327 ± 0.118	1.378 ± 0.092	1.355 ± 0.090
	Gamma	1.000	1.046 ± 0.028*	1.025 ± 0.040	1.011 ± 0.038*	1.026 ± 0.039*	0.992 ± 0.047	1.027 ± 0.058*	0.989 ± 0.036	0.978 ± 0.044
TG	Delta	1.000	1.142 ± 0.127	1.389 ± 0.163*	1.233 ± 0.169*	1.491 ± 0.260*	1.457 ± 0.153*	1.558 ± 0.274*	1.433 ± 0.228*	1.307 ± 0.080*
	Theta	1.000	1.314 ± 0.097*	1.489 ± 0.159*	1.520 ± 0.154*	1.985 ± 0.292*	1.732 ± 0.223*	1.845 ± 0.334*	1.995 ± 0.296*	1.798 ± 0.195*
	Alpha	1.000	1.319 ± 0.103*	1.525 ± 0.184*	1.571 ± 0.174*	2.158 ± 0.426*	1.878 ± 0.314*	2.084 ± 0.523	2.237 ± 0.441*	2.063 ± 0.243*
	Beta	1.000	1.176 ± 0.060*	1.293 ± 0.107*	1.291 ± 0.103*	1.643 ± 0.172*	1.551 ± 0.158*	1.602 ± 0.201*	1.735 ± 0.171*	1.815 ± 0.228*
	Gamma	1.000	1.031 ± 0.021	1.102 ± 0.046	1.048 ± 0.030	1.129 ± 0.043*	1.092 ± 0.039*	1.100 ± 0.054*	1.141 ± 0.055*	1.162 ± 0.036*

V1M	Delta	1.000	1.280 ± 0.168	1.256 ± 0.108*	1.682 ± 0.355*	2.224 ± 0.526*	2.018 ± 0.307*	1.904 ± 0.395*	2.165 ± 0.519*	2.135 ± 0.461*
	Theta	1.000	1.114 ± 0.123	1.238 ± 0.100	1.732 ± 0.252	2.047 ± 0.354	2.170 ± 0.345*	2.328 ± 0.460	2.502 ± 0.457*	2.379 ± 0.341*
	Alpha	1.000	1.134 ± 0.076	1.243 ± 0.074	1.490 ± 0.141	1.697 ± 0.197	1.809 ± 0.179	1.928 ± 0.248	2.056 ± 0.251*	2.064 ± 0.183*
	Beta	1.000	1.120 ± 0.054	1.145 ± 0.027	1.290 ± 0.053	1.297 ± 0.041	1.401 ± 0.044*	1.425 ± 0.062*	1.477 ± 0.076*	1.502 ± 0.063*
	Gamma	1.000	1.161 ± 0.058	1.134 ± 0.033	1.110 ± 0.032*	1.094 ± 0.025	1.078 ± 0.044	1.072 ± 0.052	1.088 ± 0.073	1.082 ± 0.082

LFP power/intensity changes in the delta, theta, alpha, beta, and gamma bands at the ACC, Po, TG, and V1M from freely moving animals. All data are shown as mean ± SEM. *$p < 0.05$ versus control group.

Table 10. Correlations of LFP changes among various paired brain regions from freely moving animals

Delta	ACC	Po	TG	V1M
ACC		$r(7) = .768$ $p = .016$	$r(7) = .807$ $p = .009$	$r(7) = .921$ $p < .001$
Po			$r(7) = .581$ $p = .101$	$r(7) = .922$ $p < .001$
TG				$r(7) = .745$ $p = .021$
V1M				

Theta	ACC	Po	TG	V1M
ACC		$r(7) = .950$ $p < .001$	$r(7) = .875$ $p = .002$	$r(7) = .978$ $p < .001$
Po			$r(7) = .916$ $p = .001$	$r(7) = .968$ $p < .001$
TG				$r(7) = .907$ $p = .001$
V1M				

Alpha	ACC	Po	TG	V1M
ACC		$r(7) = .957$ $p < .001$	$r(7) = .907$ $p = .001$	$r(7) = .983$ $p < .001$
Po			$r(7) = .930$ $p < .001$	$r(7) = .977$ $p < .001$

TG				$r(7) = .939$ $p < .001$
V1M				

Beta	ACC	Po	TG	V1M
ACC		$r(7) = .977$ $p < .001$	$r(7) = .930$ $p < .001$	$r(7) = .971$ $p < .001$
Po			$r(7) = .938$ $p < .001$	$r(7) = .978$ $p < .001$
TG				$r(7) = .940$ $p < .001$
V1M				

Gamma	ACC	Po	TG	V1M
ACC		$r(7) = -.274$ $p = .476$	$r(7) = .792$ $p = .011$	$r(7) = .283$ $p = .460$
Po			$r(7) = -.389$ $p = .301$	$r(7) = .553$ $p = .122$
TG				$r(7) = .152$ $p = .696$
V1M				

Table 11. Coherence alternations in each paring following vehicle injection from freely moving animals

Pairings	Delta	Theta	Alpha	Beta	Gamma
ACC and Po	0.222 ± 0.178	0.955 ± 0.275	0.252 ± 0.178	0.321 ± 0.257	0.066 ± 0.264
ACC and TG	0.550 ± 0.358	0.799 ± 0.602	0.695 ± 0.483	0.346 ± 0.567	0.151 ± 0.457
ACC and V1M	0.185 ± 0.268	0.576 ± 0.438	0.011 ± 0.199	0.401 ± 0.353	0.749 ± 0.499
Po and TG	0.314 ± 0.357	0.476 ± 0.348	0.523 ± 0.244	0.047 ± 0.185	0.316 ± 0.300
Po and V1M	0.876 ± 0.500	0.286 ± 0.251	0.313 ± 0.164	0.467 ± 0.277	0.359 ± 0.234
TG and V1M	0.166 ± 0.372	0.629 ± 0.330	0.767 ± 0.271	0.339 ± 0.565	0.220 ± 0.309

Table 12. Coherence alternations in each paring following NTG injection from freely moving animals

Pairings	Delta	Theta	Alpha	Beta	Gamma
ACC and Po	2.111 ± 0.632*	1.357 ± 0.663	1.515 ± 0.427*	1.575 ± 0.324*	1.046 ± 0.341*
ACC and TG	1.906 ± 0.474*	1.557 ± 0.496	2.451 ± 0.516*	2.926 ± 0.454*	2.672 ± 0.611*
ACC and V1M	3.409 ± 0.822*	3.971 ± 0.858*	2.112 ± 0.391*	2.264 ± 0.637*	2.855 ± 0.770*
Po and TG	2.459 ± 0.706*	2.518 ± 0.443*	1.962 ± 0.604*	1.846 ± 0.562*	2.011 ± 0.562*
Po and V1M	4.293 ± 0.505*	2.541 ± 0.704*	2.374 ± 0.462*	2.421 ± 0.419*	1.357 ± 0.350*
TG and V1M	2.883 ± 0.811*	1.921 ± 0.594	2.111 ± 0.633	2.714 ± 0.565*	3.577 ± 0.891*

*$p < 0.05$ versus control group